

Global Study of Nuclear Structure Functions

S. A. Kulagin*

Institute for Nuclear Research, 117312 Moscow, Russia

R. Petti†

CERN, CH-1211 Genève 23, Switzerland

Abstract

We present the results of a phenomenological study of unpolarized nuclear structure functions for a wide kinematical region of x and Q^2 . As a basis of our phenomenology we develop a model which takes into account a number of different nuclear effects including nuclear shadowing, Fermi motion and nuclear binding, nuclear pions and off-shell correction to bound nucleon structure functions. Within this approach we perform a statistical analysis of available data on the ratio of the nuclear structure functions F_2 for different nuclei in the range from Deuterium to ^{207}Pb . We express the off-shell effect and the effective scattering amplitude describing nuclear shadowing in terms of few parameters which are common to all nuclei and have a clear physical interpretation. We extract such parameters from a statistical analysis of data. As a result, we obtain an excellent overall agreement between our calculations and data in the entire kinematical region of x and Q^2 . We discuss a number of applications of our model which include the calculation of the deuteron structure functions, nuclear valence and sea quark distributions and nuclear structure functions for neutrino charged-current scattering.

*kulagin@ms2.inr.ac.ru

†Roberto.Petti@cern.ch

I. INTRODUCTION

The lepton Deep Inelastic Scattering (DIS) off nucleons has been since long time a powerful tool to probe the structure of hadrons and nuclei at small and intermediate scales. After the discovery of the parton structure of nucleons, DIS remains to be the primary source of experimental information on the distribution of quark and gluon fields in the nucleon and nuclei and a valuable tool to test predictions of QCD. New data from high-intensity electron (Jefferson Laboratory) and neutrino (NuMI at Fermilab and JPARC in Japan) beams will allow in future to further extend our knowledge of the nucleon and nuclear structure from high-precision experiments.

The role of nuclei in DIS studies is twofold. First, it should be noted that the study of nuclei at small space-time scales is interesting by itself and it can provide valuable insights into the origin of nuclear force and properties of hadrons in nuclear medium. On the other hand the nuclear data often serve as the source of information on hadrons otherwise not directly accessible. A typical example is the extraction of the neutron structure function which is usually obtained from deuterium and proton data in a wide kinematic region. This procedure requires, in turn, a detailed knowledge of nuclear effects in order to control the corresponding systematic uncertainties. Another example is the definition of nuclear parton distribution functions (nPDFs) which allow to describe universal high-momentum transfer characteristics of complex nuclei.

Sizable nuclear effects were discovered in charged lepton DIS experiments [1, 2, 3, 4, 5, 6, 7, 8, 9, 10, 11, 12, 13]. These observations rule out a simple picture of a nucleus as a system of quasi-free nucleons and indicate that the nuclear environment plays an important role even at energies and momenta much larger than those involved in typical nuclear ground state processes. The study of nuclei is therefore directly related to the interpretation of high-energy physics from hadron colliders to fixed target experiments. The measurements of nucleus-nucleus and proton-nucleus interactions at RHIC [15] and LHC [16] will help to clarify the nuclear modifications of the parton distributions, as well as to define the initial conditions towards the studies of new states of matter in heavy ion collisions.

The understanding of nuclear effects is particularly relevant for neutrino physics, where the tiny cross-section with matter requires the use of heavy nuclear targets in order to collect a significant number of interactions. The presence of an axial-vector component in the weak current and the quark flavour selection differentiate neutrinos from charged leptons and imply a more complex description of nuclear effects in neutrino scattering. The role of nuclear corrections to neutrino structure functions has been recently emphasized [17] after the NuTeV collaboration reported a deviation from the Standard Model prediction for the value of the weak mixing angle ($\sin^2 \theta_W$) measured in neutrino DIS [18]. One of the original motivations of the present work is indeed related to the extraction of the weak mixing angle from neutrino DIS data of the NOMAD experiment [19]. It must be remarked that nuclear effects are important not only in the determination of electroweak parameters, but also for the understanding of neutrino masses and mixing. The recent high-intensity NuMI [20] and JPARC [21] neutrino facilities offer the possibility to perform a detailed study of nuclear effects in neutrino interactions on a relatively short time scale. The construction of a future neutrino factory [22] would then allow to reach the ultimate precision of the neutrino probe.

The main experimental information on nuclear effects is coming from charged-lepton scattering DIS experiments performed at CERN [2, 3, 4, 5, 6, 7, 8], SLAC [9, 10], FNAL [11, 12] and recently at JLab [13, 23]. The measurements usually refer to the ratio R_2 of the

structure function F_2 of two nuclei (usually a complex nucleus to deuterium). Additional data from the Drell-Yan reaction of protons off nuclear targets are also available [14]. From the studies of data on the ratio R_2 one can separate a few regions of characteristic nuclear effects: depletion of nuclear structure functions at small Bjorken x ($x < 0.05$) known as shadowing region; a small enhancement of nuclear structure functions for $0.1 < x < 0.3$ (antishadowing); depletion with a minimum around $x = 0.6 \div 0.7$ followed by a rise at large x (known as “EMC effect” after the name of the experiment which discovered it). It is interesting to note that a clear Q^2 dependence has been reported only in the shadowing region, while for $0.1 < x < 0.6$ R_2 is almost Q^2 independent. However, the data available on the Q^2 dependence of nuclear effects are still scarce. One of the main drawbacks of all existing data is the strong correlation between x and Q^2 resulting from the kinematics of fixed (stationary) target experiments. As a result, significant regions of the (x, Q^2) plane are still uncovered in DIS experiments.

There were quite a few studies of nuclear structure functions and many different theoretical models have been proposed to explain the basic features of data (for a detailed summary of the current understanding of nuclear corrections we refer to recent reviews and references cited therein [24, 25, 26, 27], see also discussion in Section IV). It should be remarked that most of the theoretical efforts were focused on specific physics phenomena which are used to describe the effects observed in a limited kinematical range of x and Q^2 . Such approach is important to derive some insights on the basic physics mechanisms. However, global studies of nuclear effects on structure functions in a wide kinematical region of x and Q^2 and for a wide range of nuclei are clearly needed. Such studies not only would help to understand the origin of observed effects but they will also allow to develop a model of nuclear structure functions and cross sections applicable in the analysis of existing data and in the interpretation of future experiments. The present work is an attempt to develop such a model.

Our main goal here is not to describe separate features of nuclear effects, but rather we want to perform a quantitative study of data on the basis of a sound theoretical framework linked to other branches of nuclear physics. In order to describe nuclear data over a wide kinematical regime we take into account a number of known effects including nuclear shadowing, nuclear pion excess, Fermi motion, nuclear binding and off-shell corrections to bound nucleon structure functions. It should be noted that if some effects, such as Fermi motion and nuclear binding, are well constrained by other studies or data, the remaining ones are less known. The main example is the off-shell correction which describes the modification of structure functions of bound nucleons in nuclear environment. We study this effect phenomenologically by parameterizing the off-shell correction to the nucleon structure function in terms of a few parameters which are fixed from statistical analysis of nuclear data, together with the corresponding uncertainties. It is worth to emphasize that these parameters are universal, *i.e.* common for all nuclei, since they are related to the nucleon structure. In a certain sense the off-shell correction can be considered as a new structure function which describes the response of the nucleon parton distributions to the variation of the nucleon invariant mass. Even if this structure function is not accessible for free proton and neutron, it can be probed in nuclear reactions.

It should be also emphasized that the contributions from different nuclear effects in different kinematical regions of x are correlated by sum rules. For example, the light-cone momentum sum rule links bound nucleon and pion contributions. We use this requirement in order to constrain mesonic contributions to nuclear structure functions. Another example is

the baryon number sum rule which links shadowing and off-shell corrections. In our approach the off-shell effect provides the mechanism of cancellation of a negative nuclear-shadowing contribution to the normalization of nuclear valence quark distributions.

After fixing the parameters of our model, we compute predictions for a number of applications. In particular, we discuss nuclear valence and sea quarks at high Q^2 and compute nuclear corrections to neutrino structure functions. These subjects will be treated more extensively in future publications.

The paper is organized as follows. In Section II we briefly summarize the DIS kinematics for electron (muon) and neutrino scattering and introduce notations used in this paper. Section III provides information on the nucleon structure functions and parton distributions necessary for our analysis. Section IV is devoted to the theoretical framework to treat different nuclear corrections in our studies. In particular, in Section IV A we examine the derivation of nuclear structure functions in the approximation of incoherent scattering off bound nucleons and nuclear pions (Section IV A 3). Off-shell effects in the structure functions and quark distributions are discussed in Section IV A 6. Coherent nuclear effects leading to nuclear shadowing and antishadowing are described in Section IV B. In Section V we discuss in detail the nuclear input which is used in our analysis (Sections V A to V C), the model of off-shell effects (Section V D) and effective scattering amplitude (Section V E). The analysis of data is described in Section V F and V G. In Section VI we present the results obtained from our fits to nuclear data. The Q^2 and A dependence of nuclear effects are discussed in Section VI C to VI D. In Section VII we apply our model to study nuclear parton distributions (Section VII A) and neutrino structure functions (Section VII B). In Appendix A we provide the details of integration over the phase-space in nuclear convolution and in Appendix B the multiple scattering coefficients are given.

II. KINEMATICS OF INELASTIC SCATTERING

A. Charged lepton scattering

Consider the scattering of a *charged lepton* (electron or muon) off a nucleon with the four-momentum $p = (E_p, \mathbf{p})$ and mass M . The scattering matrix element to leading order in the electromagnetic coupling constant $\alpha = e^2/4\pi \approx 1/137$ is determined by the standard one-photon exchange process. In inclusive scattering, the final hadronic state is not detected and the differential cross section can be written as (see, *e.g.*, [28])

$$d\sigma = \frac{\alpha^2}{Q^4} L^{\mu\nu} W_{\mu\nu} \frac{d^3k'}{(p \cdot k) E'}. \quad (1)$$

Here $k = (E, \mathbf{k})$ and $k' = (E', \mathbf{k}')$ are four-momenta of incoming and outgoing lepton, respectively, $q = k - k'$ is four-momentum transfer to the target, $Q^2 = -q^2$. The tensor $L_{\mu\nu}$ describes the lepton-photon interaction. If the polarization of the incoming and outgoing lepton is not detected, then the lepton tensor is

$$L_{\mu\nu} = 2 (k_\mu k'_\nu + k_\nu k'_\mu) - Q^2 g_{\mu\nu}. \quad (2)$$

The hadronic tensor $W_{\mu\nu}$ stands for the sum of hadronic matrix elements of the electromagnetic current J_μ over all final hadronic states

$$W_{\mu\nu} = \frac{1}{4\pi} \sum_n (2\pi)^4 \delta(p + q - p_n) \langle p | J_\mu(0) | n \rangle \langle n | J_\nu(0) | p \rangle. \quad (3)$$

We do not consider the polarization effects here and assume the averaging over the target polarization.

Since the lepton tensor is symmetric, only symmetric part of the hadronic tensor contributes to the cross section. Because of the conservation of electromagnetic current $q^\mu W_{\mu\nu} = 0$. This condition, supplemented by the requirements of time reversal invariance and parity conservation in electromagnetic interaction, suggests that the symmetric hadronic tensor has only 2 independent Lorentz structures (see, *e.g.*, [28])

$$W_{\mu\nu}(p, q) = -\tilde{g}_{\mu\nu} F_1 + \tilde{p}_\mu \tilde{p}_\nu \frac{F_2}{p \cdot q}, \quad (4)$$

where $F_{1,2}$ are Lorentz-invariant structure functions, and, for simplicity, we use the following notations:

$$\tilde{g}_{\mu\nu} = g_{\mu\nu} - \frac{q_\mu q_\nu}{q^2}, \quad (5a)$$

$$\tilde{p}_\mu = p_\mu - q_\mu \frac{p \cdot q}{q^2}. \quad (5b)$$

We use the normalization of states $\langle p|p' \rangle = 2E_p(2\pi)^3 \delta(\mathbf{p} - \mathbf{p}')$ for both bosons and fermions. With this normalization the hadronic tensor and the structure functions $F_{1,2}$ are dimensionless.

The structure functions are the functions of two independent invariant variables. In deep inelastic regime the Bjorken variable $x = Q^2/(2p \cdot q)$ and four-momentum transfer squared Q^2 are usually used as the variables the structure functions depend on.

The polarization averaged differential cross section is determined by the structure functions $F_{1,2}$. In terms of the variables x and Q^2 the cross section reads

$$\frac{d^2\sigma}{dx dQ^2} = \frac{4\pi\alpha^2}{xQ^4} \left[\left(1 - y - \frac{(Mxy)^2}{Q^2} \right) F_2 + xy^2 \left(1 - \frac{2m_l^2}{Q^2} \right) F_1 \right], \quad (6)$$

where $y = p \cdot q / p \cdot k$. The variable y is not independent variable and related to x and Q^2 via the equation $xy = Q^2/(2p \cdot k)$. We keep the lepton mass term in Eq.(6) for the sake of completeness. Although it is negligible in electron deep inelastic scattering, it might be relevant for muon scattering at small momentum transfer or for τ lepton scattering.

The structure functions $F_{1,2}$ can be related to the virtual photon helicity cross sections by projecting Eq.(3) onto the states with definite photon polarizations. These states are described by the photon polation vectors. In the reference frame, in which the momentum transfer is along the z -axis, $q = (q_0, \mathbf{0}_\perp, q_z)$, $q_z = -|\mathbf{q}|$ the photon polarization vectors are

$$e_\pm = (0, 1, \pm i, 0)/\sqrt{2}, \quad (7a)$$

$$e_0 = (q_z, \mathbf{0}_\perp, q_0)/Q. \quad (7b)$$

where $Q = \sqrt{Q^2}$. The polarization vectors e_+ and e_- describe two transversely polarized states with helicities $+1$ and -1 . The vector e_0 corresponds to the longitudinally polarized (scalar) virtual photons. The polarization vectors are orthogonal to momentum transfer, $e_\pm \cdot q = e_0 \cdot q = 0$, and obey the orthogonality and normalization conditions, $e_\pm \cdot e_L = 0$, $e_\pm^* \cdot e_\pm = -1$, $e_0^2 = 1$.

The helicity structure functions are

$$W_{\pm} = e_{\pm}^{\mu*} W_{\mu\nu} e_{\pm}^{\nu} = F_1, \quad (8a)$$

$$W_0 = e_0^{\mu*} W_{\mu\nu} e_0^{\nu} = \gamma^2 F_2 / (2x) - F_1, \quad (8b)$$

where $\gamma = |\mathbf{q}|/q_0 = (1 + 4x^2 M^2/Q^2)^{1/2}$. Instead of Eq.(8), it is more convenient to use the transverse and the longitudinal structure functions defined as

$$F_T = x(W_+ + W_-) = 2xF_1, \quad (9a)$$

$$F_L = 2xW_0 = \gamma^2 F_2 - 2xF_1. \quad (9b)$$

B. Neutrino scattering

Let us first consider the *charged-current* (CC) induced neutrino (antineutrino) scattering. In the Standard Model the charged current is

$$J_{\lambda}^{\pm} = V_{\lambda}^{\pm} - A_{\lambda}^{\pm}, \quad (10)$$

with $V_{\lambda}^{\pm} = V_{\lambda}^1 \pm iV_{\lambda}^2$ and $A_{\lambda}^{\pm} = A_{\lambda}^1 \pm iA_{\lambda}^2$ the charged components of the vector and the axial-vector currents.

The differential cross section of the CC neutrino inclusive scattering is

$$d\sigma_{\text{CC}}^{(\nu, \bar{\nu})} = \frac{2\pi G_F^2 / (4\pi)^3}{(1 + Q^2/M_W^2)^2} L_{\mu\lambda}^{(\nu, \bar{\nu})} W_{\mu\lambda}^{\pm} \frac{d^3 k'}{(p \cdot k) E'}, \quad (11)$$

where the tensors $L_{\mu\lambda}^{(\nu)}$ and $W_{\mu\lambda}^+$ describe interaction of W boson with leptons and hadrons for neutrino scattering, $L_{\mu\lambda}^{(\bar{\nu})}$ and $W_{\mu\lambda}^-$ are the corresponding quantities for antineutrino scattering. If the polarization of outgoing lepton is not detected, then the neutrino and antineutrino tensors are

$$\begin{aligned} L_{\mu\lambda}^{(\nu)} &= 2 \text{Tr} [(1 - \gamma_5) \not{k} \gamma_{\mu} \not{k}' \gamma_{\lambda}] \\ &= 8 (k_{\mu} k'_{\lambda} + k_{\lambda} k'_{\mu} - k \cdot k' g_{\mu\lambda} + i\varepsilon_{\mu\lambda}(k, k')), \end{aligned} \quad (12a)$$

$$L_{\mu\lambda}^{(\bar{\nu})} = L_{\lambda\mu}^{(\nu)} \quad (12b)$$

where we denote $\varepsilon_{\mu\lambda}(a, b) = \varepsilon_{\mu\lambda\alpha\beta} a^{\alpha} b^{\beta}$. The hadronic tensor is

$$W_{\mu\lambda}^{\pm} = \frac{1}{4\pi} \int d^4 z \exp(iq \cdot z) \langle p | [J_{\mu}^{\mp}(z), J_{\lambda}^{\pm}(0)] | p \rangle. \quad (13)$$

For the scattering from unpolarized target there are five independent structure functions in the hadronic tensor (13) (see, *e.g.*, [28])

$$\begin{aligned} W_{\mu\lambda}^{\pm} &= -\tilde{g}_{\mu\lambda} F_1^{W\pm} + L_{\mu} L_{\lambda} \frac{F_2^{W\pm}}{p \cdot q} + i\varepsilon_{\mu\lambda}(p, q) \frac{F_3^{W\pm}}{2p \cdot q} \\ &\quad + \frac{q_{\mu} q_{\lambda}}{Q^2} F_4^{W\pm} + \frac{q_{\mu} p_{\lambda} + q_{\lambda} p_{\mu}}{p \cdot q} F_5^{W\pm}. \end{aligned} \quad (14)$$

The first two terms with F_1 and F_2 in Eq.(14) are similar to those in charged-lepton scattering and appear due to VV and AA transitions in Eq.(13). The term with F_3 describes parity-violating VA and AV transitions. The terms F_4 and F_5 are present because the weak current does not conserve.

Contracting the leptonic and hadronic tensors we obtain the explicit form of the differential cross section in terms of the structure functions. Using the usual variables x and y we have

$$\frac{d^2\sigma_{\text{CC}}^{(\nu,\bar{\nu})}}{dx dy} = \frac{G_F^2 ME/\pi}{(1 + Q^2/M_W^2)^2} \sum_{i=1}^5 Y_i F_i^{W^\pm}, \quad (15)$$

where the signs $+$ and $-$ refer to the neutrino and antineutrino scattering, respectively. The kinematical factors Y_i read as follows

$$Y_1 = y^2 x \frac{Q'^2}{Q^2} \left(1 - \frac{m'^2}{2Q^2}\right), \quad (16a)$$

$$Y_2 = \left(1 - \frac{yQ'^2}{2Q^2}\right)^2 - \frac{y^2 Q'^2}{4Q^2} \left(1 + \frac{p^2 Q^2}{(p \cdot q)^2}\right), \quad (16b)$$

$$Y_3 = \pm xy \left(1 - \frac{yQ'^2}{2Q^2}\right), \quad (16c)$$

$$Y_4 = \frac{yQ'^2}{4Q^2} \frac{m'^2}{p \cdot k}, \quad (16d)$$

$$Y_5 = -\frac{m'^2}{p \cdot k}. \quad (16e)$$

Here m' is the mass of outgoing charged lepton and $Q'^2 = Q^2 + m'^2$. We keep the lepton mass terms for the completeness. Even though these terms are tiny in ν_e and ν_μ scattering, they are not negligible in ν_τ scattering.

The contributions from the structure functions F_4 and F_5 to the neutrino production cross-section are suppressed by a small ratio $m'^2/(ME)$. It was also shown that $F_4 = 0$ and $2xF_5 = F_2$ in the leading order and in the limit of massless quarks (Albright–Jarlskog relations [29]). Recently it was argued that the second of these relations survives the higher order and the target mass corrections in massless QCD, while the relation for F_4 should be replaced by $F_4 = F_2/(2x) - F_1$ [30].

We now discuss kinematics of the *neutral current* (NC) induced neutrino scattering. In the standard model, the neutral current is the superposition of the isovector weak left current and electromagnetic current:

$$J_\mu^0 = \sqrt{2} (V_\mu^3 - A_\mu^3 - 2 \sin^2 \theta_W J_\mu^{\text{em}}), \quad (17)$$

where θ_W is the Weinberg weak mixing angle.

The NC hadronic tensor is given by Eq.(13), in which the charged current must be replaced by the neutral current. The leptonic tensor is determined by Eq.(12) with the overall factor $1/2$, reflecting the fact that neutrino can only be left-polarized (and antineutrino, right-polarized). As a result, the NC cross section has the overall factor $1/2$ compared to Eq.(15)

$$\frac{d^2\sigma_{\text{CC}}^{(\nu,\bar{\nu})}}{dx dy} = \frac{G_F^2 ME/(2\pi)}{(1 + Q^2/M_Z^2)^2} \sum_{i=1}^5 Y_i F_i^Z, \quad (18)$$

The kinematical factors Y_i in Eq.(18) are obtained from Eqs.(16) by taking the limit $m' \rightarrow 0$. Therefore the structure functions $F_{4,5}$ do not contribute to the NC cross section. We also comment that, since neutrino and antineutrino in NC scattering couple to the same hadronic NC, the neutrino and antineutrino NC structure functions are identical.

The relations between the helicity structure functions and the structure functions $F_{1,2,3}$ in the neutrino scattering are

$$W_{\pm} = F_1 \pm \gamma F_3, \quad (19a)$$

$$W_0 = \gamma^2 F_2 / (2x) - F_1. \quad (19b)$$

The definition of $F_{T,L}$ by Eq.(9) also apply in this case. We observe from (19) that the structure function F_3 determines the left-right asymmetry in the transverse helicity structure functions.

III. NUCLEON STRUCTURE FUNCTIONS

The structure functions remain important observables to probe QCD structure of proton and neutron and nuclei. In this section we briefly review the characteristics of nucleon structure functions necessary for our analysis.

A. QCD perturbative regime

In the region of Q^2 large compared to the nucleon scale the structure functions can be analyzed in perturbative QCD. A working tool of this analysis is the operator product expansion (OPE) [31]. Using the OPE, the contributions from different quark-gluon operators to hadronic tensors (3) and (13) can be ordered according to their *twist*. For the DIS structure functions this leads to the expansion in inverse powers of Q^2 :

$$F_a(x, Q^2) = F_a^{LT}(x, Q^2) + \frac{H_a(x, Q^2)}{Q^2} + \mathcal{O}(1/Q^4), \quad (20)$$

where a labels the type of the structure function ($a = T, 2, 3$). The first term is the leading twist (LT) contribution and H_a are the twist-4 contributions (higher twist, HT).

The LT contribution is directly related to the distributions of quarks and gluons inside the nucleon, the parton distribution functions (PDFs) (for more detail see, e.g., Ref.[32]). The HT components involve interactions between quarks and gluons and lack simple probabilistic interpretation. In what follows we briefly review the LT contribution to the structure functions, target mass correction effects, and sketch on the phenomenological studies of PDFs and HT, which will be used in our approach.

1. Leading Twist

The LT part of the structure functions is related to the PDFs via the DIS factorization theorem (see, e.g., Ref.[32] and references therein)

$$F_a^{LT}(x, Q^2) = \sum_{i=q,\bar{q},g} \int_x^1 \frac{dz}{z} C_a^i(z, \alpha_s(Q^2)) p_i(x/z, Q^2). \quad (21)$$

where $p_i(x, Q^2)$ denote the distribution of partons of the type i (PDF), the sum is taken over the different types quarks and antiquarks. The coefficients functions C_a^i depend on the process and the type of the structure function a but are independent of the target. These functions are computable as power series in α_s . The parton distributions are independent of the process but do depend on the target.

The PDFs have non-perturbative origin and cannot be calculated in perturbative QCD. However, the Q^2 dependence of the PDFs can be handled using QCD perturbation theory, and is governed by the well-known DGLAP evolution equations [33]:

$$Q^2 \frac{\partial p_i(x, Q^2)}{\partial Q^2} = \sum_{j=q,\bar{q},g} \int_x^1 \frac{dz}{z} P_{ij}(z, \alpha_s(Q^2)) p_j(x/z, Q^2), \quad (22)$$

where P_{ij} are the splitting functions. The splitting functions describe the interaction between different partons at a large scale Q^2 and, similar to the coefficient functions, are computable as power series in α_s .¹

The one-loop (NLO) coefficient and splitting functions have been computed since long time [34]. The two-loop (NNLO) coefficient functions [35] and the corresponding splitting functions [36] are now also available. For all the calculations described in this paper we use both the coefficient function and the PDFs to NNLO approximation in order to calculate LT structure functions.

2. Target Mass Corrections

It must be commented that the twist expansion is derived in the massless target limit. If a finite mass for the nucleon target is considered, new terms arise in Eq.(20) that mix operators of different spin, leading to additional power terms of kinematical origin – the so-called target mass corrections (TMC). In the approximation that $x^2 M^2/Q^2$ is small, the TMC series can be absorbed in the leading twist term [37]. Therefore, Eq.(20) remains valid with the LT terms replaced by

$$F_T^{\text{TMC}}(x, Q^2) = \frac{x^2}{\xi^2 \gamma} F_T^{\text{LT}}(\xi, Q^2) + \frac{2x^3 M^2}{Q^2 \gamma^2} \int_\xi^1 \frac{dz}{z^2} F_2^{\text{LT}}(z, Q^2), \quad (23a)$$

$$F_2^{\text{TMC}}(x, Q^2) = \frac{x^2}{\xi^2 \gamma^3} F_2^{\text{LT}}(\xi, Q^2) + \frac{6x^3 M^2}{Q^2 \gamma^4} \int_\xi^1 \frac{dz}{z^2} F_2^{\text{LT}}(z, Q^2), \quad (23b)$$

$$xF_3^{\text{TMC}}(x, Q^2) = \frac{x^2}{\xi^2 \gamma^2} \xi F_3^{\text{LT}}(\xi, Q^2) + \frac{2x^3 M^2}{Q^2 \gamma^3} \int_\xi^1 \frac{dz}{z^2} z F_3^{\text{LT}}(z, Q^2), \quad (23c)$$

where $\gamma = (1 + 4x^2 M^2/Q^2)^{1/2}$ and $\xi = 2x/(1 + \gamma)$ is the Nachtmann variable [38].

However, it must be remarked that the derivation of [37] was given in the zeroth order in α_s , assuming that the target quarks are on-shell and neglecting the transverse degrees of freedom. Both, higher order α_s corrections and quark off-shell effects modify Eqs.(23). Furthermore, Eqs.(23) suffer the so called threshold problem. Indeed, it follows from Eqs.(23)

¹ We note also that both Eq.(21) and Eq.(22) are presented for the factorization and the renormalization scales set to Q^2 .

that the target mass corrected inelastic structure functions F_2^{TMC} remain finite as $x \rightarrow 1$ even if the LT terms vanish in this limit. Clearly, the region x close to 1 is beyond the applicability of Eqs.(23). However, in the applications to nuclear structure functions at large x it is important to meet the threshold condition. One possible way to deal with this problem is to expand Eqs.(23) in power series in Q^{-2} and keep a finite number of terms. In particular, keeping the LT and the $1/Q^2$ term we have

$$F_T^{\text{TMC}}(x, Q^2) = F_T^{\text{LT}}(x, Q^2) + \frac{x^3 M^2}{Q^2} \left(2 \int_x^1 \frac{dz}{z^2} F_2^{\text{LT}}(z, Q^2) - \frac{\partial}{\partial x} F_T^{\text{LT}}(x, Q^2) \right), \quad (24a)$$

$$F_2^{\text{TMC}}(x, Q^2) = \left(1 - \frac{4x^2 M^2}{Q^2} \right) F_2^{\text{LT}}(x, Q^2) + \frac{x^3 M^2}{Q^2} \left(6 \int_x^1 \frac{dz}{z^2} F_2^{\text{LT}}(z, Q^2) - \frac{\partial}{\partial x} F_2^{\text{LT}}(x, Q^2) \right), \quad (24b)$$

$$xF_3^{\text{TMC}}(x, Q^2) = \left(1 - \frac{2x^2 M^2}{Q^2} \right) xF_3^{\text{LT}}(x, Q^2) + \frac{x^3 M^2}{Q^2} \left(2 \int_x^1 \frac{dz}{z^2} z F_3^{\text{LT}}(z, Q^2) - \frac{\partial}{\partial x} xF_3^{\text{LT}}(x, Q^2) \right). \quad (24c)$$

In this approximation the structure functions have a correct threshold behavior and vanish in the limit of $x \rightarrow 1$, provided that the LT terms and their derivatives vanish in this limit.

The target mass corrections should also be applied to the HT terms in the higher order terms in the twist expansion (20). For this reason we do not consider $1/Q^4$ terms in the TMC formula, which are small in the considered kinematical range. We also note, that the target mass corrections for an off-shell target, *i.e.* when $p^2 \neq M^2$, should be treated as part of the nuclear effects and will be discussed in Sect. IV A 6.

B. Structure function phenomenology

The twist expansion and PDFs as universal, process-independent characteristics of the target are at the basis of extensive QCD phenomenology of high-energy processes. In phenomenological studies, the PDFs are extracted from QCD global fits. A number of such analyses are available [39, 40, 41]. In our studies of nuclear data described in Sect. V F to V D we use the results by Alekhin [39]² who provides the set of the nucleon PDFs obtained with coefficient and splitting functions calculated to the NNLO approximation. Furthermore, the HT terms and the PDF uncertainties have also been evaluated in [39].

It should be also remarked that the twist expansion and perturbative QCD apparently breaks down at low Q^2 . Furthermore, the conservation of electromagnetic current requires the structure function F_2 to vanish as Q^2 for $Q^2 \rightarrow 0$. The data seem to indicate the presence of a transition region between perturbative and non-perturbative regimes at Q^2 about 1 GeV². In our studies of nuclear effects in the structure functions some data points

² In our analysis we use PDFs obtained from new fits optimized in the low Q^2 region and including additional data with respect to [39]. This extraction of PDFs also takes into account the nuclear corrections to D data described in the present paper (Section V G). Results from the new fits will be reported elsewhere.

at small x are in the low- Q^2 region. In order to match low- Q and high- Q regions we apply spline interpolations for the structure functions which obeys the current conservation requirements.

IV. NUCLEAR STRUCTURE FUNCTIONS

In this Section we describe a theoretical framework which will be the basis of phenomenological studies of nuclear DIS data discussed in Sections V to VI.

The mechanisms of nuclear DIS appear to be different for small and large Bjorken x as viewed from the laboratory system. The physics scale for this separation comes from the comparison of a characteristic DIS time, which is also known as Ioffe length $L_I = 1/Mx$ (see, *e.g.*, Ref.[28]), and an average distance between bound nucleons in nuclei which is about 2 Fm. At large $x > 0.1$ the characteristic DIS time is smaller than average internucleon distance. This observation justifies the use of the incoherent approximation for the nuclear Compton amplitude in this region. Within this approximation the nuclear structure functions are treated as a convolution of the nucleon light-cone distribution in a nucleus and the nucleon structure functions. It was realized before the EMC effect that the nucleon momentum distribution (*Fermi motion*) is the major nuclear effect at large Bjorken x and provides the rise of the EMC ratio at very large $x > 0.7$ [43]. After the discovery of the EMC effect [1] a number of calculations was performed in different versions of the impulse approximation [44, 46, 48, 49, 50], *i.e.* assuming no medium modification of bound nucleon structure. It was clarified that *nuclear binding* correction explains a significant part of the observed dip at $x \sim 0.6$ (for a review of the EMC effect and more references see [25, 26, 27]).

Effects beyond the impulse approximation are important. It should be noted that because of binding, the nucleons do not carry all of the light-cone momentum of the nucleus and the momentum sum rule is violated in the impulse approximation. A natural way to correct this problem is to explicitly consider the pion contribution to the structure functions [54] which balances missing momentum. Several calculations of the *pion correction* to nuclear structure functions have been performed in different approaches and approximations [47, 55]. Although all calculations predict some enhancement at small x , the concrete predictions are model-dependent. In this paper we calculate nuclear pion correction following the approach of Ref.[47] in which the pion contribution was constrained using the equations of motion for interacting pion-nucleon system. By using the light-cone momentum balance equation we effectively constrain the contribution from all mesonic fields responsible for nuclear binding.

It should be also noted that bound nucleons are off-shell particles. *Off-shell effects* in nuclear DIS were discussed in a number of papers [45, 46, 48, 50, 51, 52]. The fact that the nucleon has spin 1/2 makes this problem technically more involved. In particular it was shown in [48, 49, 50, 51] that the off-shell nucleon generally has larger number of structure functions which depend on the nucleon off-shellness as an additional variable. This effect violate simple nuclear convolution model. However, if the nucleon virtuality is small (which seems to be the case for bound nucleons) the number of structure functions remains unchanged [48, 49, 50]. Nevertheless, the off-shell effect remains an important correction through which the modification of the internal structure of the bound nucleon in nuclear environment is assessed. It should be also emphasized that the off-shell effect provides the specific mechanism of balancing a negative contribution to the nuclear baryon number sum rule from nuclear shadowing effect (for details see Sections VIA and VIB). In Section IV A we discuss the derivation of the nuclear structure functions in the presence of off-shell effects

with the full consideration of the nucleon spin. The treatment of off-shell effect in the structure functions and parton distributions is discussed in more detail in Sections IV A 6 and V D.

In the small- x region the space-time picture of DIS is different. For $x \ll 0.1$ the characteristic DIS time is large on nuclear scale, the nuclear DIS becomes “stretched” in time and in the longitudinal direction. The process can be viewed as the intermediate boson first fluctuates into a quark pair which can form a complex configuration (hadronic or quark-gluon) and then scatters off the target. As an average time of life of such fluctuation is large compared to average distance between bound nucleons, the photon interaction with nuclear targets resembles hadronic properties [57, 59]. In particular, since the scattering amplitude is dominated by the Pomeron and almost imaginary, the double scattering correction to the DIS cross-section is negative leading to nuclear *shadowing* effect, similar to that in hadron scattering [56]. Nuclear shadowing in DIS was subject to intensive studies [61] (for a review of nuclear shadowing and more references see, *e.g.*, [24, 27]). In the present paper we treat nuclear shadowing effect in a semi-phenomenological approach by introducing phenomenological amplitude which describes interaction of hadronic component of the intermediate boson with the nucleon and consider the propagation of this state in nuclear environment using multiple scattering theory. Details are discussed in Sect. IV B.

Summarizing we write the nuclear structure functions as the sum of incoherent and coherent contributions

$$F_a^A = F_a^{p/A} + F_a^{n/A} + F_a^{\pi/A} + \delta F_a^A, \quad (25)$$

where $F_a^{p/A}$, $F_a^{n/A}$, $F_a^{\pi/A}$ denote the contributions to the structure function of type a from bound protons, neutrons, and nuclear pions, respectively. The last term in Eq.(25) is a correction due to nuclear coherent interaction. The exact meaning of all these terms will be explained in the following sections.

A. Incoherent scattering approximation

The DIS hadronic tensor is given by the imaginary part of the virtual photon Compton amplitude in the forward direction. In the incoherent scattering regime (large x) taking into account the nucleon spin the nuclear hadronic tensor can be written as (see also [47, 48, 49])

$$W_{\mu\nu}^A(P_A, q) = \sum_{\tau=p,n} \int [dp] \text{Tr} \left(\widehat{\mathcal{W}}_{\mu\nu}^\tau(p, q) \mathcal{A}^\tau(p; A) \right) \quad (26)$$

where the sum is taken over the bound protons and neutrons, Tr is taken in the nucleon Dirac space and the integration is performed over the nucleon four-momentum, $[dp] = d^4p/(2\pi)^4$. The quantity $\mathcal{A}^\tau(p; A)$ is the imaginary part of the proton ($\tau = p$) or the neutron ($\tau = n$) propagator in the nucleus

$$\mathcal{A}_{\alpha\beta}^\tau(p; A) = \int dt d^3\mathbf{r} e^{ip_0 t - i\mathbf{p}\cdot\mathbf{r}} \langle A | \bar{\Psi}_\beta^\tau(t, \mathbf{r}) \Psi_\alpha^\tau(0) | A \rangle, \quad (27)$$

with $\Psi_\alpha^\tau(t, \mathbf{r})$ the nucleon field operator and α and β the Dirac spinor indices. The quantity $\widehat{\mathcal{W}}_{\mu\nu}^\tau(p, q)$ is the off-shell nucleon electromagnetic tensor, which is the matrix in the Dirac space. On the mass shell $p^2 = M^2$, averaging $\widehat{\mathcal{W}}_{\mu\nu}^\tau(p, q)$ over the nucleon polarizations we

obtain the nucleon hadronic tensor (4)

$$W_{\mu\nu}^\tau(p, q) = \frac{1}{2} \text{Tr} \left[(\not{p} + M) \widehat{\mathcal{W}}_{\mu\nu}^\tau(p, q) \right]. \quad (28)$$

In off-shell region, the Lorentz tensor structure of $\widehat{\mathcal{W}}_{\mu\nu}$ is more involved than the corresponding structure of the on-shell nucleon tensor. In order to establish the tensor structure of $\widehat{\mathcal{W}}_{\mu\nu}$ we expand the latter in terms of a complete set of Dirac matrices $\{I, \gamma^\alpha, \sigma^{\alpha\beta}, \gamma^\alpha \gamma_5, \gamma_5\}$. The various coefficients in this expansion must be constructed from the vectors p and q , and from the symmetric tensor $g_{\alpha\beta}$ and the antisymmetric tensor $\epsilon_{\mu\nu\alpha\beta}$. We consider first the symmetric part of $\widehat{\mathcal{W}}_{\mu\nu}$ and keep only those terms which are even under time-reversal and parity transformations, since only such terms can contribute to $F_{1,2}$. Keeping only current-conserving terms we have 7 independent Lorentz–Dirac structures which can be written as [48, 51]

$$\begin{aligned} 2 \widehat{\mathcal{W}}_{\mu\nu}^{\text{sym}}(p, q) = & -\tilde{g}_{\mu\nu} \left(\frac{f_1^{(0)}}{M} + \frac{f_1^{(1)}}{M^2} \not{p} + \frac{f_1^{(2)}}{p \cdot q} \not{q} \right) \\ & + \frac{\tilde{p}_\mu \tilde{p}_\nu}{p \cdot q} \left(\frac{f_2^{(0)}}{M} + \frac{f_2^{(1)}}{M^2} \not{p} + \frac{f_2^{(2)}}{p \cdot q} \not{q} \right) + \frac{f_2^{(3)}}{p \cdot q} \tilde{p}_{\{\mu} \tilde{g}_{\nu\}} \gamma^\alpha, \end{aligned} \quad (29)$$

where $\tilde{g}_{\mu\nu}$ and \tilde{p}_μ are given by Eq.(5). The curly braces in the last term denote symmetrization over Lorentz indices, *i.e.* $a_{\{\mu} b_{\nu\}} = \frac{1}{2}(a_\mu b_\nu + a_\nu b_\mu)$. The coefficients $f_i^{(j)}$ are the dimensionless Lorentz-invariant functions of x , Q^2 , and the nucleon offshellness p^2 .

Similar analysis have also been carried out for the antisymmetric part of $\widehat{\mathcal{W}}_{\mu\nu}$ for the neutrino scattering. This term is described by the structure functions F_3 in Eq.(14). For off-shell nucleon the result can be written as [50]

$$2 \widehat{\mathcal{W}}_{\mu\nu}^{\text{asym}}(p, q) = i \epsilon_{\mu\nu\alpha\beta} q^\alpha \widehat{\mathcal{G}}^\beta / (2 p \cdot q), \quad (30a)$$

$$\widehat{\mathcal{G}}^\beta = \left(\frac{f_3^{(0)}}{M} + \frac{f_3^{(1)}}{M^2} \not{p} + \frac{f_3^{(2)}}{p \cdot q} \not{q} \right) p^\beta + f_3^{(3)} \gamma^\beta, \quad (30b)$$

where the coefficients $f_3^{(j)}$ are the dimensionless Lorentz-invariant functions of x , Q^2 , and the nucleon offshellness p^2 .

By substituting Eqs. (29) and (30) into Eq.(28) one observes that at $p^2 = M^2$ Eqs. (4) and (14) are recovered with the nucleon structure functions given by

$$F_1 = f_1^{(0)} + f_1^{(1)} + f_1^{(2)}, \quad (31a)$$

$$F_2 = f_2^{(0)} + f_2^{(1)} + f_2^{(2)} + f_2^{(3)}, \quad (31b)$$

$$F_3 = f_3^{(0)} + f_3^{(1)} + f_3^{(2)} + f_3^{(3)}. \quad (31c)$$

It should be noted that the Dirac equation is the basic reason of simplification of the Lorentz structure of the hadronic tensor of the on-shell nucleon.

One important observation which follows from the outlined analysis is that Eq.(26) does not factorize into completely separate nuclear and nucleon parts. The off-shell nucleon is described by 7 independent structure functions in the symmetric P -even hadronic tensor ($f_1^{(i)}$

and $f_2^{(i)}$). Four independent structure functions $f_3^{(i)}$ are required in order to parameterize P -odd antisymmetric part of the hadronic tensor. These functions depend on p^2 as an additional variable and weighted in Eq.(26) with generally different nuclear distributions.

Clearly, the fact that we have to deal with unknown functions not present for the on-shell nucleon introduces an uncertainty into the problem. However, in practice it may be quite sufficient to treat nuclei as nonrelativistic systems. In this limit the nuclear hadronic tensor considerably simplifies, as will be discussed in the next Section.

1. The limit of weak nuclear binding

Let us now discuss Eq.(26) in the limit of weak nuclear binding. We assume that the nucleus is a non-relativistic system with small characteristic momentum and energy of bound nucleons, $|\mathbf{p}| \ll M$, $|p_0 - M| \ll M$. The antinucleon degrees of freedom are neglected in this approximation. A nonrelativistic approximation to Eq.(26) is derived using the relation between the relativistic four-component nucleon field Ψ and the nonrelativistic two-component operator ψ (for simplicity we suppress the isospin index τ)

$$\Psi(\mathbf{p}, t) = e^{-iMt} \begin{pmatrix} (1 - \mathbf{p}^2/8M^2) \psi(\mathbf{p}, t) \\ (\boldsymbol{\sigma} \cdot \mathbf{p}/2M) \psi(\mathbf{p}, t) \end{pmatrix}, \quad (32)$$

where the nucleon operators are taken in a mixed (\mathbf{p}, t) representation. The renormalization operator $1 - \mathbf{p}^2/(8M^2)$ is introduced to provide a correct normalization of nonrelativistic nucleon field ψ , *i.e.* the operator $\psi^\dagger \psi$ is normalized to the nucleon number to order \mathbf{p}^2/M^2 .

In order to make the nonrelativistic reduction of Eq.(26), we separate the nucleon mass from the energy p_0 and write the four-momentum of the bound nucleon as $p = (M + \varepsilon, \mathbf{p})$. We then substitute Eq.(32) into Eq.(26), and then reduce the four-dimensional Dirac basis to the two-dimensional spin matrices. In this way we examine all Lorentz-Dirac structures in Eqs. (29) and (30) and keep the terms to order ε/M and \mathbf{p}^2/M^2 and drop higher order terms. The result can be summarized as follows:

$$\frac{1}{M_A} \text{Tr} \left(\mathcal{A}(p; A) \widehat{\mathcal{W}}_{\mu\nu}(p, q) \right) = \frac{1}{M + \varepsilon} \mathcal{P}(\varepsilon, \mathbf{p}) W_{\mu\nu}(p, q), \quad (33)$$

where M_A is the mass of a nucleus A ,

$$\mathcal{P}(\varepsilon, \mathbf{p}) = \int dt \exp(-i\varepsilon t) \langle A | \psi^\dagger(\mathbf{p}, t) \psi(\mathbf{p}, 0) | A \rangle / \langle A | A \rangle \quad (34)$$

is the nonrelativistic nuclear spectral function normalized to the number of nucleons in the corresponding isospin state

$$\int [dp] \mathcal{P}^{p,n}(\varepsilon, \mathbf{p}) = (Z, N). \quad (35)$$

Note that the factor M_A in the left side of (33) is absorbed in the normalization of nuclear states $\langle A | A \rangle$ in Eq.(34). The hadronic tensor $W_{\mu\nu}(p, q)$ in Eq.(33) is given by Eq.(4) with

the structure functions

$$F_1(x, Q^2, p^2) = f_1^{(0)} \left(1 + \frac{p^2 - M^2}{2M^2} \right) + f_1^{(1)} \frac{p^2}{M^2} + f_1^{(2)}, \quad (36a)$$

$$F_2(x, Q^2, p^2) = f_2^{(0)} \left(1 + \frac{p^2 - M^2}{2M^2} \right) + f_2^{(1)} \frac{p^2}{M^2} + f_2^{(2)} + f_2^{(3)}, \quad (36b)$$

$$F_3(x, Q^2, p^2) = f_3^{(0)} \left(1 + \frac{p^2 - M^2}{2M^2} \right) + f_3^{(1)} \frac{p^2}{M^2} + f_3^{(2)} + f_3^{(3)}. \quad (36c)$$

From Eq.(33) we obtain a nonrelativistic approximation to the nuclear hadronic tensor (26)

$$\frac{W_{\mu\nu}^A(P_A, q)}{M_A} = \sum_{\tau=p,n} \int \frac{[dp]}{M + \varepsilon} \mathcal{P}^\tau(\varepsilon, \mathbf{p}) W_{\mu\nu}^\tau(p, q), \quad (37)$$

which is a basic equation for further analysis of nuclear DIS.

A few comments are in order. It must be emphasized that the nonrelativistic limit is taken with respect to the nucleon momentum. In the derivation of Eq.(33) we keep terms to order \mathbf{p}^2/M^2 and ε/M and neglect the higher-order terms. Furthermore, Eq.(33) is valid for arbitrary momentum transfer q . In Eq.(33) the high-energy amplitude ($W_{\mu\nu}$) factorizes from the low-energy (\mathcal{P}) domain. We observe that the problem of “splitting” of structure functions in the off-shell region (i.e. the problem of additional nucleon structure functions) can be avoided in the vicinity of the mass shell for non-relativistic values of energy and momentum. In this region the off-shell hadronic tensor involves the same number of independent structure functions as the on-shell does. Equations (36) define analytical continuation of the nucleon structure functions to the off-shell region in the vicinity of the mass-shell. It is easy to see that Eqs.(36) reduce to Eqs.(31) at $p^2 = M^2$ thus assuring a correct on-shell limit of our analytic continuation of the structure functions.

We now extract the relations between the nuclear and the nucleon structure functions from Eq.(37). Nuclear structure functions are given by Eq.(4) with p replaced by P_A and x by $x_A = Q^2/(2M_A q_0)$. However, it is convenient to consider the nuclear structure functions as the functions of the variable $x = Q^2/(2M q_0)$ instead of the “natural” nuclear scaling variable x_A . We then define $F_{T,L}^A(x, Q^2) = F_{T,L}^A(x_A, Q^2)$ and $x F_3^A(x, Q^2) = x_A F_3^A(x_A, Q^2)$. In order to separate the structure functions we contract the both sides of Eq.(37) with the virtual photon polarization vectors (7) and consider the helicity structure functions. As a result we have

$$F_T^A(x, Q^2) = \sum_{\tau=p,n} \int [dp] \mathcal{P}^\tau(\varepsilon, \mathbf{p}) \left(1 + \frac{\gamma p_z}{M} \right) \left(F_T^\tau + \frac{2x'^2 \mathbf{p}_\perp^2}{Q^2} F_2^\tau \right), \quad (38a)$$

$$F_L^A(x, Q^2) = \sum_{\tau=p,n} \int [dp] \mathcal{P}^\tau(\varepsilon, \mathbf{p}) \left(1 + \frac{\gamma p_z}{M} \right) \left(F_L^\tau + \frac{4x'^2 \mathbf{p}_\perp^2}{Q^2} F_2^\tau \right) \quad (38b)$$

where in the integrand F_a^τ with $a = T, L, 2$ are the structure functions of bound proton ($\tau = p$) and neutron ($\tau = n$) with the four-momentum $p = (M + \varepsilon, \mathbf{p})$, \mathbf{p}_\perp is the transverse component of the nucleon momentum with respect to the momentum transfer. The off-shell nucleon structure functions depend on the Bjorken variable x' , momentum transfer square

Q^2 and the virtuality p^2 as additional variable

$$\begin{aligned} x' &= \frac{Q^2}{2p \cdot q} = \frac{x}{1 + (\varepsilon + \gamma p_z)/M}, \\ p^2 &= M^2 + 2M\varepsilon - \mathbf{p}^2. \end{aligned} \quad (39)$$

In Eq.(38) the off-shell transverse and longitudinal structure functions are given by equations similar to (9) with M^2 replaced by p^2 , *i.e.* $F_T = 2x'F_1$, $F_L = \gamma'^2 F_2 - F_T$ with $\gamma'^2 = 1 + 4x'^2 p^2/Q^2$. Using Eqs.(38) we have for the nuclear structure function F_2^A

$$\gamma^2 F_2^A(x, Q^2) = \sum_{\tau=p,n} \int [dp] \mathcal{P}^\tau(\varepsilon, \mathbf{p}) \left(1 + \frac{\gamma p_z}{M}\right) \left(\gamma'^2 + \frac{6x'^2 \mathbf{p}_\perp^2}{Q^2}\right) F_2^\tau. \quad (40)$$

The nuclear structure function F_3 can be extracted from the left-right asymmetry in the helicity amplitudes, Eq.(19). We have [50]

$$xF_3^A(x, Q^2) = \sum_{\tau=p,n} \int [dp] \mathcal{P}^\tau(\varepsilon, \mathbf{p}) \left(1 + \frac{p_z}{\gamma M}\right) x' F_3^\tau. \quad (41)$$

Equations (38) to (41) allow us to compute the structure functions of a generic nucleus as a convolution of nuclear spectral function, which describes the distribution of the bound nucleons over momentum and separation energy, with the bound proton and neutron structure functions.

We also comment that the transverse motion of the bound nucleon in the nuclear rest frame causes the mixture of different structure functions in Eqs. (38a) and (38b) to order Q^{-2} . For this reason the additional term proportional to $x'^2 \mathbf{p}_\perp^2 F_2/Q^2$ appears in Eq.(40).

2. Convolution representation

If Q^2 is high enough to neglect power terms in equations (38a) to (41) then these equations can be written as two-dimensional convolution. For example, for the structure function F_2 we have

$$F_2^A(x, Q^2) = \int_{y>x} dy dv [f_{p/A}(y, v) F_2^p(x/y, Q^2, v) + f_{n/A}(y, v) F_2^n(x/y, Q^2, v)], \quad (42)$$

where $f_{p/A}(y, v)$ and $f_{n/A}(y, v)$ are the proton and the neutron distributions over the fraction of light-cone momentum y and virtuality $v = p^2$. The proton (neutron) distribution function is given in terms of the proton (neutron) spectral function as follows [47, 48]

$$f(y, v) = \int [dp] \mathcal{P}(\varepsilon, \mathbf{p}) \left(1 + \frac{p_z}{M}\right) \delta\left(y - 1 - \frac{\varepsilon + p_z}{M}\right) \delta(v - p^2). \quad (43)$$

The distribution functions are normalized to the number of bound protons (neutrons), as clear from Eq.(35). Equations similar to (42) hold for other structure functions with the same nucleon distribution functions. If we further neglect off-shell effects in the structure functions, Eq.(42) reduces to the familiar one-dimensional convolution.

It is instructive to calculate the average nucleon light-cone momentum $\langle y \rangle_N$ per one nucleon. Using Eq.(43) we have

$$\langle y \rangle_N = 1 + \frac{\langle \varepsilon \rangle + \frac{2}{3} \langle T \rangle}{M}, \quad (44)$$

where $\langle \varepsilon \rangle$ and $\langle T \rangle$ are the average nucleon separation and kinetic energies. Because of binding effect we have $\langle y \rangle_N < 1$, *e.g.* for iron the calculations with realistic nuclear spectral function, which are discussed in more detail in Section V B, gives $\langle y \rangle_N = 0.966$. The missing nuclear light-cone momentum apparently should be carried by fields responsible for nuclear binding. In our approach the missing light-cone momentum is balanced by nuclear pion field. Note that this situation is similar to the balance of light-cone momentum in the nucleon in which about a half of the nucleon momentum is carried by gluons. However, in the case of nuclei the fraction of nuclear light-cone momentum carried by pions is much smaller because nuclei are weakly-bound systems. The pion contribution to nuclear hadronic tensor and structure functions is derived in Sect. IV A 3 and specific model of nuclear pion distribution is discussed in Sect. V C.

3. Pion contribution to nuclear structure functions

The lepton can scatter off virtual pions which are exchanged by bound nucleons. The pion correction to nuclear hadronic tensor can be written as follows (see, *e.g.*, [47])

$$W_{\mu\nu}^{\pi/A}(P_A, q) = \frac{1}{2} \int [dk] D_{\pi/A}(k) W_{\mu\nu}^{\pi}(k, q) \quad (45)$$

where $W_{\mu\nu}^{\pi}(k, q)$ is hadronic tensor of a pion with four-momentum k and the function $D_{\pi/A}$ describes the distribution of pions in a nucleus. The latter can be expressed in terms of the pion propagator in a nucleus as

$$D_{\pi/A}(k) = \int d^4x \exp(ik \cdot x) \langle A | \varphi(x) \varphi(0) | A \rangle, \quad (46)$$

where $\varphi = (\varphi_1, \varphi_2, \varphi_3)$ is the pion field operator. The π^0 state is described by real pseudoscalar field φ_3 , while the charged pion states are described by the complex pseudoscalar fields $(\varphi_1 \pm i\varphi_2)/\sqrt{2}$. The factor 1/2 in Eq.(45) is because of the chosen representation of the pion field operator in Eq.(46) in which particle and antiparticle are identical.

In the further discussion of pion effect it is convenient to consider the normalized pion distribution, *i.e.* independent of normalization of the target state. We define this as follows

$$\mathcal{D}_{\pi/A}(k) = \int dt \exp(ik_0 t) \langle A | \varphi^*(\mathbf{k}, t) \varphi(\mathbf{k}, 0) | A \rangle / \langle A | A \rangle, \quad (47)$$

$$\varphi(\mathbf{k}, t) = \int d^3\mathbf{r} \exp(i\mathbf{k} \cdot \mathbf{r}) \varphi(\mathbf{r}, t), \quad (48)$$

where $\varphi(\mathbf{k}, t)$ is the pion field operator in momentum representation. Using translational invariance it is easy to verify that $\mathcal{D}_{\pi/A}(k) = D_{\pi/A}(k)/(2M_A)$ in the nucleus rest frame.

In order to extract the pion contribution to nuclear structure functions we contract both sides of Eq.(45) with the photon polarization vectors. Assuming that the hadronic tensor for off-shell pions by Eq.(4) we obtain from Eq.(45)

$$F_T^{\pi/A}(x, Q^2) = \int [dk] \mathcal{D}_{\pi/A}(k) (k_0 + \gamma k_z) \left(F_T^\pi + \frac{2x'^2 \mathbf{k}_\perp^2}{Q^2} F_2^\pi \right), \quad (49a)$$

$$F_L^{\pi/A}(x, Q^2) = \int [dk] \mathcal{D}_{\pi/A}(k) (k_0 + \gamma k_z) \left(F_L^\pi + \frac{4x'^2 \mathbf{k}_\perp^2}{Q^2} F_2^\pi \right), \quad (49b)$$

$$\gamma^2 F_2^{\pi/A}(x, Q^2) = \int [dk] \mathcal{D}_{\pi/A}(k) (k_0 + \gamma k_z) \left(\gamma'^2 + \frac{6x'^2 \mathbf{k}_\perp^2}{Q^2} \right) F_2^\pi, \quad (49c)$$

$$xF_3^{\pi/A}(x, Q^2) = \int [dk] \mathcal{D}_{\pi/A}(k) (k_0 + k_z/\gamma) x' F_3^\pi, \quad (49d)$$

where $F_a^{\pi/A}$ denotes the pion correction to the nuclear structure function F_a^A . In the integrand F_a^π are the structure functions of virtual pion with four-momentum k , \mathbf{k}_\perp is transverse component of the pion momentum relative to the direction of momentum transfer and $x' = Q^2/(2k \cdot q)$ is the pion Bjorken variable. The pion structure functions in Eqs.(49) depend on x' , Q^2 and pion invariant mass $k^2 = k_0^2 - \mathbf{k}^2$ as an additional variable. The transverse and longitudinal structure functions are related to F_1 and F_2 as $F_T = 2x'F_1$, $F_L = \gamma'^2 F_2 - F_T$ with $\gamma'^2 = 1 + 4x'^2 k^2/Q^2$. The mixture of the structure functions F_T and F_L in Eqs.(49) is because of transverse motion of nuclear pions, similar to the corresponding effect in Eqs.(38) for bound nucleons.

At high Q^2 Eqs.(49) can be written in a convolution form. For example, pion correction to F_2 can be written as

$$F_2^{\pi/A}(x, Q^2) = \int_{x < y} dy dv f_{\pi/A}(y, v) F_2^\pi(x/y, Q^2, v), \quad (50)$$

$$f_{\pi/A}(y, v) = 2yM \int [dk] \mathcal{D}_{\pi/A}(k) \delta\left(y - \frac{k_0 + k_z}{M}\right) \delta(v - k^2), \quad (51)$$

Similar equations hold for other structure functions in Eqs.(49). If one neglects off-shell dependence of pion structure functions then Eq.(50) reduces to the standard one-dimensional convolution with the pion light-cone distribution which is given by Eq.(51) integrated over v . We note that the distribution function by Eq.(51) is antisymmetric function, $f_{\pi/A}(-y) = -f_{\pi/A}(y)$. This property allows us to derive the sum rules for the odd moments of the pion distribution function which will be discussed in more detail in Section V C.

4. Application to the deuteron

So far the discussion did not refer to particular nuclear target. In this section we apply the discussed formalism to the *deuteron*. The deuteron is an isoscalar bound state of the proton and the neutron. The residual nuclear system is, therefore, the proton or neutron and the spectral function is given in terms of the deuteron wave function $\Psi_D(\mathbf{p})$

$$\mathcal{P}^{p,n}(\varepsilon, \mathbf{p}) = 2\pi\delta\left(\varepsilon - \varepsilon_D + \frac{\mathbf{p}^2}{2M}\right) |\Psi_D(\mathbf{p})|^2, \quad (52)$$

where $\varepsilon_D = M_D - 2M$ and $\mathbf{p}^2/2M$ are the deuteron binding energy and the spectator nucleon recoil energy, respectively. The deuteron structure functions then become

$$F_T^D(x, Q^2) = \int \frac{d^3\mathbf{p}}{(2\pi)^3} |\Psi_D(\mathbf{p})|^2 \left(1 + \frac{\gamma p_z}{M}\right) \left(F_T^N + \frac{2x'^2 \mathbf{p}_\perp^2}{Q^2} F_2^N\right), \quad (53a)$$

$$F_L^D(x, Q^2) = \int \frac{d^3\mathbf{p}}{(2\pi)^3} |\Psi_D(\mathbf{p})|^2 \left(1 + \frac{\gamma p_z}{M}\right) \left(F_L^N + \frac{2x'^2 \mathbf{p}_\perp^2}{Q^2} F_2^N\right), \quad (53b)$$

$$\gamma^2 F_2^D(x, Q^2) = \int \frac{d^3\mathbf{p}}{(2\pi)^3} |\Psi_D(\mathbf{p})|^2 \left(1 + \frac{\gamma p_z}{M}\right) \left(\gamma'^2 + \frac{6x'^2 \mathbf{p}_\perp^2}{Q^2}\right) F_2^N, \quad (53c)$$

$$xF_3^D(x, Q^2) = \int \frac{d^3\mathbf{p}}{(2\pi)^3} |\Psi_D(\mathbf{p})|^2 \left(1 + \frac{p_z}{\gamma M}\right) x' F_3^N \quad (53d)$$

where $F_a^N = (F_a^p + F_a^n)/2$ with $a = T, 2, 3$ are the structure functions of the isoscalar nucleon. The variables of these structure functions are similar to those of Eqs.(38,40,41) and we do not write them explicitly.

5. Application to complex nuclei

Unlike the deuteron, the spectral function of complex nuclei does not reduce to the ground state wave function but includes, generally infinite, set of excited residual states. This can be seen directly from Eq.(34) by inserting the complete set of intermediate states. For simplicity we suppress the explicit notations for different isospin states and write

$$\mathcal{P}(\varepsilon, \mathbf{p}) = 2\pi \sum_n |\langle (A-1)_n, -\mathbf{p} | \psi(\mathbf{p}) | A \rangle|^2 \delta(\varepsilon + E_n^{A-1} + E_R - E_0^A). \quad (54)$$

Here the sum runs over the quantum numbers of the states of $A-1$ nucleons, which include the bound states as well as the continuum states, E_n^{A-1} and E_0^A are respectively the energy of the residual nucleus (in the recoil nucleus rest frame) and the ground state energy of the target nucleus. The residual system balances momentum of the removed nucleon and acquires the recoil energy $E_R = \mathbf{p}^2/2M_{A-1}$.

The integration of Eq.(54) over energy gives nucleon momentum distribution,

$$n(\mathbf{p}) = \int \frac{d\varepsilon}{2\pi} \mathcal{P}(\varepsilon, \mathbf{p}). \quad (55)$$

The nuclear spectral function determines the rate of nucleon removal reactions such as $(e, e'p)$ that makes it possible to extract the spectral function from experimental data.³ For low separation energies (for $|\varepsilon| < \varepsilon_F \sim 30 - 50$ MeV) the experimentally observed spectrum is similar to that predicted by the mean-field model [66]. In this model the nucleus is viewed

³ However, the direct connection between the cross sections and the spectral function holds only in the impulse approximation, and should be corrected by other effects such as final state interactions and meson exchange currents.

as Fermi gas of nucleons bound to self-consistent mean field potential [67]. The spectral function (54) can be readily calculated in this model

$$\mathcal{P}_{\text{MF}}(\varepsilon, \mathbf{p}) = 2\pi \sum_{\lambda < \lambda_F} n_\lambda |\phi_\lambda(\mathbf{p})|^2 \delta(\varepsilon - \varepsilon_\lambda + E_R), \quad (56)$$

where $\phi_\lambda(\mathbf{p})$ is the wave functions of the single-particle level with quantum numbers λ and n_λ is the number of nucleons on this level. The sum in Eq.(56) runs over the occupied single-particle levels with energies below the Fermi level λ_F .

Equation (56) gives a good approximation to nuclear spectral function in the vicinity of the Fermi level, where the excitation energies of the residual nucleus are small, as was established in nuclear $(e, e'p)$ reactions [66]. As excitation energy becomes higher, Eq.(56) becomes less accurate. Because of interaction effects the single-particle (hole) states are not the eigenstates of nuclear Hamiltonian. For this reason the energy δ -functions in Eq.(56) are smeared and acquire a width, as observed in nucleon removal experiments.

The fragmentation of deep-hole states is not the only interaction effect in the nuclear ground state. High-energy and high-momentum components of nuclear spectrum can not be described by the mean-field model and driven by correlation effects in nuclear ground state as witnessed by numerous studies (for a review see [68]). We denote the contribution to the spectral function which absorbs the correlation effects as $\mathcal{P}_{\text{cor}}(\varepsilon, \mathbf{p})$. The leading contribution to \mathcal{P}_{cor} comes from 2h1p states, i.e. for configurations of $A-1$ nucleons with one nucleon in continuum and remaining $A-2$ nucleons being in the state with low momentum and low excitation energy. The energy dependence of \mathcal{P}_{cor} is completely different from that of \mathcal{P}_{MF} . \mathcal{P}_{cor} has a widespread background extending to large values of p and $|\varepsilon|$. The maximum of \mathcal{P}_{cor} for the given p is at $\varepsilon \sim -p^2/2M$. The model spectral function which is used in this paper is discussed in Sect.VB.

Complex nuclei typically have different numbers of protons and neutrons and, in contrast to the deuteron case, the calculation of nuclear structure functions requires both the isoscalar and the isovector contributions. In order to take into account this effect we explicitly separate the isoscalar and isovector contributions to Eqs.(38,40,41). To this end we consider generic integrand in convolution formulas and write

$$\sum_{\tau=p,n} \mathcal{P}^\tau F_a^\tau = \mathcal{P}^{p+n} F_a^N + \frac{1}{2} \mathcal{P}^{p-n} F_a^{p-n}, \quad (57)$$

where we denote $\mathcal{P}^{p\pm n} = \mathcal{P}^p \pm \mathcal{P}^n$ and $F_a^N = \frac{1}{2}(F_a^p + F_a^n)$ and $F_a^{p-n} = F_a^p - F_a^n$ for the structure function of type a .

In an isoscalar nucleus with equal number of protons and neutrons Eq.(57) is dominated by the isoscalar contribution and one generally assumes $\mathcal{P}^{p-n} = 0$. However, it must be remarked that this equation is violated by a number of effects even in the isoscalar nucleus. The finite difference between the proton and neutron spectral functions is generated by the Coulomb interaction and isospin-dependent effects in the nucleon–nucleon interaction. The discussion of these effects goes beyond the scope of this paper and we leave them for future studies. Instead we focus on the neutron excess effect for heavy nuclei.

We write the isoscalar and isovector spectral functions in terms of reduced functions \mathcal{P}_0 and \mathcal{P}_1 as

$$\mathcal{P}^{p+n} = A\mathcal{P}_0, \quad (58a)$$

$$\mathcal{P}^{p-n} = (Z - N)\mathcal{P}_1. \quad (58b)$$

The functions \mathcal{P}_0 and \mathcal{P}_1 are normalized to unity as follows from Eq.(35). These spectral functions are quite different. The function \mathcal{P}_0 involves the averaging over all isoscalar intermediate states. The model spectral function which is used in this paper is described in Sect. VB. The function \mathcal{P}_1 probes the isovector component in a nucleus. We now discuss the term \mathcal{P}_1 in more detail and argue that its contribution is peaked about the Fermi surface. We assume that \mathcal{P}_{cor} is mainly isoscalar and cancels out in the $p - n$ difference. Then \mathcal{P}^{p-n} is determined by the difference of the corresponding mean-field contributions. If we further neglect small differences between the energy levels of protons and neutrons then the term \mathcal{P}^{p-n} is determined by the occupation numbers n_λ for protons and neutrons. Because of Pauli principle, an additional particle can be added to a Fermi system only on an unoccupied level. In a complex nucleus all but the Fermi level are usually occupied (the Fermi level has a large degeneracy factor). Therefore, the term \mathcal{P}_1 is determined by the contribution from the Fermi level

$$\mathcal{P}_1 = |\phi_F(\mathbf{p})|^2 \delta(\varepsilon - \varepsilon_F), \quad (59)$$

where ε_F and ϕ_F are the energy and the wave function of the Fermi level and we have neglected the recoil of the $A-1$ nucleus.⁴

We now make use the results of this Section in order to write Eqs.(38,40,41) in terms of \mathcal{P}_0 and \mathcal{P}_1 . Using Eqs. (57) and (58) we can write for each structure function $a = T, 2, 3$

$$F_a^A = A \langle F_a^N \rangle_0 + \frac{Z-N}{2} \langle F_a^{p-n} \rangle_1, \quad (60)$$

where the averaging $\langle F_a \rangle_{0,1}$ denotes the integration in Eqs.(38,40,41) with the reduced spectral functions \mathcal{P}_0 and \mathcal{P}_1 , respectively.

We conclude this section by commenting that data are sometimes naively corrected for the neutron excess effect neglecting Fermi motion and binding effects (as well as any other nuclear effects) in the isovector and the isoscalar distributions. As follows from the present discussion, the Fermi motion and binding effects are quite different in the isoscalar and the isovector distributions in heavy nuclei. If neglected, this effect may cause an additional systematic uncertainty in data and a distortion of final results.

6. Off-shell effects

The bound proton and neutron are off-mass-shell and their structure functions differ from those of the free proton and neutron. The off-shell nucleon structure functions depend on the nucleon virtuality p^2 as an additional variable. Therefore, the off-shell effects in the structure functions are closely related to the target mass corrections. Target mass effects in the off-shell nucleon can be of two different kinds. First, similarly to the on-shell nucleon, we have to take into account the kinematical target mass dependence due to the finite p^2/Q^2 ratio. We assume that this effect is described by Eqs.(23), where the nucleon mass squared is replaced by p^2 (this leads in turn to the modification of the parameter γ and the variable ξ in the off-shell region). Furthermore, the dependence on p^2 appears already at leading

⁴ It must be remarked that both the isospin-dependent correlation effects in the ground state and Coulomb field effects modify this simple relation. However, we leave the analysis of these effects for future studies and discuss in this paper the non-isoscalarity effect by Eq.(59).

twist (LT) at the PDF level as was argued in [46, 48, 50, 51]. Thus off-shell effects in the LT structure functions can be viewed as a measure of the nucleon's deformation inside the nuclear medium.

Since we treat nuclei as nonrelativistic systems it would be enough to consider the off-shell effect as a correction. We expand the LT structure functions in the vicinity of the mass shell in series in $p^2 - M^2$. Keeping only the linear term we have for F_2 ⁵

$$F_2^N(x; p^2) = F_2(x) \left(1 + \delta f_2(x) \frac{p^2 - M^2}{M^2} \right), \quad (61)$$

$$\delta f_2(x) = \frac{\partial \ln F_2(x; p^2)}{\partial \ln p^2}, \quad (62)$$

where the first term is the structure function of the on-mass-shell nucleon and the derivative is evaluated at $p^2 = M^2$. Similar expressions can be written for the other structure functions.

The function δf_2 can be written in terms of the corresponding off-shell functions for valence and sea-quark PDF in the nucleon. In order to find this relation we consider F_2 for he isoscalar nucleon at high Q^2 and write it in the leading order as

$$F_2 = \frac{5}{18} (x q_{\text{val}} + x q_{\text{sea}}), \quad (63)$$

where $q_{\text{val}} = u - \bar{u} + d - \bar{d}$ and $q_{\text{sea}} = 2(\bar{u} + \bar{d}) + \frac{2}{5}(s + \bar{s}) + \frac{8}{5}(c + \bar{c})$. We define the functions describing off-shell deformation of valence and sea quarks similar to δf_2

$$\delta f_{\text{val}}(x) = \frac{\partial \ln q_{\text{val}}(x; p^2)}{\partial \ln p^2}, \quad (64a)$$

$$\delta f_{\text{sea}}(x) = \frac{\partial \ln q_{\text{sea}}(x; p^2)}{\partial \ln p^2}. \quad (64b)$$

For simplicity we do not consider isospin dependence of off-shell effect and assume the function $\delta f_{\text{val}}(x)$ to be identical for u and d quarks. However, the off-shell deformations of the valence and sea quarks are generally different. Using Eq.(63) the function δf_2 can be expressed in terms of δf_{val} and δf_{sea}

$$\delta f_2 = \frac{\delta f_{\text{val}} + r(x) \delta f_{\text{sea}}}{1 + r(x)}, \quad (65)$$

where $r(x) = q_{\text{sea}}(x)/q_{\text{val}}(x)$. The off-shell deformation of the structure function F_3 in the leading order is given by the corresponding effect for valence quarks, $\delta f_3 = \delta f_{\text{val}}$. We observe from Eq.(65) that at large x , where $r \ll 1$ and the contribution from the sea can be neglected, the off-shell effects in F_2 and F_3 are similar and described by the function δf_{val} . On the other hand, at small x where the sea-quark distribution dominates over the valence one, the contribution due to δf_{val} to δf_2 is suppressed by a small valence/sea ratio.

Off-shell effects in nucleon structure functions were discussed in [48, 50] using the spectral

⁵ For simplicity we suppress the explicit notation of the Q^2 dependence of structure functions.

representation of the quark distributions

$$q_N(x; p^2) = \int ds \int_{t_{\min}}^{t_{\max}} dt D_{q/N}(s, t, x; p^2), \quad (66)$$

$$t_{\max} = x \left(p^2 - \frac{s}{1-x} \right), \quad (67)$$

where $q_N(x; p^2)$ is the quark distribution in the nucleon with four-momentum p . The integration in Eq.(66) is taken over the mass spectrum of spectator states s and the quark virtuality $t = k^2$ with the kinematical maximum t_{\max} for the given s and p^2 . The invariant spectral density $D_{q/N}$ measures the probability to find in a nucleon with momentum p , a quark with light-cone momentum x and virtuality t and the remnant system in a state with invariant mass s .

One observes from Eq.(66) that the p^2 dependence of quark distributions has two sources: the one in the upper limit of t integration (kinematical off-shell dependence), and an explicit p^2 dependence of the quark spectral function $D_{q/N}$ (dynamical off-shell dependence).

The kinematical off-shell effect causes a negative correction to the bound nucleon structure functions that results in an enhanced EMC effect, as first noticed in [46, 48]. However, if only the kinematical off-shell effects are taken into account the number of valence quarks in the nucleon would change with p^2 . It can be seen directly from Eq.(66) that the normalization of the quark distribution decreases as p^2 decreases, provided that the spectral density is positively defined. This observation indicates that off-shell effect of dynamical origin must also be present. A method to estimate the dynamical off-shell effects minimizing the model dependence was suggested in [48], in which the conservation of the valence quark number in off-shell nucleon was used as a constraint

$$\frac{d}{dp^2} \int_0^1 dx q_{\text{val}}(x; p^2) = 0. \quad (68)$$

A partial cancellation between the kinematical and dynamical off-shell effects was found in [48, 50]. However, the off-shell effect in the structure functions remains an important correction. In this paper we treat the function δf_2 phenomenologically and fix it from the studies of nuclear data as discussed in more detail in Section V.

B. Coherent nuclear effects

Nuclear shadowing effect was extensively discussed in the literature. A recent paper [24] provides a review of both data and theoretical models of nuclear shadowing.

It appears to be a common wisdom that nuclear shadowing is a result of coherent interaction of hadronic component of virtual photon with target nucleus. The structure functions at small x can be presented as a superposition of contributions from different hadronic states. We consider the helicity structure functions W_0 and W_{\pm} , as defined in Eq.(8), that will allow us to discuss nuclear effects in charged-lepton and neutrino interactions on the same ground. We have

$$W_a = \sum_v w_v \sigma_a^v(s), \quad (69)$$

where $\sigma_a^v(s)$ is the total cross section of scattering of the hadronic state v with the given helicity $a = 0, \pm 1$ off the target nucleon (or nucleus) with the center-of-mass energy $s = Q^2(1/x-1) + M^2$ and the quantities w_v describe the weight of different hadronic states.

At low Q^2 the vector meson dominance model (VMD) appears to be a good tool to evaluate nuclear corrections in structure functions [59]. In VMD the structure functions are saturated by contributions from a few vector meson states, σ^v are the meson cross sections. The mesonic cross sections are approximately constant at high energy and have similar magnitude for different mesons with lowest masses (ρ , ω , A_1). The weights for the electromagnetic current are $w_v = Q^2/(\pi f_v^2)(1 + Q^2/m_v^2)^{-2}$ with f_v the photon-meson coupling constants and m_v the vector meson mass. Usually only the lowest mass vector mesons (ρ^0 , ω , ϕ) are important at low $Q^2 < 1 \text{ GeV}^2$. The structure functions in this model have strong Q^2 dependence.⁶ In the generalized versions of VMD, the higher-mass states including continuum have also been considered that made it possible to apply the model at higher Q^2 .

In this paper we approximate the sum over hadronic states in Eq.(69) by a factorized form

$$W_a(x, Q^2) = w_a(x, Q^2)\bar{\sigma}_a(s), \quad (70)$$

where $\bar{\sigma}_a$ is an effective cross section averaged over hadronic configurations and w_a is remaining normalization factor. At low Q^2 the quantity $\bar{\sigma}_a$ corresponds to the average over a few vector meson states. As Q^2 increases, the averaging in (70) involves the rising number of hadronic configurations. Since the relative weight of higher-mass states increases with Q^2 and the cross section decreases with the mass, one can qualitatively conclude that $\bar{\sigma}$ should decrease with Q^2 . In the approach adopted in this paper we will treat $\bar{\sigma}$ phenomenologically.

In this paper we are concerned with the relative effect of nuclear interactions

$$\delta R_a^{A/N}(x, Q^2) = \frac{\delta W_a^A(x, Q^2)}{W_a^N(x, Q^2)}, \quad (71)$$

where δW_a^A is the nuclear structure function of helicity a subtracted incoherent contribution (cf. Eq.(25)). From Eq.(70) we conclude that the relative nuclear effect on the structure functions equals the corresponding effect for the effective cross sections

$$\delta R_a^{A/N} = \delta \bar{\sigma}_a^A / \bar{\sigma}_a^N, \quad (72)$$

where $\delta \bar{\sigma}^A$, similar to δW^A , is the nuclear cross section subtracted incoherent contribution. The problem of calculation of nuclear corrections to structure functions thus reduces to the calculation of multiple scattering effects in hadronic cross sections.

1. Application to deuteron

We now consider this effect in application to the deuteron. In order to calculate the shadowing correction we consider hadron elastic scattering amplitude $f(s, k)$ with s the center-of-mass energy and k the momentum transfer. We chose the normalization of the amplitude such that the optical theorem reads $\text{Im} f(s, 0) = \sigma(s)/2$ and parametrize the

⁶ Note that the VMD contribution is formally a higher twist because of strong Q^2 dependence of the weights.

scattering amplitude as $f = (i + \alpha)\sigma/2$, where $\alpha = \text{Re } f / \text{Im } f$. The hadron-deuteron scattering amplitude in forward direction can be written as follows [56]

$$f^D = f^p + f^n + \delta f^D, \quad (73)$$

$$\delta f^D = i f^p f^n \mathcal{C}_2^D, \quad (74)$$

where f^p and f^n are the scattering amplitudes off the proton and the neutron and δf^D the double scattering correction. \mathcal{C}_2^D can be written in terms of the deuteron wave function as

$$\mathcal{C}_2^D = \frac{1}{(2\pi)^2} \int d^2 \mathbf{k}_\perp S_D(\mathbf{k}_\perp, k_L) e^{-B \mathbf{k}_\perp^2}, \quad (75)$$

$$S_D(\mathbf{k}) = \int d^3 \mathbf{r} e^{i \mathbf{k} \cdot \mathbf{r}} |\Psi_D(\mathbf{r})|^2. \quad (76)$$

The dependence of the elastic scattering amplitudes on the momentum transfere was assumed to be exponential, hence the exponential factor in Eq.(75). Such dependence is confirmed experimentally and for low mass vector mesons the parameter B populates the region from 4 to 10 GeV^2 depending on Q^2 (see, *e.g.*, [59]).

Note that Eq.(73) is the scattering amplitude of an off-shell hadron with four-momentum q . For this reason there appears a finite longitudinal momentum transfere $k_L = Mx(1 + m^2/Q^2)$, which accounts for a finite longitudinal correlation length of a virtual hadron ($k_L = 0$ for the scattering of on-shell particles).

We apply Eqs. (72) and (73) in order to calculate coherent nuclear effects for different structure functions. It should be remarked that helicity conserves in multiple scattering interactions and the scattering matrix is diagonal in helicity basis. For this reason the multiple scattering corrections involve the amplitudes with the same helicity. We also assume that effective scattering amplitudes of the given helicity are equal for proton and neutron (but they, of course, depend on helicity). Let us first discuss the transverse structure function F_T . The relative shadowing correction to the transverse structure function is

$$\delta R_T^D(x, Q^2) = \sigma_T(\alpha_T^2 - 1)\mathcal{C}_2^D/2, \quad (77)$$

where σ_T and α_T are parameters of effective scattering amplitude of transversaly polarized virtual photon. A model for effective scattering amplitude is discussed in Section V E.

We now use Eq.(73) in order to find relation between shadowing corrections for the longitudinal and transverse structure functions. It follows from Eq.(70) that the ratio $R = F_L/F_T$ equals the corresponding ratio of the effective cross sections σ_L/σ_T provided that the normalization factor $w(x, Q^2)$ is independent of helicity. This holds in the VMD for low-lying meson resonances and we also assume that this is approximately true for the contribution from higher-mass states. Thus using Eq.(77) we find that the relative shadowing corrections for longitudinal and transverse structure functions is simply determined by R

$$\frac{\delta R_L^D(x, Q^2)}{\delta R_T^D(x, Q^2)} = R(x, Q^2), \quad (78)$$

where $R(x, Q^2)$ is calculated for the nucleon.⁷

⁷ We neglect the contribution from the real part of the scattering amplitude in ratio (78). In particular we assume $(\alpha_L^2 - 1)/(\alpha_T^2 - 1) \approx 1$.

Using Eqs. (77) and (78) we can compute the nuclear shadowing effect for the structure function F_2 in terms of the corresponding correction to F_T . Indeed, recalling Eqs.(9) we have

$$\delta R_2^D = \frac{\delta R_T^D + R\delta R_L^D}{1 + R}. \quad (79)$$

Taking into account (78) we find the factor $(1 + R^2)/(1 + R)$ difference between shadowing effect for F_2 and F_T .

We now discuss the shadowing effect for the structure function $x F_3$. This structure function is given by the left-right asymmetry in helicity structure functions $W_+ - W_-$. Therefore, in this case the problem reduces to computing the multiple scattering effect for the difference of the corresponding scattering amplitudes. We denote $f_3 = f_+ - f_-$. The non-zero difference f_3 is generated because of vector-axial vector current transitions in the hadronic tensor. The double scattering correction to f_3 can readily be derived from Eq.(73)

$$\delta f_3^D = 2i f_3 f_T \mathcal{C}_2^D, \quad (80)$$

where we denote $f_T = (f_+ + f_-)/2$. It follows from Eq.(80) that the relative shadowing effect for the cross-section asymmetry is determined by the cross-section σ_T . Using Eqs. (73) and (80) we find

$$\frac{\delta R_3^D}{\delta R_T^D} = 2 \frac{1 - \alpha_3 \alpha_T}{1 - \alpha_T^2}. \quad (81)$$

We observe from this equation that the shadowing effect is enhanced for the cross section asymmetry by the factor of 2 with respect to the shadowing effect for the cross section σ_T if we neglect the effect of real part of the amplitudes [62]. To clarify the origin of this enhancement we consider a somewhat simplified VMD model with the single vector meson (ρ meson) and the axial-vector meson (a_1 meson). In this model the structure functions F_L and F_T are determined by the diagonal vector-vector and axial vector-axial vector transitions $VN \rightarrow VN$ and $AN \rightarrow AN$, while the structure function F_3 is driven by the off-diagonal transitions $VN \rightarrow AN$ and $AN \rightarrow VN$. The cross section of the off-diagonal transitions is much smaller than the cross sections of the direct processes. For this reason, $x F_3 \ll F_2$ at small x . However, the multiple scattering corrections to off-diagonal process $V \rightarrow A$ on a nucleus are determined by a strong cross section of the diagonal processes $V \rightarrow V$ and $A \rightarrow A$. This becomes clear if we consider the double scattering term for the off-diagonal nuclear amplitude. To this order the nuclear scattering proceeds via two steps: the off-diagonal scattering from one nucleon followed by the diagonal scattering from the second nucleon. The off-diagonal scattering can be interchanged with the diagonal scattering that leads to the factor of 2 enhancement, which appears to have the combinatorical origin.⁸

2. Application to complex nuclei

We now turn to the discussion of the shadowing effect in complex nuclei. We apply the Glauber-Gribov multiple scattering theory to calculate the multiple scattering effect on

⁸ Shadowing in neutrino structure functions including $x F_3$ at small and intermediate Q^2 will be discussed in more detail in [80].

effective cross sections. Let f^A be the nuclear scattering amplitude in forward direction. We will assume no isospin dependence of the scattering amplitude, *i.e.* $f^p = f^n$. Then f^A can be written as (see, *e.g.*, [59] and references therein)

$$f^A = A f + \delta f^A, \quad (82)$$

$$\delta f^A = i f^2 \mathcal{C}_2^A(f), \quad (83)$$

where f is the corresponding nucleon amplitude and \mathcal{C}_2^A incorporates the multiple scattering effects and read as follows

$$\mathcal{C}_2^A(f) = \int_{z_1 < z_2} d^2 \mathbf{b} dz_1 dz_2 \rho_A(\mathbf{b}, z_1) \rho_A(\mathbf{b}, z_2) \exp \left[i \int_{z_1}^{z_2} dz' (f \rho_A(\mathbf{b}, z') - k_L) \right]. \quad (84)$$

Here ρ_A is the nucleon density distribution normalized to the number of nucleons A and the integration is performed along the collision axis, which is chosen to be z -axis, and over the transverse positions of nucleons (impact parameter \mathbf{b}). If only the double scattering approximation is considered then the exponential factor in Eq.(84) should be omitted. The exponential factor in Eq.(84) accounts for multiple scattering effects (see, *e.g.*, [59]).

We note that Eqs. (82) and (84) were derived assuming that the wave function factorizes into the product of the single particle wave functions and neglecting short-range correlation effects between bound nucleons (optical approximation). We comment in this respect that the correlations are relevant only if the coherence length $L_c = 1/k_L$ is comparable to the short-range repulsive part of the nucleon–nucleon force, which is about 0.5 Fm. This takes place at relatively large x , for which shadowing effect is small (see discussion in Ref.[24]).

The transverse momentum dependence of elastic scattering amplitudes was also neglected, since the transverse size of the meson-nucleon amplitude in the impact parameter space is of order $B^{-1/2}$, much smaller than the radius of the nucleus.

We first discuss multiple scattering correction to the transverse structure function. The relative shadowing correction is determined by effective scattering amplitude f_T of transversely polarized virtual photon

$$\delta R_T^A = \sigma_T \text{Re}(i + \alpha_T)^2 \mathcal{C}_2^A(f_T)/2. \quad (85)$$

If the real part of the amplitude is small then multiple scattering correction is negative because of destructive interference of forward scattering amplitudes on the upstream nucleons that causes *shadowing* of virtual hadron interactions. It should be also noted that if the real part is large then the interference in the double scattering term is constructive that would lead to antishadowing effect.

If the coherence length of hadronic fluctuation is small compared to average nuclear radius, $L_c \ll R_A$, then the oscillating factor in Eq.(84) suppresses multiple scattering effect. The onset point of coherent nuclear effects can be estimated by comparing the coherence length of hadronic fluctuation L_c with the averaged distance between bound nucleons in the nucleus r_{NN} . The coherent nuclear effects take place if the coherence length is large enough $L_c > r_{\text{NN}}$. Since for any mass m^2 of intermediate hadronic state $L_c < (Mx)^{-1}$ the region of coherent nuclear effects is limited to small x for any Q^2 , $x < (Mr_{\text{NN}})^{-1}$. Nuclear shadowing saturates if the coherence length L_c exceeds average nuclear radius that happens at small

x and the condition $L_c \sim R_A$ defines the transition region with strong x dependence of the shadowing correction.

The rate of multiple scattering interactions is controlled by mean free path of hadronic fluctuation in a nucleus $l_f = (\rho_A \sigma)^{-1}$. If l_f is small enough compared with nuclear radius, which is the case for heavy nuclei, then multiple scattering effects are important.

It can be easily seen from Eqs. (82) and (84) that if the dependence of \mathcal{C}_2^A on the scattering amplitude can be neglected, then Eq.(78) generalizes to complex nuclei. This corresponds to the case when the double scattering saturates the multiple scattering corrections. Generally, for heavy nuclei Eq.(78) should be replaced by

$$\frac{\delta R_L^A(x, Q^2)}{\delta R_T^A(x, Q^2)} = R(x, Q^2) \frac{\text{Re}(i + \alpha_L)^2 \mathcal{C}_2^A(f_L)}{\text{Re}(i + \alpha_T)^2 \mathcal{C}_2^A(f_T)}, \quad (86)$$

with f_L and f_T the effective scattering amplitudes for longitudinally and transversely polarized photons. The relation between the nuclear shadowing effect for F_2 and F_T in heavy nuclei can be derived from Eqs.(79), (85) and (86).

We now discuss the multiple scattering corrections to the right-left asymmetry in the helicity scattering amplitudes and the generalization of Eq.(81) to heavy nuclei. The multiple scattering correction to the difference $f_3 = f_+ - f_-$, as follows from Eqs. (82) and (84), can be written as

$$\delta(f_+^A - f_-^A) = i[f_+^2 \mathcal{C}_2^A(f_+) - f_-^2 \mathcal{C}_2^A(f_-)], \quad (87)$$

where f_{\pm} are the corresponding nucleon amplitudes. We now use the fact that $|f_3| \ll |f_T|$, where $f_T = (f_+ + f_-)/2$ is the amplitude averaged over the transverse polarizations of the intermediate boson, and expand Eq.(87) in f_3 keeping only the linear term. We have

$$\delta f_3^A = 2i f_3 f_T \mathcal{C}_2^A(f_T) - f_3 f_T^2 \mathcal{C}_3^A(f_T), \quad (88)$$

where

$$\begin{aligned} \mathcal{C}_3^A(f) = & -i \partial \mathcal{C}_2^A(f) / \partial f = \\ & \int_{z_1 < z_2 < z_3} d^2 \mathbf{b} dz_1 dz_2 dz_3 \rho_A(\mathbf{b}, z_1) \rho_A(\mathbf{b}, z_2) \rho_A(\mathbf{b}, z_3) \\ & \exp \left[i \int_{z_1}^{z_3} dz' (f \rho_A(\mathbf{b}, z') - k_L) \right]. \end{aligned} \quad (89)$$

The first term in the right side of Eq.(88) is similar to that in Eq.(80). This term is driven by the double scattering term (quadratic f^2 term in multiple scattering series). However, the higher order multiple scattering terms also contribute to (88) through nonlinear effects in \mathcal{C}_2^A and \mathcal{C}_3^A . Note in this respect that the expansion of the term \mathcal{C}_3^A in the multiple scattering series starts from the tripple scattering term ρ^3 . The analytical expressions for \mathcal{C}_2^A and \mathcal{C}_3^A calculated for uniform density distribution, which is used in our analysis described in Sect. V G, are given in Appendix B.

Using Eq.(88) it is straightforward to compute the relative multiple scattering correction to the cross section asymmetry $\delta R_3^A = \delta \sigma_3^A / \sigma_3$ that also determines the nuclear shadowing effect for the structure function F_3 . The resulting experection for δR_3^A is somewhat cumbersome in general case and we do not give it explicitly here. It should be noted that δR_3^A does not depend on the cross section asymmetry σ_3 for the nucleon but does depend on $\alpha_3 = \text{Re } f_3 / \text{Im } f_3$. If we keep only the double scattering term then δR_3^A is given by Eq.(81) also in the case of complex nuclei. However, this relation is violated by higher order multiple scattering terms.

V. DESCRIPTION OF THE MODEL

In the following we discuss in detail the model which is used to describe nuclear structure functions. The model incorporates the treatment of both the coherent and incoherent processes as described in Section IV. Our general strategy in constructing the model is to include constraints from other branches of nuclear physics. In particular, we use the model nuclear spectral function (Section VB) calculated in a many-body approach, which describes well electron scattering off nuclei at low and intermediate energies. The model pion distribution function is constrained by light-cone momentum conservation and equations of motion of pion field (Section VC). The nuclear shadowing effect is described in terms of effective scattering amplitude of intermediate hadronic states of virtual boson off the nucleon (see Section IVB). In order to describe data on nuclear structure functions we introduce an off-shell correction to the nucleon structure functions, which provides a measure of the modification of the nucleon structure in the nuclear environment. This effect and the effective scattering amplitude are treated phenomenologically in terms of few universal parameters, which are independent from nuclei and are extracted from nuclear DIS data in a wide kinematic range of x and Q^2 . The parameterizations of the off-shell effect and of the effective amplitude are discussed in Sections VD and VE. Sections VF to VG 3 describe the data used, the analysis procedure and our main results.

A. Deuteron wave function

Nuclear spectral function \mathcal{P} describes the probability to find the nucleon with the momentum \mathbf{p} and the (non-relativistic) energy ε in the ground state of the nucleus. We first discuss the *deuteron* for which the spectral function is determined by the wave function (see Eq.(52)). The deuteron wave function is the superposition of s - and d -wave states. In the momentum space it can be written as follows

$$\Psi_{D,m}(\mathbf{p}) = \sqrt{2\pi^2} \left(\psi_0(p) - \psi_2(p) \frac{S_{12}(\hat{\mathbf{p}})}{\sqrt{8}} \right) \chi_{1m}, \quad (90)$$

where ψ_0 and ψ_2 are respectively the s - and d -wave function in the momentum space,⁹ m is the projection of the total angular momentum on the spin quantization axis, χ_{1m} is the spin 1 wave function with $S_z = m$, and $S_{12}(\hat{\mathbf{p}})$ is the tensor operator

$$S_{12}(\hat{\mathbf{p}}) = 3(\boldsymbol{\sigma}_1 \cdot \hat{\mathbf{p}})(\boldsymbol{\sigma}_2 \cdot \hat{\mathbf{p}}) - \boldsymbol{\sigma}_1 \cdot \boldsymbol{\sigma}_2, \quad (91)$$

where $\hat{\mathbf{p}} = \mathbf{p}/|\mathbf{p}|$ and $\boldsymbol{\sigma}_1$ and $\boldsymbol{\sigma}_2$ are the Pauli matrices acting on the spin variables of the bound proton and neutron, respectively. The momentum distribution in the deuteron is

⁹ In terms of the standard wave functions in the coordinate space $u(r)$ and $w(r)$ the functions ψ_0 and ψ_2 are $\psi_0(p) = (2/\pi)^{1/2} \int dr r j_0(rp) u(r)$ and $\psi_2(p) = (2/\pi)^{1/2} \int dr r j_2(rp) w(r)$, where j_0 and j_2 are the spherical Bessel functions. Note also a different sign of the d -wave term in Eq.(90) with respect to the wave function in the coordinate space.

given by the wave function (90) squared

$$|\Psi_{D,m}(\mathbf{p})|^2 = 2\pi^2 \left[\psi_0^2(p) + \psi_2^2(p) - \chi_{1m}^\dagger S_{12} \chi_{1m} \left(\frac{\psi_0(p)\psi_2(p)}{\sqrt{2}} + \frac{\psi_2^2(p)}{4} \right) \right], \quad (92)$$

where the last term in the right side appears due to the tensor operator (91). This term vanishes after averaging over the deuteron polarizations, which is the case for the present paper. The momentum space partial wave functions are normalized according to

$$\int_0^\infty dp p^2 (\psi_0^2(p) + \psi_2^2(p)) = 1. \quad (93)$$

In order to study the sensitivity of our result to the choice of the deuteron wave function we used two different deuteron wave functions: the one which corresponds to the Bonn potential [64] and the Paris wave function [65]. These two wave functions have different high-momentum component and in this respect represent two extreme situations.

B. Nuclear spectral function

In this paper we consider a phenomenological model for the spectral function which incorporates both the single particle nature of the spectrum at low energy and high-energy and high-momentum components due to NN-correlations in the ground state. We first discuss the isoscalar spectral function which we write as

$$\mathcal{P}_0(\varepsilon, \mathbf{p}) = \mathcal{P}_{\text{MF}}(\varepsilon, \mathbf{p}) + \mathcal{P}_{\text{cor}}(\varepsilon, \mathbf{p}). \quad (94)$$

The low-energy part is described by the mean-field spectral function (56). In practice we use an approximate expression motivated by closure in which the sum over occupied levels is substituted by its average value:

$$\mathcal{P}_{\text{MF}}(\varepsilon, \mathbf{p}) = 2\pi n_{\text{MF}}(\mathbf{p}) \delta(\varepsilon + E^{(1)} + E_R(\mathbf{p})), \quad (95)$$

with $E_R(\mathbf{p}) = \mathbf{p}^2/2M_{A-1}$ being the recoil energy of residual nucleus, $E^{(1)} = E^{A-1} - E_0^A$ the nucleon separation energy averaged over single-particle levels, and $n_{\text{MF}}(\mathbf{p})$ the corresponding part of the nucleon momentum distribution.

The correlated part of the spectral function \mathcal{P}_{cor} is determined by excited states in (54) with one or more nucleons in the continuum. We follow [69] and assume that \mathcal{P}_{cor} at high momentum and high energy is dominated by ground state configurations with a correlated nucleon-nucleon pair and remaining $A-2$ nucleons moving with low center-of-mass momentum

$$|A-1, -\mathbf{p}\rangle \approx \psi^\dagger(\mathbf{p}_1) |(A-2)^*, \mathbf{p}_2\rangle \delta(\mathbf{p}_1 + \mathbf{p}_2 + \mathbf{p}). \quad (96)$$

The corresponding matrix element in Eq.(54) can be parametrized in terms of the wave function of the nucleon-nucleon pair embedded into nuclear environment,

$$\langle (A-2)^*, \mathbf{p}_2 | \psi(\mathbf{p}_1) \psi(\mathbf{p}) | A \rangle = \psi_{\text{rel}}(\mathbf{k}) \psi_{\text{CM}}^{A-2}(\mathbf{p}_{\text{CM}}) \delta(\mathbf{p}_1 + \mathbf{p}_2 + \mathbf{p}). \quad (97)$$

In the right side of Eq.(97) where we have assumed the factorization into the wave functions describing the relative motion in the nucleon-nucleon pair with relative momentum $\mathbf{k} = (\mathbf{p} - \mathbf{p}_1)/2$ and the center-of-mass (CM) motion of the pair in the field of $A-2$ nucleons, $\mathbf{p}_{\text{CM}} = \mathbf{p}_1 + \mathbf{p}$. The CM wave function ψ_{CM} generally depends on the quantum numbers of the state of $A-2$ nucleons, however the corresponding dependence of the ψ_{rel} is assumed to be weak.

Using Eq.(97) we sum over the spectrum of states of $A-2$ nucleons and obtain an approximate expression for \mathcal{P}_{cor} :

$$\mathcal{P}_{\text{cor}}(\varepsilon, \mathbf{p}) = 2\pi \int d^3\mathbf{p}_1 d^3\mathbf{p}_2 n_{\text{rel}}(\mathbf{k}) n_{\text{CM}}(\mathbf{p}_2) \delta(\mathbf{p}_1 + \mathbf{p}_2 + \mathbf{p}) \delta\left(\varepsilon + \frac{\mathbf{p}_1^2}{2M} + \frac{\mathbf{p}_2^2}{2M_{A-2}} + E^{(2)}\right). \quad (98)$$

Here n_{rel} and n_{CM} are the relative and the CM momentum distributions respectively and $E^{(2)} = E^{A-2} - E_0^A$ is the energy needed to separate two nucleons from the ground state averaged over configurations of $A-2$ nucleons with low excitation energy. Note that the minimum two nucleon separation energy $E^{(2)} = E_0^{A-2} - E_0^A$ is of order 20 MeV for medium-range nuclei like ^{56}Fe .

We can further simplify Eq.(98) if the momentum p is high enough and $|\mathbf{p}| \gg |\mathbf{p}_2|$. This allows us to take the relative momentum distribution out of the integral over the CM momentum at the point $\mathbf{k} = \mathbf{p}$. Then we have

$$\mathcal{P}_{\text{cor}}(\varepsilon, \mathbf{p}) = 2\pi n_{\text{rel}}(\mathbf{p}) \left\langle \delta\left(\varepsilon + \frac{\mathbf{p}^2}{2M} + \frac{\mathbf{p} \cdot \mathbf{p}_2}{M} + \frac{\mathbf{p}_2^2}{2M_*} + E^{(2)}\right) \right\rangle_{\text{CM}}, \quad (99)$$

where the averaging is done with respect to the CM motion of the correlated pair and $M_* = M(A-2)/(A-1)$ is effective mass of the system of the residual nucleus of $A-2$ nucleons and the nucleon with momentum \mathbf{p}_1 . In this approximation the high momentum part of nuclear momentum distribution is given by relative momentum distribution in the correlated nucleon-nucleon pair embedded into nuclear environment, $n_{\text{cor}}(\mathbf{p}) = n_{\text{rel}}(\mathbf{p})$.

The characteristic momenta of the CM motion of the NN-pair are similar to the one in the mean field model. The average CM momentum of the pair squared can be estimated from the balance of the overall nucleus momentum [69], $\langle (\sum \mathbf{p}_i)^2 \rangle = 0$, where the sum is taken over all bound nucleons and the expectation value is performed with respect to the intrinsic wave function of the nucleus. This gives $\langle \mathbf{p}_{\text{CM}}^2 \rangle = 2\langle \mathbf{p}^2 \rangle (A-2)/(A-1)$, with $\langle \mathbf{p}^2 \rangle$ the mean value of the squared single nucleon momentum. We consider configurations in which characteristic CM momenta are small. For this reason we should also exclude the high-momentum part in estimating $\langle \mathbf{p}^2 \rangle$ and we will assume that this quantity is given by averaging over mean-field configurations. We follow [69] and parameterize the CM momentum distribution of the correlated NN pair in the field of other $A-2$ nucleons by a Gaussian distribution,

$$n_{\text{CM}}(\mathbf{p}_{\text{CM}}) = (\alpha/\pi)^{3/2} \exp(-\alpha \mathbf{p}_{\text{CM}}^2), \quad (100)$$

with the parameter α determined from the averaged CM momentum of the nucleon-nucleon pair, $\alpha = 3/(2\langle \mathbf{p}_{\text{CM}}^2 \rangle)$.

Using Eq.(100) we find that the integration over the CM momentum in (99) can be performed analytically and the result reads,

$$\mathcal{P}_{\text{cor}}(\varepsilon, \mathbf{p}) = n_1(\mathbf{p}) \frac{2M}{p} \sqrt{\alpha\pi} \left(\exp(-\alpha p_{\text{min}}^2) - \exp(-\alpha p_{\text{max}}^2) \right), \quad (101)$$

where $p = |\mathbf{p}|$, p_{\min} and p_{\max} are respectively the minimum and the maximum CM momenta allowed by the energy-momentum conservation in Eq.(98) for the given ε and \mathbf{p} ,

$$p_{\max} = \frac{M_* p}{M} + p_T, \quad (102a)$$

$$p_{\min} = \left| \frac{M_* p}{M} - p_T \right|, \quad (102b)$$

where $p_T = (2M_*(|\varepsilon| - E_{\text{th}}))^{1/2}$ and $E_{\text{th}} = E^{(2)} + E_R(\mathbf{p})$. The latter is the threshold value of the nucleon separation energy for discussed configurations. Note that in our notations $\varepsilon < 0$. We also remark that p_T has the meaning of the maximum CM momentum in the correlated NN-pair in the direction transverse to \mathbf{p} for the given ε and p [71].

In numerical evaluations we use the parameterizations for $n_{\text{MF}}(A, \mathbf{p})$ and $n_{\text{cor}}(A, \mathbf{p})$ of [69] which fit nicely the results of many-body calculation of nuclear momentum distribution. It follows from this calculation that low-momentum part incorporates about 80% of the total normalization of the spectral function while the other 20% are taken by the high-momentum part. The momentum distributions are presented in [69] for a limited range of nuclei. In order to evaluate the momentum distributions for other values of the nucleus mass number A , we interpolate the values of the momentum distributions for each value of momentum $|\mathbf{p}|$. For the parameter $E^{(2)}$ we take the two-nucleon separation energy, i.e. the difference $E_0^{A-2} - E_0^A$ between the ground state energies (note that $E^{(2)} > 0$). The remaining parameter $E^{(1)}$ of \mathcal{P}_{MF} is fixed using the Koltun sum rule [72]

$$\langle \varepsilon \rangle + \langle T \rangle = 2\varepsilon_B, \quad (103)$$

where $\langle \varepsilon \rangle$ and $\langle T \rangle$ are the nucleon separation and kinetic energies averaged with the full spectral function

$$\langle \varepsilon \rangle = A^{-1} \int [dp] \mathcal{P}(\varepsilon, \mathbf{p}) \varepsilon, \quad (104a)$$

$$\langle T \rangle = A^{-1} \int [dp] \mathcal{P}(\varepsilon, \mathbf{p}) \frac{\mathbf{p}^2}{2M}, \quad (104b)$$

and $\varepsilon_B = E_0^A/A$ is nuclear binding energy per bound nucleon. This sum rule is exact for nonrelativistic systems with two-body forces.

For the isovector spectral function Eq.(59) we use the the Fermi gas model to evaluate the wave function ϕ_F , which is supposed to be a reasonable approximation for heavy nuclei. In this model $|\phi_F(p)|^2 \propto \delta(p_F - p)$, where p_F is the Fermi momentum which is determined by average nucleon density $\rho = 4p_F^3/(6\pi^2)$. The proportionality coefficient can be found from the normalization condition (35), according to which \mathcal{P}_1 is normalized to unity. As a result we have

$$\mathcal{P}_1 = \delta(p - p_F) \delta(\varepsilon - \varepsilon_F) / (4\pi p_F^2). \quad (105)$$

C. Nuclear pion distribution function

In calculating the pion effect in nuclear structure functions the relevant quantity is the distribution of pion excess in a nucleus since the nucleon pion cloud effect is taken into account in the nucleon structure functions. The inspection of Eqs.(50) and (51) suggests

that the pion correction is located at small $x < p_F/M$, which is also confirmed by model calculations. In this region a good approximation is to neglect x^2/Q^2 terms in Eqs.(49) as well as target mass corrections to structure functions. We also assume no off-shell dependence of pion structure function and base our discussion on convolution approximation by Eqs. (50) and (51).

Before doing model calculations it is important to realize that the pion distribution function is constrained by a number of sum rules. The first moment of (51) gives an average pion ligh-cone momentum

$$\langle y \rangle_\pi = \int dy y f_{\pi/A}(y) = \langle \theta_{++}^\pi \rangle / M, \quad (106)$$

where $\theta_{++}^\pi = (\partial_0 \varphi)^2 + (\partial_z \varphi)^2$ is the light-cone component of pion energy-momentum tensor. The averaging in Eq.(106) means

$$\langle \mathcal{O} \rangle = \int d^3 \mathbf{r} \langle A | \mathcal{O}(\mathbf{r}) | A \rangle / \langle A | A \rangle \quad (107)$$

for any operator \mathcal{O} . It is also useful to consider average inverse y for which we obtain

$$\langle y^{-1} \rangle_\pi = \int \frac{dy}{y} f_{\pi/A}(y) = M \langle \varphi^2 \rangle, \quad (108)$$

where the average φ^2 is given by Eq.(107).

The pion and nucleon fractions of nuclear light-cone momentum are related by the momentum balance equation

$$\langle y \rangle_\pi + \langle y \rangle_N = \frac{M_A}{AM}. \quad (109)$$

Equation (109), although being intuitively obvious, can formally be derived in a meson-nucleon field-theoretic model of nuclear Hamiltonian [47]. Several constraints on nuclear pion distribution $\mathcal{D}_{\pi/A}(k)$ can be obtained in this model using the equations of motion for pion and nucleon operators and energy-momentum conservation condition. In particular, for a model nuclear Hamiltonian with nucleons and pions with pseudo-scalar interaction this constraints lead to the following relations [47]

$$m_\pi^2 \langle \varphi^2 \rangle = \varepsilon_B + \langle T \rangle, \quad (110a)$$

$$\langle (\partial_0 \varphi)^2 \rangle = \varepsilon_B - \frac{1}{2} (\langle \varepsilon \rangle + \langle T \rangle), \quad (110b)$$

$$\langle (\nabla \varphi)^2 \rangle = -\frac{3}{2} \langle \varepsilon \rangle - \frac{1}{2} \langle T \rangle. \quad (110c)$$

A few comments are in order. Pion field in nuclei is generated mainly by nucleon sources. Time variation of the pion field describes retardation effects in the nucleon–nucleon interaction. In a nonrelativistic system this effect is small since typical energy variations are small compared to the pion mass. We, therefore, take the static approximation $\partial_0 \varphi = 0$. Then Eq.(110b) is equivalent to the Koltun sum rule (103). For the pion energy-momentum tensor we have $\langle \theta_{++}^\pi \rangle = \frac{1}{3} \langle (\nabla \varphi)^2 \rangle$. Then using Eq.(44) we conclude that Eqs. (110c) and (109) are equivalent. For this reason only Eq.(110a) gives independent constraint.

We make use the constraints on average pion light-cone momentum y and $1/y$ which follow from Eqs. (110a) and (109) in order to evaluate pion contribution to nuclear structure

functions. It should be remarked that in this approach by using momentum balance equation (109) we effectively take into account the contributions from all mesons. In order to quantitatively evaluate the pion effect in the structure functions we use a model distribution

$$f_{\pi/A}(y) = C y(1-y)^n, \quad (111)$$

which is motivated by the asymptotics of pion distribution function at small and large y . The normalization constant C and the exponent n are fixed from Eqs.(109) and (108) using Eqs. (44) and (110a). The nucleon average separation and kinetic energies are calculated with the spectral function described in Section V B.

D. Parameterization of off-shell effects

The relative variations of the quark distributions in the vicinity of the mass shell are described by the function $\delta f(x)$ defined in Section IV A 6. This function can serve as a measure of the modification of the nucleon structure in the nuclear environment. In the analysis of data, described in detail in Section V G, we consider a phenomenological model for the off-shell function. In order to choose the parametrization of $\delta f(x)$ we note that in the absence of off-shell corrections, the effects of nuclear binding and Fermi motion on the normalization of valence quarks cancel. Therefore, we expect that the off-shell function δf should have least one zero at some intermediate x to avoid a large violation of the integral valence nuclear quark number (see Section VI A). Moreover, the explicit consideration of nuclear pion correction as discussed in Section V C suggest that $\delta f(x)$ can have two zeros. These motivate us to choose the following parameterization for the off-shell function:

$$\delta f(x) = C_N(x-x_1)(x-x_0)(h-x), \quad (112)$$

where C_N is an overall normalization constant and $h > 1$. The analysis of data indicates that the parameters h and x_0 are fully correlated. For this reason we set $h = 1 + x_0$ and the expression (112) has only three independent parameters. We use this model to describe off-shell effects in the analysis of Section V G 2.

It should be remarked that the determination of δf at small x is correlated with the treatment of pion and shadowing corrections. The data available for the extraction of δf is limited to F_2 and for this reason it is difficult to unambiguously disentangle different effects at small x . We can study the interplay between pion and off-shell effects by absorbing the pion contribution to nuclear F_2 into an effective off-shell function $\delta f'_2$. To this end we write the effective off-shell correction to F_2^A as:

$$\langle F_2^N \delta f'_2 v \rangle = \langle F_2^N \delta f v \rangle + \delta F_2^{\pi/A}(x), \quad (113)$$

where δf is the actual off-shell function and the last term in Eq.(113) is the nuclear pion correction discussed in Sections IV A 3 and V C. The averaging is taken over the nuclear spectral function according to Eq.(40) and we denote $v = (p^2 - M^2)/M^2$, the nucleon virtuality in the units of nucleon mass M . One can simplify Eq.(113) by observing that the functions $\delta f'_2$ and δf differ mainly at small x , where the pion field contribution is essential. In this region the integrand structure function can be taken out of the averaging in (113) at $x' = x$ to a good approximation. As a result we then have:

$$\delta f'_2(x) = \delta f(x) + \frac{\delta F_2^{\pi/A}(x)}{\langle v \rangle F_2^N(x)}, \quad (114)$$

Experiment	Targets	# of points	x range	Q^2 range [GeV ²]
NMC [2]	D/p	12	$7.0 \times 10^{-3} \div 0.70$	4.0
NMC [4]	⁴ He/D	18	$3.5 \times 10^{-3} \div 0.65$	$0.77 \div 44.0$
NMC [3]	⁷ Li/D	24	$1.4 \times 10^{-4} \div 0.65$	$0.034 \div 39.0$
NMC [5]	⁹ Be/ ¹² C	15	$1.25 \times 10^{-2} \div 0.70$	$3.4 \div 66.7$
NMC [3]	¹² C/D	24	$1.5 \times 10^{-4} \div 0.65$	$0.035 \div 41.0$
NMC [4]	¹² C/ ⁷ Li	25	$8.5 \times 10^{-3} \div 0.60$	$0.8 \div 17.0$
NMC [5]	²⁷ Al/C	15	$1.25 \times 10^{-2} \div 0.70$	$3.4 \div 63.9$
NMC [4]	⁴⁰ Ca/D	18	$3.5 \times 10^{-3} \div 0.65$	$0.6 \div 41.0$
NMC [4]	⁴⁰ Ca/ ⁷ Li	25	$8.5 \times 10^{-3} \div 0.60$	$0.8 \div 17.0$
NMC [4]	⁴⁰ Ca/ ¹² C	25	$8.5 \times 10^{-3} \div 0.60$	$0.8 \div 17.0$
NMC [5]	⁵⁶ Fe/ ¹² C	15	$1.25 \times 10^{-2} \div 0.70$	$3.4 \div 66.6$
EMC [7]	⁶³ Cu/D	10	$1.5 \times 10^{-2} \div 0.61$	$3.3 \div 46.4$
NMC [6]	¹¹⁹ Sn/ ¹² C	161	$1.25 \times 10^{-2} \div 0.70$	$1.3 \div 110.0$
NMC [5]	²⁰⁷ Pb/ ¹² C	15	$1.25 \times 10^{-2} \div 0.70$	$3.4 \div 66.1$
E139 [10]	⁴ He/D	21	$0.125 \div 0.88$	$2.0 \div 10.0$
E139 [10]	⁹ Be/D	21	$0.125 \div 0.88$	$2.0 \div 10.0$
E139 [10]	¹² C/D	17	$0.205 \div 0.80$	$3.5 \div 10.0$
E139 [10]	²⁷ Al/D	21	$0.125 \div 0.88$	$2.0 \div 10.0$
E139 [10]	⁴⁰ Ca/D	17	$0.205 \div 0.80$	$3.5 \div 10.0$
E139 [10]	⁵⁶ Fe/D	23	$0.084 \div 0.88$	$2.0 \div 10.0$
E139 [10]	¹⁰⁸ Ag/D	17	$0.205 \div 0.80$	$3.5 \div 10.0$
E139 [10]	¹⁹⁷ Au/D	22	$0.125 \div 0.88$	$2.0 \div 10.0$
E140 [9]	⁵⁶ Fe/D	8	$0.200 \div 0.50$	$1.0 \div 5.0$
E140 [9]	¹⁹⁷ Au/D	1	0.200	1.0
BCDMS [8]	⁵⁶ Fe/D	10	$0.07 \div 0.65$	$17.0 \div 113.0$
E665 [11]	D/p	21	$2.0 \times 10^{-5} \div 0.25$	$0.005 \div 35.6.0$
E665 [12]	²⁰⁷ Ca/ ¹² C	10	$1.2 \times 10^{-4} \div 0.027$	$0.15 \div 7.9$
E665 [12]	²⁰⁷ Pb/D	10	$1.2 \times 10^{-4} \div 0.027$	$0.15 \div 7.9$
E665 [12]	²⁰⁷ Pb/ ¹² C	10	$1.2 \times 10^{-4} \div 0.027$	$0.15 \div 7.9$

TABLE I: List of nuclear data used in the analysis. See text for details.

where $\langle v \rangle$ denotes the virtuality v averaged over the nuclear spectral function. We calculate $\delta F_2^{\pi/A}$ using the distribution of nuclear pion excess of Section V C and the parameterization of pion structure function of Ref.[42]. It should be noted that we choose sufficiently high Q^2 ($> 10 \text{ GeV}^2$) in order to calculate $\delta f'_2$ and that the calculation shows only a weak dependence on Q^2 . We have also performed calculations of the ratio in Eq.(114) for different nuclei and we always obtained similar shape and magnitude, indicating that the nuclear pion correction scales as $\langle v \rangle$. As a cross-check we will extract both δf and $\delta f'_2$ from data and we will compare the results with the calculation based upon Eq.(114).

E. Effective scattering amplitude

In the coherent region, the interaction of intermediate hadronic states with the nucleon is described in terms of an average effective cross section $\bar{\sigma}$ (see Section IV B and in particular Eq.(70)). As described in Section IV B, one can qualitatively expect that $\bar{\sigma}_T$ decreases with Q^2 since the relative weight of higher mass states increases with Q^2 and the cross-section decreases with the meson mass. In order to parametrize effective transverse cross section we use then the following expression

$$\bar{\sigma}_T = \sigma_1 + \frac{\sigma_0 - \sigma_1}{(1 + Q^2/Q_0^2)}. \quad (115)$$

The parameter σ_0 describes the cross section at small Q^2 , while σ_1 corresponds to high- Q^2 regime. The choice of both these parameters will be discussed in detail in Section V G 1. The free parameter Q_0^2 describes the transition between low- and high- Q^2 regions. We note that in our approach we only consider relative corrections to the effective cross-section and thus the calculation is not very sensitive to the detailed modelling of such cross-section. The low- Q^2 extrapolation of nucleon structure functions (Section III B) effectively provides the absolute LT and HT terms.

As described in Section IV B 1, we parameterize the effective scattering amplitude of transversely polarized photons as $f_T = (i + \alpha_T)\bar{\sigma}_T/2$ where $\alpha_T = \text{Re } f_T / \text{Im } f_T$. The presence of non-zero real part of the amplitude is required by both theoretical arguments and phenomenology. The choice of α_T in our analysis will be discussed in Section V G 1.

We now discuss the amplitude f_3 which describes the asymmetry in the scattering of left- and right-polarized virtual boson. This amplitude enters the calculation of coherent nuclear corrections to the structure F_3 and does not affect F_2 and F_1 . However, f_3 enters our analysis indirectly since it affects the normalization of nuclear valence number as described in Section VI A. It should be noted that the nuclear shadowing correction to F_3 does not depend on the cross-section σ_3 but does depend on $\alpha_3 = \text{Re } f_3 / \text{Im } f_3$ as explained in Section IV B 2. Therefore, we need to fix α_3 . To this end we use the approach based on Regge phenomenology of high-energy hadronic amplitudes. We recall that f_3 is the C -odd amplitude. A simple proper contribution is the ω -reggeon pole. Its energy dependence and Re/Im ratio is fully determined by the intercept [73]. According to Regge phenomenology the value of the intercept for this Regge pole is about 0.5 that leads to $\alpha_3 = 1$. We use this value in the calculation of nuclear shadowing correction to the valence quark distribution in Section VI A.

F. Nuclear data

Table I summarizes the list of experimental data used in this paper. They include both muon (EMC, NMC, BCDMS, FNAL E665) and electron (SLAC E139, E140) scattering on a variety of targets: p, D, ^4He , ^7Li , ^9Be , ^{12}C , ^{27}Al , ^{40}Ca , ^{56}Fe , ^{63}Cu , ^{108}Ag , ^{119}Sn , ^{197}Au , ^{207}Pb . For each target and kinematic region, we select the most precise and recent data and we do not use earlier results characterized by larger uncertainties, since their contribution to the present analysis would be negligible.¹⁰ Most of the data come from NMC for the small

¹⁰ Note also that the addition of unnecessary data points with large uncertainties can produce an artificial reduction of the χ^2 of fits.

x region and SLAC E139 for the region $x > 0.1$.

We note that, since all available nuclear data is provided by fixed-target experiments, there is always an implicit correlation between x and Q^2 in data points. Usually low- x regions also correspond to low- Q^2 values. As described in the following, this reduces the possibility to check the Q^2 dependence of the model in a complete way.

G. Extraction of parameters

The numerical values of the parameters in the model are determined from the data listed in Table I¹¹ with two main steps. Initially, we verify the consistency of our model with F_2 data from charged-lepton scattering, without imposing specific constraints. We then discuss in detail the deconvolution of different physical effects which contribute to the overall nuclear modification of the structure functions. The procedure applied in this paper can be viewed as a measurement of the deformation of bound nucleons in the nuclear medium.

It must be noted that the extraction of nuclear parameters is correlated with the determination of PDFs (see Section III B), which requires both proton and deuterium data to obtain the distributions of d and u quarks. Nuclear effects can produce significant distortions on parton densities and will be the subject of a future publication. Since our approach describes bound nucleon structure functions, nuclear data can be treated in the same way as proton data. Therefore, in principle, it would be possible to extract simultaneously PDFs and nuclear parameters by applying QCD analysis to the extended set of data including nuclear data. However, in order to limit correlations we follow a different approach.

The parameters of the model are extracted only from measured ratios $R_2(A'/A) = F_2^{A'}/F_2^A$, where A' and A are two different nuclei (usually the denominator corresponds to deuterium). The description of the nucleon structure functions largely cancels in the ratios, thus effectively removing the correlation with PDFs. In order to verify this we applied an iterative procedure. We first extracted the parameters using PDFs obtained without our nuclear corrections. Then we repeated the procedure after updating the PDF extraction using the information on nuclear effects in deuterium from the results of the previous step (Section III B). Results indicated that the fitted parameters were stable, demonstrating the absence of strong correlations.

Nuclear data are usually available in bins of x (Δx), while only the average \bar{Q}^2 in each bin is provided. We perform a fit to the experimental data with MINUIT [74] by minimizing $\chi^2 = \sum (R_2^{\text{exp}} - R_2^{\text{th}})^2 / \sigma^2(R_2^{\text{exp}})$, where $\sigma^2(R_2^{\text{exp}})$ represents the uncertainty on the measurements and the sum includes all data points. For each experimental point, the model is evaluated at the given average \bar{Q}^2 and integrated over the size of the x bin:¹²

$$R_2^{\text{th}}(x, \bar{Q}^2, A'/A) = \frac{\int_{x-\Delta x/2}^{x+\Delta x/2} F_2^{A'}(x', \bar{Q}^2) dx'}{\int_{x-\Delta x/2}^{x+\Delta x/2} F_2^A(x', \bar{Q}^2) dx'}. \quad (116)$$

Both the normalization and point-to-point uncorrelated uncertainties, as published by experiments, are taken into account. We would like to emphasize that the lack of knowledge

¹¹ We note that D/ p data were not used in our fits. However, these data are used in the comparison with model calculations in Sect. VI D

¹² In a few cases, in which the explicit Q^2 dependence is provided, the model is averaged over the corresponding Q^2 bins.

of the experimental Q^2 distribution in the x bins can potentially result in a mismatch between data and predictions in the regions where a significant Q^2 dependence is present. As discussed in the following, this increases the systematic uncertainties of the calculation for $x > 0.75$ and $x < 0.01$, although we have verified that it does not alter the central values of the extracted parameters.

As explained in Section III B, we use a phenomenological extrapolation of free nucleon structure functions for $Q^2 < 1.0 \text{ GeV}^2$. We can therefore calculate nuclear corrections to structure functions also in the limit of very small Q^2 . However, we restrict the fits to extract the free parameters of our model to the data with $Q^2 \geq 1.0 \text{ GeV}^2$ in order to reduce systematic uncertainties on the parameters. We then validate our predictions against the data points with $Q^2 < 1.0 \text{ GeV}^2$, which are included in all comparisons shown in the following.

1. Choice of fixed parameters

We start our fits by treating σ_0 and σ_1 , the asymptotic values for the effective transverse cross-section in Eq.(115), and the real part of the effective scattering amplitude $\alpha_T = \text{Re } f_T / \text{Im } f_T$ (Section IV B 1) as additional free parameters. This procedure allows a preliminary estimate of their correlation with the remaining parameters and a consistency check with the expected values.

The best fit value obtained for σ_1 is consistent with zero. By setting $\sigma_1 \neq 0$ we can still obtain an acceptable description of data provided $\sigma_1 < 1.0 \text{ mb}$ (at 90%CL), due to the (anti)correlation of σ_1 with Q_0^2 in Eq.(115). After verifying the correlation between σ_1 and the off-shell parameters in Eq.(112) is negligible, we then fix $\sigma_1 = 0$ in all our fits.

We note that a non-vanishing shadowing component at large Q^2 can be related to the normalization of the valence quark number per nucleon (Section VI A). In this respect we have two possible constraints at large Q^2 . The first condition is the conservation of the overall valence number in nuclei through a balance between the shadowing and the off-shell corrections. In addition, it is also possible to impose a conservation of the valence number in the bound nucleon, which, together with the previous condition, implies both off-shell effect and shadowing conserve independently the valence quark number. In our approach, initially we do not assume any specific normalization constraint. Instead, we verify a posteriori the size of the renormalization introduced by the actual off-shell effect (Section VI A) and its balance with the shadowing correction. We then use the normalization condition for nuclear valence number to further bound some of the parameters. This procedure will be discussed in more detail in Sections V G 2 and VI A.

The fits to DIS data on nuclear targets show a strong (positive) correlation between σ_0 and α_T . In addition, the value of σ_0 is also correlated with Q_0^2 so that it is not possible to unambiguously disentangle the three parameters from the fits. If we fix $\alpha_T = 0$ we obtain $\sigma_0 = 36 \text{ mb}$ from data. However, data clearly prefer $\alpha_T \neq 0$, with a somewhat lower value of σ_0 . The best fit solution corresponds to $\alpha_T = -0.179 \pm 0.038(\text{stat.})$ and $\Delta\chi^2 \sim 29$ with respect to the fit with fixed $\alpha_T = 0$. This can be interpreted as evidence for a sizeable real part in the effective scattering amplitude. If we impose $\sigma_0 = 27 \text{ mb}$, as expected for electromagnetic interactions by averaging ρ^0 , ω and ϕ vector mesons, we obtain $\alpha_T = -0.182 \pm 0.037(\text{stat.})$. Our results are in good agreement with the analysis of ρ^0 photoproduction experiments [60] at low- Q^2 . Since our phenomenological model correctly reproduces the photoproduction limit, we then fix $\sigma_0 = 27 \text{ mb}$ and $\alpha_T = -0.20$ according

Data set	C_N	x_0	Q_0^2 [GeV ²]	χ^2 / d.o.f.
⁴ He/D	6.00 ± 1.03	0.476 ± 0.033	1.76 ± 0.47	14.1 / 35
⁷ Li/D; ⁹ Be/D	7.08 ± 0.90	0.443 ± 0.020	0.91 ± 0.31	29.1 / 35
¹² C/D	9.33 ± 0.72	0.455 ± 0.012	1.22 ± 0.24	23.0 / 31
²⁷ Al/D; ²⁷ Al/ ¹² C	6.73 ± 0.71	0.474 ± 0.017	3.56 ± 2.38	22.7 / 33
⁴⁰ Ca/D; ⁴⁰ Ca/ ¹² C	7.08 ± 0.77	0.486 ± 0.015	1.73 ± 0.15	60.7 / 58
⁵⁶ Fe/D; ⁶³ Cu/D; ⁵⁶ Fe/ ¹² C	8.04 ± 0.42	0.457 ± 0.009	1.47 ± 0.34	69.1 / 63
¹⁰⁸ Ag/D; ¹¹⁹ Sn/ ¹² C	8.93 ± 0.98	0.414 ± 0.020	1.44 ± 0.34	22.1 / 29
¹⁹⁷ Au/D; ²⁰⁷ Pb/D; ²⁰⁷ Pb/ ¹² C	7.86 ± 0.93	0.391 ± 0.025	1.36 ± 0.36	19.9 / 42
All data	7.84 ± 0.26	0.453 ± 0.005	1.54 ± 0.08	476.5 / 556

TABLE II: Values of the parameters extracted from independent fits to different sub-sets of data with $Q^2 > 1.0$ GeV². Uncertainties are startistical only. The column on the right gives the χ^2 from each fit and the corresponding number of degrees of freedom. The last row shows the result of the global fit.

C_{ij}	$j = C_N$	$j = x_0$	$j = Q_0^2$
$i = C_N$	1.000	-0.065	-0.072
$i = x_0$	-0.065	1.000	0.006
$i = Q_0^2$	-0.072	0.006	1.000

TABLE III: Correlation coefficients between the nuclear parameters from the global combined fit.

to [60].

In our model we use the pionic parton distributions extracted from real pion scattering data [42] to approximate the structure functions of virtual pions in nuclei. To this end we perform fits with and without the pionic sea distributions and we find a significantly better description of data in the latter case. Therefore we only consider the valence contribution to the pionic structure functions in the following.

2. Results

In our model we assume three main free parameters: C_N , x_0 (Section V D) and Q_0^2 (Section V E). In addition, the actual off-shell function $\delta f(x)$ is characterized by the presence of a second zero, x_1 . This specific feature has important consequences, as it is discussed in Section VI B. Since the parameter x_1 turns out to be strongly correlated with C_N and Q_0^2 , we perform several fits with different fixed values of x_1 in the range $0.030 \leq x_1 \leq 0.065$ and we evaluate the corresponding effect on the normalization of the valence quarks at large Q^2 . Among the fits with comparable χ^2 with respect to data, we choose a fixed value $x_1 = 0.050$, since this value provides a good cancellation between off-shell correction and shadowing for all nuclei (see Section VI A for details).

In order to check our hypothesis about the universality of parameters in Eqs. (112) and

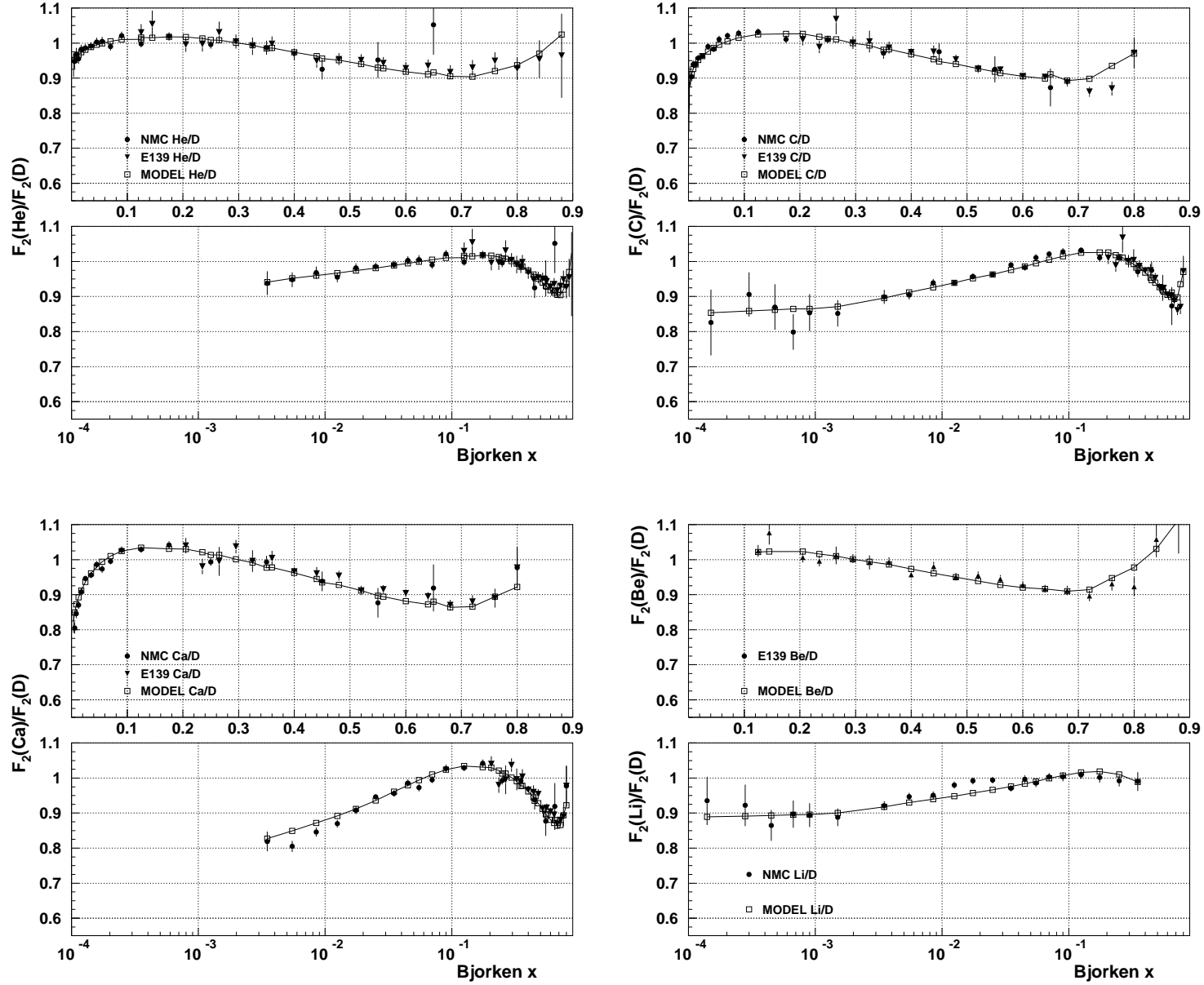


FIG. 1: Ratios $R_2(x, A'/A)$ for $^4\text{He}/\text{D}$, $^{12}\text{C}/\text{D}$, $^{40}\text{Ca}/\text{D}$, $^7\text{Li}/\text{D}$ and $^9\text{Be}/\text{D}$ (left to right and top to bottom). The curves with open squares show the corresponding model calculations (with same parameters). For data points the error bars correspond to the sum in quadrature of statistical and systematic uncertainties, while the normalization uncertainty is not shown.

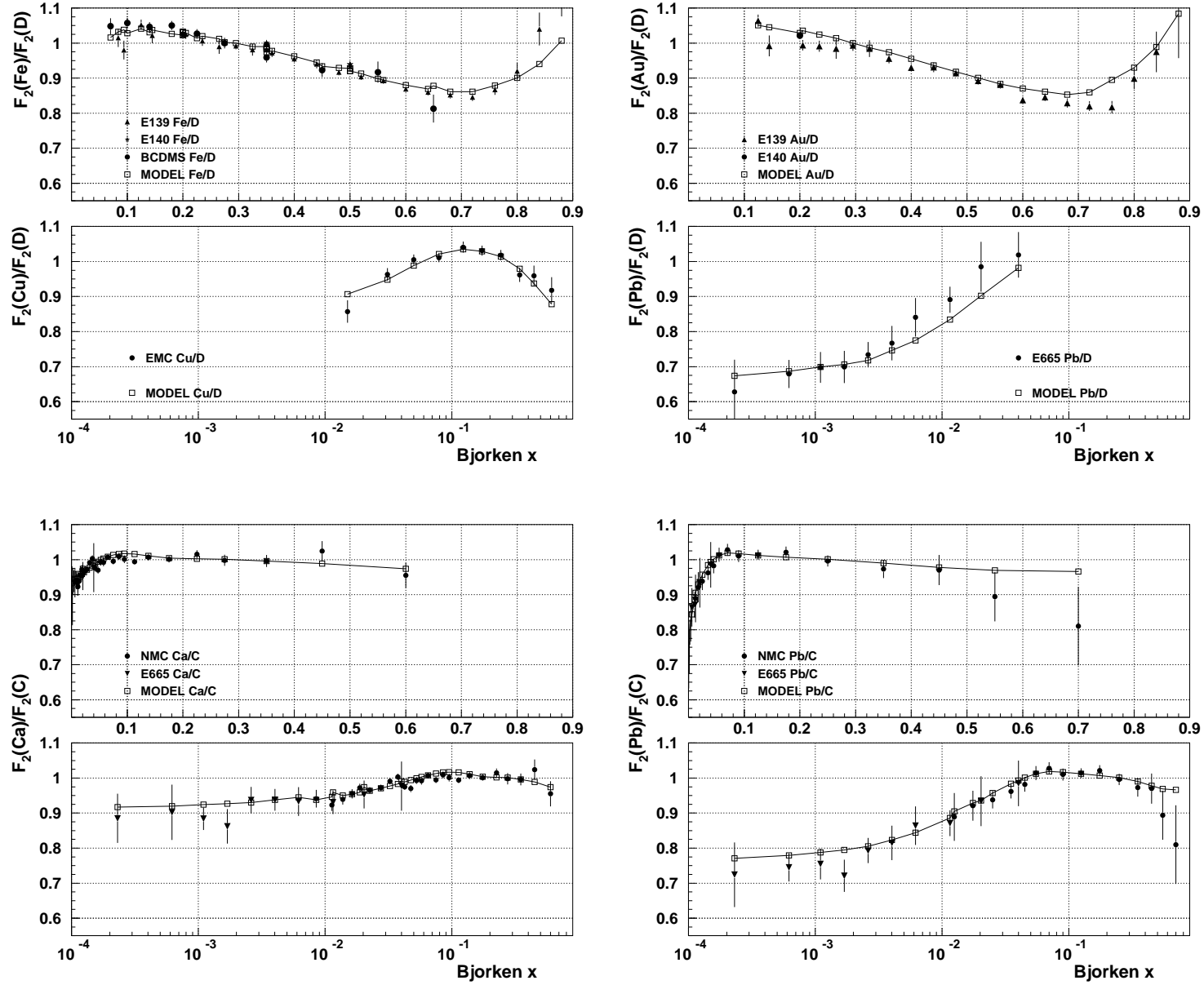


FIG. 2: Ratios $R_2(x, A'/A)$ for $^{56}\text{Fe}/\text{D}$, $^{63}\text{Cu}/\text{D}$, $^{197}\text{Au}/\text{D}$, $^{207}\text{Pb}/\text{D}$, $^{40}\text{Ca}/^{12}\text{C}$ and $^{207}\text{Pb}/^{12}\text{C}$ (left to right and top to bottom). The curves with open squares show the corresponding model calculations (with same parameters). For data points the error bars correspond to the sum in quadrature of statistical and systematic uncertainties, while the normalization uncertainty is not shown.

(115), we perform independent fits to different sub-sets of nuclei (from ^4He to ^{207}Pb) and we compare the corresponding values of the parameters with the ones obtained from a combined fit to all data. As can be seen from Table II, the results are compatible within uncertainties, thus allowing a unified treatment.¹³ The values of $\chi^2/\text{d.o.f.}$ indicate an excellent consistency between the model and the data points for all nuclei.

The final values of C_N , x_0 and Q_0^2 obtained from a global fit to nuclear data are given in the last line of Table II. The correlation between the parameters is small and mainly related to the normalization constant, as can be seen from Table III.

Figures 1 and 2 show the excellent overall agreement between the calculation and the data points for many different nuclei. A few comments are in order. The region at $x > 0.75$ is characterized by a significant Q^2 dependence and therefore the calculation based upon the average \bar{Q}^2 provided by the experiments is approximate. It must also be noted that in some cases the data points from different experiments are not fully consistent. In particular, the data points on $^{12}\text{C}/\text{D}$ and $^{40}\text{Ca}/\text{D}$ ratios from E665 experiment [12] at low x seem to be systematically above the corresponding NMC measurements, which have smaller uncertainties. Similarly, a normalization problem could be present for $^{207}\text{Pb}/\text{D}$ data from E665. Assuming the effect is common to all heavy targets, in our fits we use instead the double ratios $(^{40}\text{Ca}/\text{D})/(^{12}\text{C}/\text{D})$ and $(^{207}\text{Pb}/\text{D})/(^{12}\text{C}/\text{D})$ and the E665 measurement of the ratio $^{207}\text{Pb}/\text{D}$. The double ratios are in good agreement with NMC data (noticed also in [5]) as well as with our predictions, while the $^{207}\text{Pb}/\text{D}$ points lie slightly above our calculations. Furthermore, the ratio $^7\text{Li}/\text{D}$ shown in Figure 1 indicates a small excess in the region of x between 0.01 and 0.03, which produces corresponding reductions in the ratios $^{12}\text{C}/^7\text{Li}$ and $^{40}\text{Ca}/^7\text{Li}$. The effect is much larger than the quoted systematic uncertainties. For instance, the exclusion of three points at $x = 0.0125, 0.0175, 0.0250$ from our fit leads to the reduction of overall $\chi^2/\text{d.o.f.}$ for the ratio $^7\text{Li}/\text{D}$ from 1.95 to 0.72.¹⁴ We also comment that the value of the $^{207}\text{Pb}/^{12}\text{C}$ ratio at $x = 0.7$ from NMC (Fig. 2) is marginally compatible with the corresponding value of $^{197}\text{Au}/\text{D}$ ratio from E139 experiment.

In the approach followed in this paper DIS F_2 data constrain only the overall shape of the nuclear corrections. We emphasize that at low x there is an interplay between the off-shell function, the pion contribution and the coherent nuclear effects. This results in significant correlations between the corresponding parameterizations and does not allow an unambiguous extraction of individual components without external constraints. In our approach the pion (meson) excess in nuclei is fixed by energy-momentum conservation. In order to disentangle the actual off-shell function from the remaining coherent correction, we use additional information from photoproduction experiments (Section V G 1). The agreement between our independent extraction of the average VMD parameters and the photoproduction limit makes us confident in the deconvolution of the different components.

We further check the interplay between the nuclear pion excess and the off-shell function in our analysis by fitting F_2 data without taking into account explicitly the pion contribution. We use for this test a higher order polynomial with respect to Eq.(112), without any fixed parameter. This is intended to avoid biases from the functional form used to model the off-

¹³ Unfortunately it is not possible to have data points covering both the high and low x regions for all nuclei.

This can result in a small sensitivity to some of the parameters for specific nuclei, as can be seen from the uncertainties in Table II.

¹⁴ The comment is only intended to quantify the effect. We keep all data in our fits, regardless of the inconsistencies described above.

shell function. The results obtained for the effective $\delta f'_2$ are consistent with the calculation from Eq.(115). Moreover, the best fit corresponds to a value of Q_0^2 in agreement with our previous determination.

Figure 3 illustrates different nuclear corrections to the ratio of F_2 of ^{197}Au to that of the isoscalar nucleon (*i.e.* $F_2^N = \frac{1}{2}(F_2^p + F_2^n)$) calculated in our model using the final parameters shown in the last line of Table II.

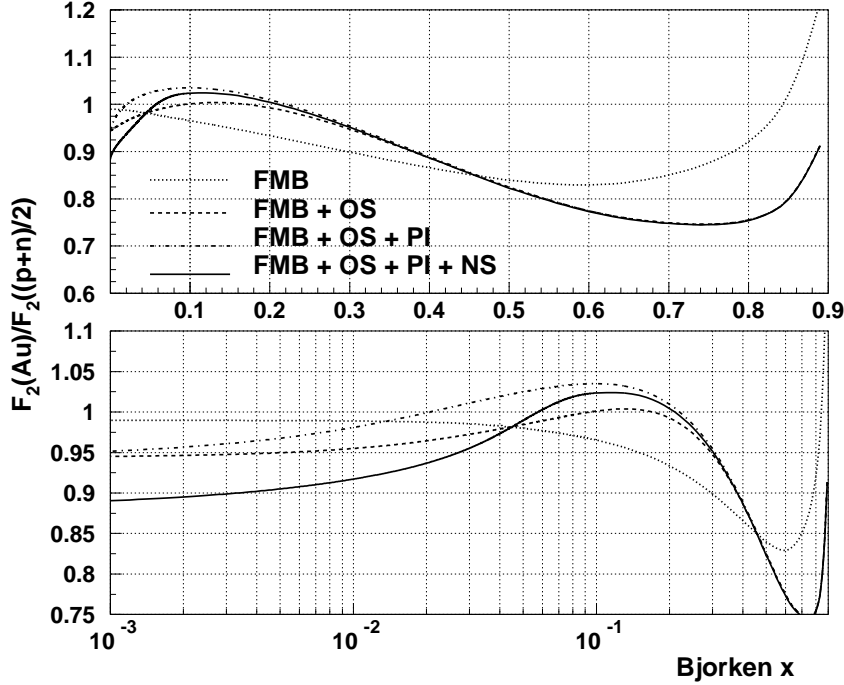


FIG. 3: Different nuclear effects on the ratio of ^{197}Au to isoscalar nucleon for F_2 at $Q^2 = 10 \text{ GeV}^2$. The labels on the curves correspond to effects due to Fermi motion and nuclear binding (FMB), off-shell correction (OS), nuclear pion excess (PI) and coherent nuclear processes (NS). All curves include target mass and the neutron excess corrections.

3. Systematic uncertainties

Systematic uncertainties of the model are evaluated by varying each of the contributions from the deuterium wave function, the spectral function, the parton distributions, the pion structure function and the functional forms of $\delta f(x)$ and $\bar{\sigma}(Q^2)$. New fits are then performed and systematics are defined from the corresponding variation of the nuclear parameters and from the global χ^2 values. Results are listed in Table IV.

Although we do not use directly deuterium data for the fits, most of the data points come from the ratios R_2 of a heavy target to deuterium. In order to study the sensitivity of our result to the choice of the deuteron wave function we performed independent fits with two different choices of the deuteron wave function: the one which corresponds to the Bonn

Systematics	δC_N	δx_0	δQ_0^2 [GeV ²]
Deuteron wave function	0.238	0.0016	0.026
Nuclear spectral function	0.451	0.0046	0.021
Parton distributions	0.005	0.0007	0.023
Pion structure function	0.050	0.0020	0.065
Functional form	0.120	0.0040	0.070
Cross-sections σ_0 and σ_1	0.015	0.0005	0.165
Total	0.526	0.0067	0.195

TABLE IV: The estimate of systematic uncertainties on the extraction of nuclear parameters. See text for a detailed explanation.

potential [64] and the Paris wave function [65]. These two wave functions have different high-momentum component and in this respect represent two extreme situations.

Similarly, we modify the high-momentum component of the momentum distribution $n_1(\mathbf{p})$ in the spectral function by multiplying it by the ratio of the Bonn and Paris deuteron wave functions squared. This is motivated by the observation [69, 70] that for finite nuclei and nuclear matter the nuclear momentum distributions at high momenta ($|\mathbf{p}| > p_F$ with p_F the Fermi momentum) are proportional to the deuteron wave function. We then repeat our fits with modified spectral functions in order to estimate the corresponding variations on the parameters of the model.

The systematic uncertainty related to the parton distributions is estimated by varying the PDFs within their uncertainty ($\pm 1\sigma$). In addition, we also use different sets of parton distributions, extracted from fits to different data samples, with different Q^2 boundaries and different parameterization for the low Q^2 extrapolation.

For the pion structure function, we repeat our fits by using both the LO and the NLO approximations of the pionic parton distributions from [42]. We also arbitrarily change the parameterizations [42] within $\pm 10\%$.

We tried different functional forms in Eqs. (112) and (115) to parameterize δf and $\bar{\sigma}$. In particular, for the off-shell function δf we have tried a generic higher order polynomial parameterization in Eq.(112) and also used a parametrization with an additional x^k term, with free parameter k . In spite of the new parameters, all acceptable results (i.e. with χ^2 values comparable to our best fit solution) extracted from fits to data were very similar to expression (112). We emphasize that the behaviour of the function $\delta f(x)$ for $x < 0.75$ is well constrained by data and only small variations on both the shape and the position of the zero x_0 are allowed. This observation in turn results in reduced systematic uncertainties of the model.

For the coherent processes, we varied σ_0 within the uncertainty estimated by averaging over ρ^0 , ω and ϕ mesons, ± 3 mb (Section V E). As explained in Section V G 1, this parameter is strongly correlated with α_T and Q_0^2 . Similarly, we varied σ_1 within the 1σ allowed range (Section V G 1). We also tried to change the exponent controlling Q^2 dependence in Eq.(115). We obtained almost equally good fits with the dipole and monopole forms in Eq.(115). The monopole form of Eq.(115) had lower $\chi^2/\text{d.o.f.}$ for the overall data set.

Figure 4 shows the off-shell function $\delta f(x)$ and the effective cross-section $\bar{\sigma}(Q^2)$ obtained in Section V G 2, together with the corresponding total uncertainty bands (including both

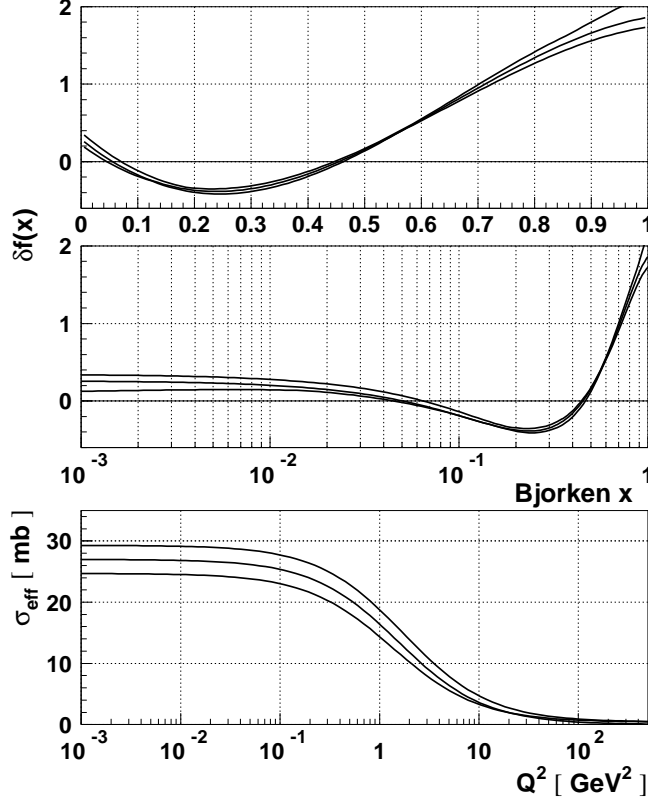


FIG. 4: Off-shell function $\delta f(x)$ and effective cross-section $\bar{\sigma}(Q^2)$ corresponding to the parameters from Table II. The curves show the size of the uncertainty bands ($\pm 1\sigma$), including both statistical and systematic (Table IV) uncertainties. The effect of different functional forms is also included, as explained in Section V G 3.

statistical and systematic uncertainties).

The final results are dominated by systematic uncertainties, as can be seen from Tables II and IV. However, we note that the size of systematic uncertainties is constrained by the value of χ^2 of a global fit to data, as explained above. Therefore, the availability of more accurate (or with wider coverage of kinematics and nuclei) experimental measurements would significantly improve our results.

VI. DISCUSSION

We now discuss the results obtained from our fit to nuclear data in Section V G. In Section VI A we address the problem of the normalization of the valence quark number and Section VI B is focused on the implication of this constraint for our analysis. Section VI C is devoted to the Q^2 and A dependence of nuclear effects predicted by our model. In Section VI D we discuss nuclear effects on the deuteron structure functions.

A. Valence quark number

It is instructive to study the contributions due to different nuclear effects to the normalization of valence quark distribution in a nucleus. Common wisdom is that this quantity should not be corrected by nuclear effects since it counts the baryon number of the system. Therefore, it is important to verify if different nuclear effects cancel out in the normalization. In the impulse approximation, *i.e.* if no shadowing and off-shell effects are taken into account, the cancellation of nuclear binding and Fermi motion effects in the normalization is explicit and it is guaranteed by the normalization of nucleon distribution function (43) to the number of nucleons. It should be also noted that nuclear pions do not contribute to nuclear valence distribution. In the presence of off-shell (OS) and nuclear shadowing (NS) effects different contributions to the valence quark normalization per one nucleon can be written as follows

$$N_{\text{val}/A} = \int_0^A dx q_{\text{val}/A}(x) = N_{\text{val}/N} + \delta N_{\text{val}}^{\text{OS}} + \delta N_{\text{val}}^{\text{NS}}, \quad (117)$$

$$\delta N_{\text{val}}^{\text{OS}} = \int_0^1 dx q_{\text{val}/N}(x) \delta f_{\text{val}}(x) \langle v \rangle, \quad (118)$$

$$\delta N_{\text{val}}^{\text{NS}} = \int_0^1 dx q_{\text{val}/N}(x) \delta R_{\text{val}}(x) \quad (119)$$

where $N_{\text{val}/N} = 3$ is the number of valence quarks in the nucleon and $\langle v \rangle = \langle p^2 - M^2 \rangle / M^2$ is the bound nucleon off-shellness averaged over nuclear spectral function. The notation $q_{\text{val}/N}(x)$ denotes the nucleon valence quark distribution, while $\delta R_{\text{val}}(x)$ is the shadowing correction to the valence quark distribution (for more details see Section VII A).

Following the approach of Section V G we determine the phenomenological function $\delta f_2(x)$, which describes off-shell effects for F_2 , from available data on the ratio R_2 . We need then to examine the relation between $\delta f_2(x)$ and the corresponding off-shell corrections for valence and sea quark distributions in the bound nucleon. We recall that $\delta f_2(x)$ is related to $\delta f_{\text{val}}(x)$ and $\delta f_{\text{sea}}(x)$ by Eq.(65). Therefore, at large x , at which the contribution from sea quarks can be neglected, $\delta f_2 = \delta f_{\text{val}}$. At smaller x values the contribution from the sea quark term is enhanced by the sea/valence ratio r .

In the present work we use only information on F_2 from DIS data. For this reason it is difficult to unambiguously disentangle off-shell effects for valence and sea distributions. We then test different assumptions by evaluating the corresponding off-shell corrections to the nuclear valence quark number. The analysis of additional data from either Drell-Yan production or neutrino scattering would be also very important for such studies. While we defer a detailed analysis of the existing Drell-Yan data from nuclear targets [14] to a future publication, no sensitive neutrino data about nuclear effects on structure functions is currently available (see also the discussion in Section VII B).

Let us first assume $\delta f_{\text{val}} = \delta f_2$ for any x . From Eq.(65) we then also have $\delta f_{\text{sea}} = \delta f_2$, that implies that we have a universal off-shell function for both valence and sea quark distributions. We evaluate $\delta N_{\text{val}}^{\text{OS}}$ by Eq.(118) as a function of Q^2 using the parameters of $\delta f(x)$ from Table II and the nucleon valence distribution of [39]. The results for iron and lead are reported in Fig. 5, indicating a positive off-shell correction of about 1.5 – 2% that decreases with Q^2 . We then compute the shadowing correction $\delta N_{\text{val}}^{\text{NS}}$ by Eq.(125b) using the effective cross section extracted from our fits (see Section V E). The results are shown

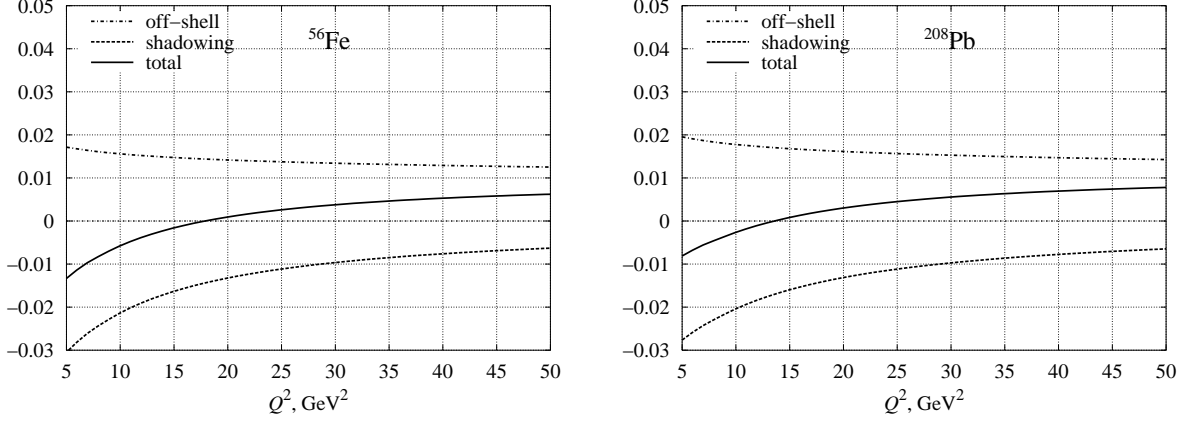


FIG. 5: Relative off-shell ($\delta N_{\text{val}}^{\text{OS}}/3$) and nuclear shadowing ($\delta N_{\text{val}}^{\text{NS}}/3$) corrections to the normalization of the valence quark distribution for ^{56}Fe and ^{208}Pb nuclei (left and right panel, respectively) computed as described in Section VI A. The solid curve shows the sum of the off-shell and the nuclear shadowing corrections.

in Fig. 5. It is important to observe that $\delta N_{\text{val}}^{\text{NS}}$ is negative and there is large cancellation between off-shell and shadowing effects in the normalization over a wide range of Q^2 .

Let us now discuss a different hypothesis, namely no off-shell effect in the sea of bound nucleon $\delta f_{\text{sea}} = 0$. From Eq.(65) we then have $\delta f_{\text{val}} = (1+r)\delta f_2$. It should be remarked that the presence of the factor $r = q_{\text{sea}}/q_{\text{val}}$ results in a strong rise of δf_{val} at small x , which is hard to justify. In particular, the off-shell correction to valence quark number is dominated by the small x region in this case and it even becomes divergent.¹⁵ Therefore, this assumption leads to unphysical results and we have to rule out this case.

B. Normalization constraints

In the following we will favor the assumption of a single universal off-shell function $\delta f(x)$, according to discussion of Section VI A. This is supported by the existing R_2 data we used to extract the phenomenological off-shell function. The universality of $\delta f(x)$ should be further verified with both Drell-Yan data and future precise neutrino data. In our analysis we use the normalization condition in order to fix parameters of the function $\delta f(x)$, in particular the parameter x_1 . As explained in Section V G 2, within all possible values of x_1 providing comparable descriptions of data (χ^2) we selected the one minimizing the overall correction $\delta N_{\text{val}}^{\text{OS}} + \delta N_{\text{val}}^{\text{NS}}$.

We note that in a certain sense $\delta f(x)$ can be considered as a new structure function of bound nucleon which measures the change of nucleon quark-gluon structure in nuclear environment (see discussion in Section V G 2). This structure function is not accessible in experiments with isolated proton and/or neutron but can generally be probed in nuclear reactions.

¹⁵ We obtain $\delta N_{\text{val}}^{\text{OS}}/3 \approx -0.5$ for iron if we cut off the contribution of the region $x < 10^{-5}$. Changing the lower limit to $x = 10^{-6}$ increases the magnitude of this correction by about factor of 2.

The phenomenological cross section in Eq.(115) effectively incorporates contributions to structure functions due to all twists since it is extracted from data. Higher twists are known to be important at low and intermediate Q^2 and for this reason we should not expect an exact cancellation between $\delta N_{\text{val}}^{\text{OS}}$ and $\delta N_{\text{val}}^{\text{NS}}$ calculated with phenomenological cross section. Nevertheless, we observe from Fig. 5 that the cancellation becomes more accurate at higher Q^2 indicating transition to the leading twist regime. In particular, the exact cancellation takes place at $Q^2 \approx 15 \text{ GeV}^2$. We performed similar calculation for several nuclei and we thus verified that this effect is independent of the choice of the nucleus.

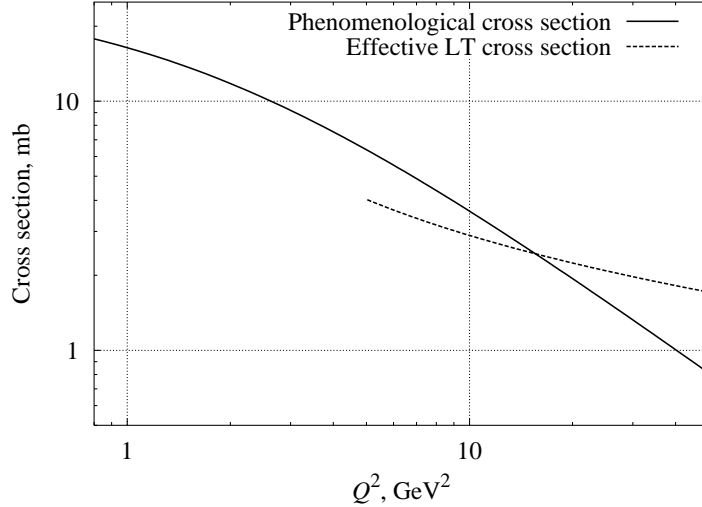


FIG. 6: Phenomenological cross section $\bar{\sigma}_T$ extracted from our fits (solid curve) and effective LT cross section (dashed curves) computed for iron and lead nuclei as described in Section VIA.

It should be noted that the nuclear data available in the shadowing region are limited to relatively low Q^2 and for this reason the phenomenological cross section (115) is not constrained at high Q^2 . In this work we evaluate the effective cross section at high Q^2 by treating the condition $\delta N_{\text{val}}^{\text{OS}} + \delta N_{\text{val}}^{\text{NS}} = 0$ as an equation on the cross section. We solve this equation numerically using the off-shell function $\delta f(x)$ from Section VG 2. The resulting cross section is presented in Fig. 6 together with phenomenological cross section extracted from our fits. In this paper we use the following simple model for the effective cross section. For Q^2 below the crossing point in Fig. 6 we use phenomenological cross section (115) extracted from the fits, and for higher Q^2 we use the cross section calculated from the normalization condition. The difference between the two curves in Fig. 6 below the crossing point is attributed to high-twist effects.

The function $\delta f(x)$ is positive for $x < x_1$ (see Fig. 4). This implies a negative off-shell correction to the structure functions at small Bjorken x because the offshellness v of a bound nucleon is negative. Thus the off-shell correction at small x appears as a leading twist shadowing correction. Therefore, in this region there is a certain interplay between nuclear effects due to coherent nuclear interactions and off-shell effect. In the region $x_1 < x < x_0$ the function $\delta f(x)$ is negative that provides an enhancement of bound nucleon structure functions. Thus in our approach the antishadowing at $x \sim 0.1$ is linked to off-shell effects. It is important to note that for the valence distributions there is additional antishadowing mechanism due to coherent nuclear interactions. Indeed, the presence of substantial real

part in the C -odd channel ($\alpha_3 = 1$) results in the constructive interference of multiple scattering interactions at $x \sim 0.1$ for valence distributions as will be discussed in more detail in Section VII A.

C. The Q^2 and A dependence

In order to illustrate the Q^2 dependence of R_2 in our model, in Fig. 7 we plot the ratio $R_2(\text{Fe}/N)$, where N is isoscalar nucleon $(p+n)/2$, as a function of x for a few fixed Q^2 . We observe from Fig. 7 significant variations of the ratio R_2 with Q^2 at small $x < 0.1$ and large $x > 0.65$. This Q^2 dependence can be attributed to several effects. In the nuclear shadowing region at small x the Q^2 dependence of the ratio R_2 is due to the corresponding dependence of effective cross section $\bar{\sigma}$ (see Eq.(115) and Fig. 4). It must be also noted that in the region of x between 0.01 and 0.1 the Q^2 dependence of R_2 is affected by the Q^2 dependence of longitudinal correlation length $1/k_L$ (see Section IV B and Eqs. (73) and (84)). For $0.1 < x < 0.65$ the Q^2 dependence of R_2 is negligible. At large x the Q^2 dependence is due to the target mass correction effect by Eq.(23) in convolution equations.

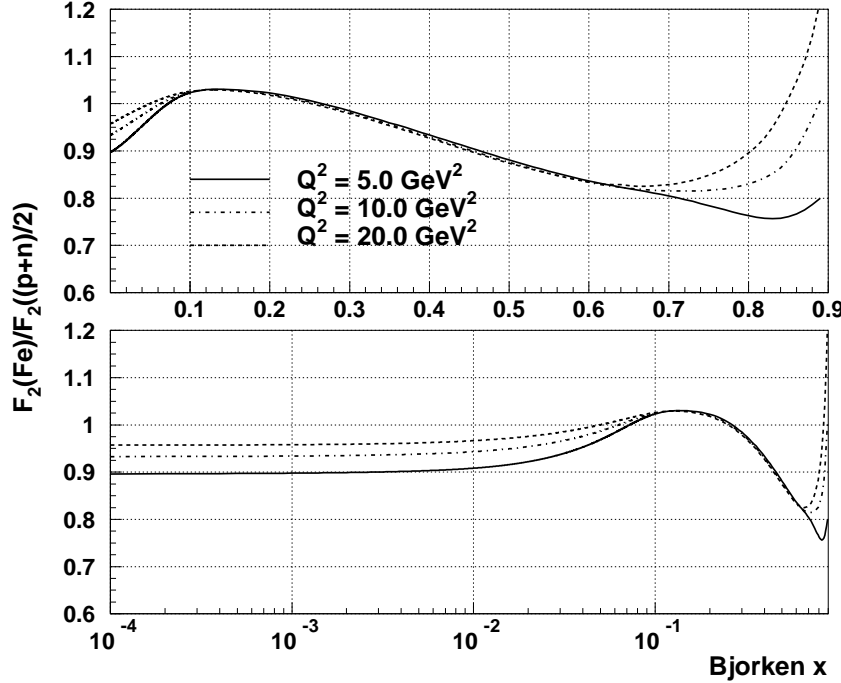


FIG. 7: Our predictions for the ratio of ^{56}Fe and isoscalar nucleon structure functions calculated for $Q^2 = 5, 10, 20 \text{ GeV}^2$. The calculation takes into account the non-isoscalarity correction for iron by Eq.(60).

In Fig. 8 we compare the NMC data on Q^2 dependence of the ratio $R_2(\text{Sn}/\text{C})$ with our calculations. We observe an overall good agreement between data and model calculations for all values of x within available region of Q^2 . However, it should be remarked that available data on Q^2 dependence of nuclear effects are still too scarce to make thorough

phenomenological studies of this effect. In particular, the correlation between x and Q^2 for fixed target experiments and the lack of information about the Q^2 distributions of data in each of the x bins used (typically only the average Q^2 is provided) can potentially bias the calculations where a significant Q^2 dependence is expected.

Figures 1 and 2 show that the model reproduces correctly the ratios R_2 over a wide range of nuclei and kinematic regions. The A dependence of the ratio R_2 is illustrated in Fig. 9 for a few fixed values of x . At small x the A dependence is related to the multiple scattering coefficients in Eqs. (84) and (89), through the nucleon number density distributions. The increase in the nuclear shadowing effect with A has "geometrical" origin and can be attributed to the rising size of heavy nuclei. At large x the A dependence of the ratio R_2 is determined by the corresponding dependence of parameters of nuclear spectral function. The slope of R_2 as a function of x at intermediate $x = 0.5$ – 0.6 increases with A because of the corresponding increase in the average separation and kinetic energy of bound nucleons. It is interesting to note that at $x \approx 0.3$ the ratio R_2 depends on neither A nor Q^2 .

D. Nuclear effects in Deuterium

Understanding of nuclear effects in deuterium is an important issue since deuterium data are often used as the source of information on neutron structure functions. As explained in Section V G, the determination of d and u parton distributions is sensitive to nuclear corrections to deuterium data (Section III B). In this Section we apply the off-shell function $\delta f(x)$ and effective cross section $\bar{\sigma}$ from our fit to data from heavy nuclei in order to calculate nuclear modifications in deuterium and compare our predictions with data. The calculation of the deuteron structure function directly follows from Eqs.(53), nuclear shadowing and pion corrections as explained in Sections IV B 1, IV A 3, V C. It should be emphasized that our approach does not require any extrapolation from heavy nuclei to deuterium.

The ratio of the deuteron and the proton structure functions $R_2(D/p) = F_2^D/F_2^p$ was measured by the E665 and NMC collaborations [2, 11] in a wide kinematical region of x and Q^2 . A comparison with these data provide a good test of the applicability of our model to D, since these data were not used in the fits described in Section V G. In Fig. 10 we show the E665 and NMC data together with the results of our calculations. A good agreement is found between data and the model described in this paper. In particular, our prediction of a small shadowing effect in D seems to be supported by the measured values of $R_2(D/p)$ at small values of x . We note the ratio $R_2(D/p)$ also provides a check of the parton distributions used in our calculation and in particular of the difference between d and u quark contents. This was not the case for all the remaining data listed in Table I which were corrected by experiments for non-isoscalarity, thus providing an effective cancellation of PDFs in the ratios $R_2(A'/A)$ (Section V G).

Unlike the ratio $R_2(D/p)$ the ratio $R_2(D/N) = F_2^D/F_2^{p+n}$ cannot be measured directly because a free neutron target is not available. A phenomenological model of the EMC effect in the deuterium was discussed in Ref.[10]. In this model the ratio $R_2(D/N)$ was extracted by extrapolating the measured ratios $R_2(A/D)$ using nuclear density model of Ref.[27]. The key assumption was made in Ref.[10] that the quantity $R_2(A/N) - 1$ scales as nuclear number density. It was also assumed that this ratio is independent of Q^2 . The values of $R_2(D/N)$ were given in [10] for x corresponding to the x bins of SLAC data. The results are shown in Fig. 11 together with our calculation of the ratio $R_2(D/N)$ for the same kinematics of

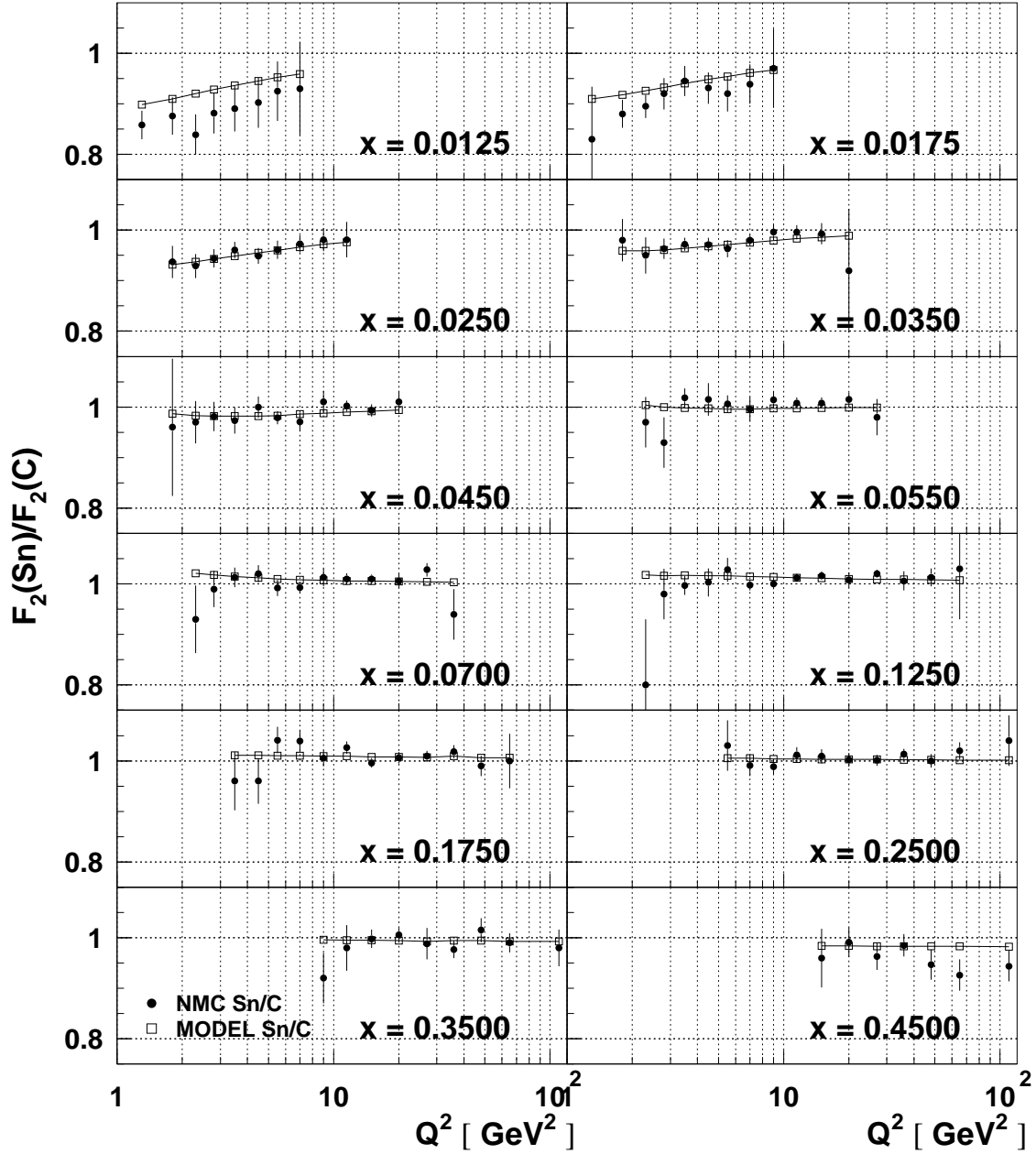


FIG. 8: The Q^2 dependence of the ratio $R_2(\text{Sn/C})$ for different values of x as measured by the NMC [5]. The curves with open squares show the corresponding model calculations. For data points the error bars correspond to the sum in quadrature of statistical and systematic uncertainties, while the normalization uncertainty is not shown.

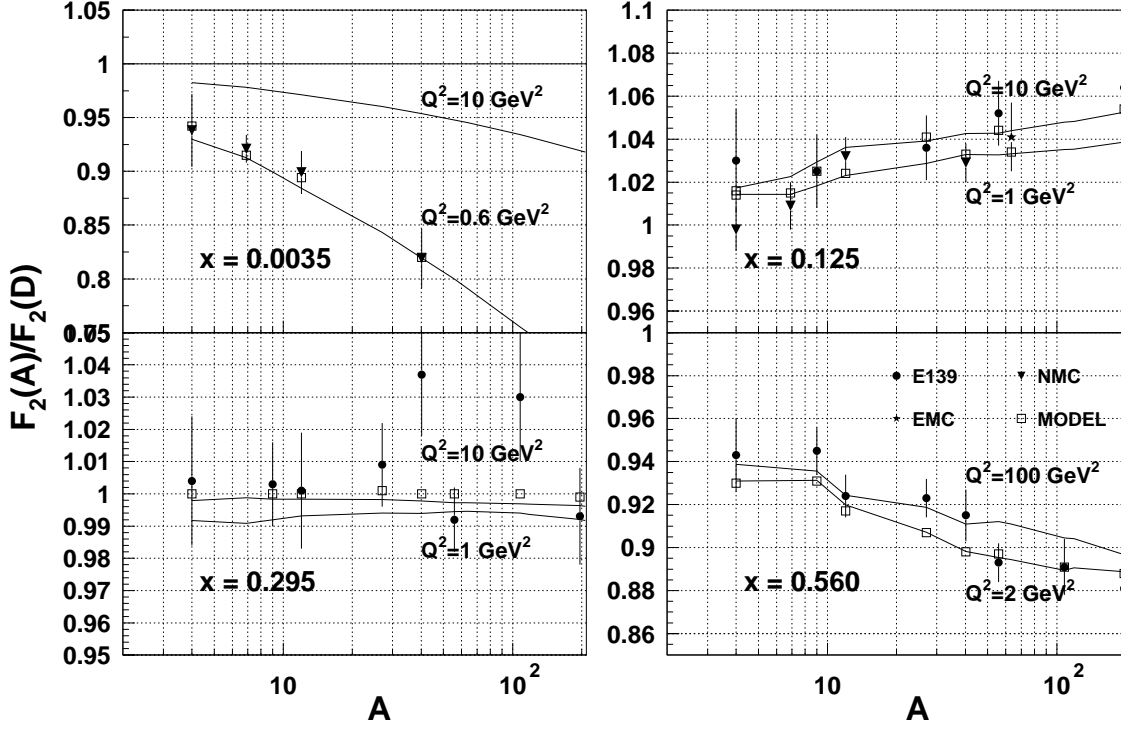


FIG. 9: The ratio $R_2(A/D)$ as a function of A for different values of x . The open squares show the model calculations corresponding to the average Q^2 of the data points. For data points the error bars correspond to the sum in quadrature of statistical and systematic uncertainties, while the normalization uncertainty is not shown. Two curves calculated at constant Q^2 values are also shown for comparison.

the points presented in Ref.[10].¹⁶ In Fig. 12 we show our prediction for the ratio $R_2(D/N)$ at fixed $Q^2 = 10 \text{ GeV}^2$ and the corresponding uncertainty band ($\pm 1\sigma$), including model systematics.

VII. APPLICATIONS

In this Section we apply our results to evaluate nuclear parton distributions (Section VII A) and make the predictions of nuclear effects for neutrino structure functions (Section VII B).

¹⁶ The theoretical uncertainties of such extrapolation were not estimated in Ref.[10]. See also discussion in Ref.[52].

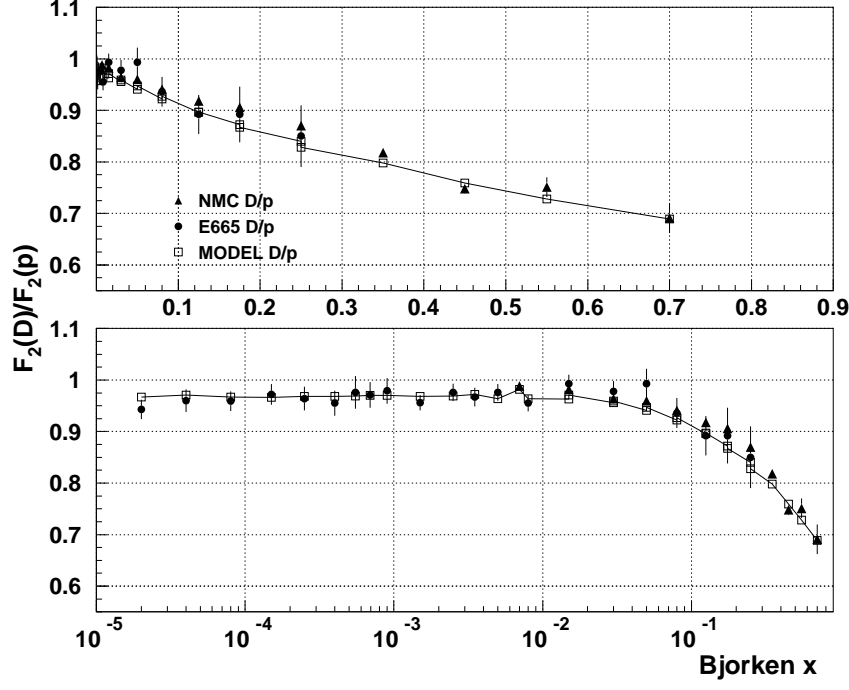


FIG. 10: Comparison of E665 and NMC data to our calculations (curve with open squares) for the ratio $R_2(x, D/p)$. For data points the error bars correspond to the sum in quadrature of statistical and systematic uncertainties, while the normalization uncertainty is not shown.

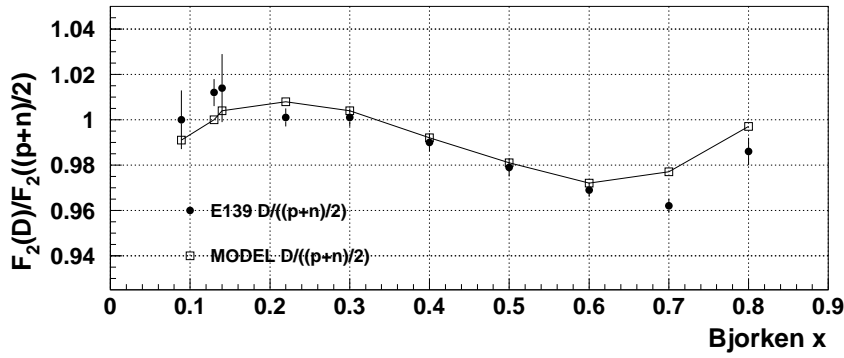


FIG. 11: Comparison of the extrapolations of E139 nuclear data within the nuclear density model of Ref.[10] to our calculations (curve with open squares) for the ratio $R_2(x, D/N)$. The error bars on the E139 points correspond to the sum in quadrature of statistical and systematic uncertainties. For each x value, the model calculation was performed at the average Q^2 of the experimental points quoted in Ref.[10].

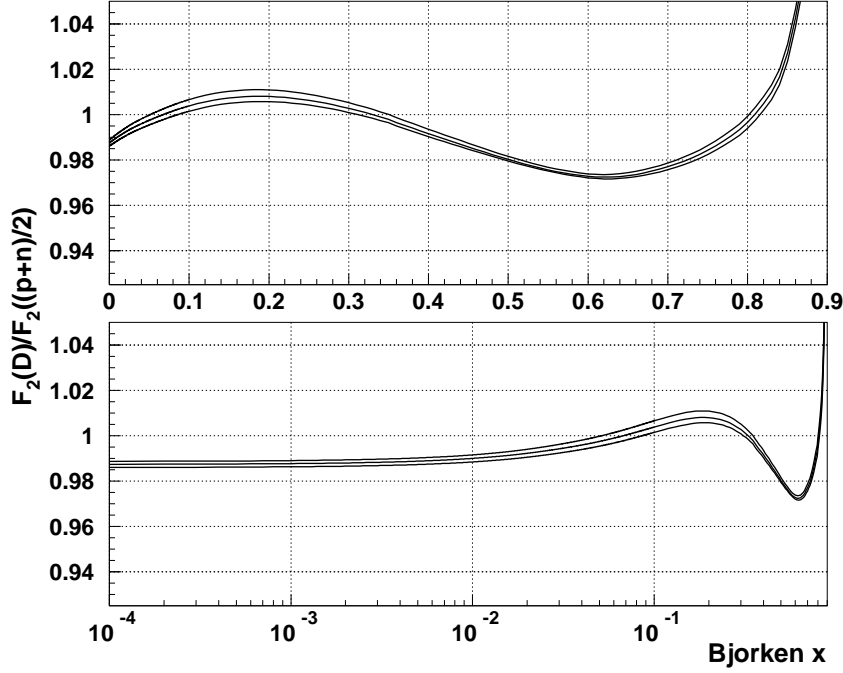


FIG. 12: Our predictions for the ratio $R_2(x, D/N)$ of deuteron to isoscalar nucleon at a fixed $Q^2 = 10 \text{ GeV}^2$. The $\pm 1\sigma$ band is also given, including both statistical and systematic uncertainties.

A. Nuclear parton distributions

At high Q^2 the structure functions are described in terms of parton distributions as discussed in Section III A 1. The PDFs are independent of the process but do depend on the considered target. Different phenomenological approaches to the extraction of nuclear PDFs (nPDFs) can be found in Refs. [75, 76, 77, 78]. It should be remarked at this point that physics observables are the cross sections and the structure functions, which include contributions from all twists. The higher-twist terms are generally process-dependent, can be essential in the region of relatively low Q^2 , and, furthermore, can be substantially affected by nuclear environment. Therefore, the applicability of leading twist calculations must be considered in comparison with data as well as in any attempt to extract nPDFs. In our approach, the calculation of nPDFs follows directly from the analysis of Sections V G 2 and V I B, which allows us to determine both nPDFs and their uncertainties from existing data. However, this paper is not aimed at the full nPDF analysis, which can be published elsewhere [80]. We rather want to discuss different physics effects which cause modifications of nuclear quark distributions. The numerical results shown in this Section were obtained using the NNLO approximation of proton and neutron PDFs described in Section III B.

1. Nuclear convolution

As discussed in Sect. IV, in the region of high Q^2 and large x the nuclear structure functions can be approximated by incoherent contributions from different nuclear constituents which can be presented in a convolution form (see Eqs. (42) and (50)). The convolution formulas look very similar for all type of nuclear structure functions suggesting that the convolution equations hold for the parton distributions. We denote $q_{a/T}(x, Q^2)$ the distribution of quarks of type a in a target T . Then the quark distribution in a nucleus can be written as

$$q_{a/A}(x, Q^2) = \sum_{c=p,n,\pi} f_{c/A} \otimes q_{a/c}, \quad (120)$$

where the function $f_{c/A}(y, v)$ can be interpreted as the distribution of particles of type c in a nucleus over light-cone momentum y and invariant mass (virtuality) v (for bound nucleons and nuclear pions see Eqs. (43) and (51), respectively). The operation $f \otimes q$ denotes the convolution

$$f \otimes q = \int_{x < y} \frac{dy dv}{y} f(y, v) q(x/y, Q^2, v). \quad (121)$$

Equations similar to (120) can be written for antiquark and gluon distributions in nuclei. Note also that the distribution functions are independent of Q^2 and, therefore, the Q^2 evolution of nuclear PDFs is governed by the evolution of PDFs of nuclear constituents.

It is useful to sort out the contributions to the convolution equation according to isospin. Let us consider the isoscalar and isovector quark distributions, $q_0 = u + d$ and $q_1 = u - d$. We first consider the contributions from bound protons and neutrons to nuclear quark distributions. Assuming exact isospin invariance of PDFs in the proton and neutron we have simple relations between the isoscalar and the isovector distributions in the proton and the neutron

$$q_{0/p}(x, Q^2) = q_{0/n}(x, Q^2), \quad (122a)$$

$$q_{1/p}(x, Q^2) = -q_{1/n}(x, Q^2). \quad (122b)$$

Using these relations we observe that the quark distributions with different isospin decouple in the convolution equation. In particular, for the isoscalar ($q_{0/A}$) and the isovector ($q_{1/A}$) nuclear quark distributions we have

$$q_{0/A}(x, Q^2) = A f_0 \otimes q_{0/p}, \quad (123a)$$

$$q_{1/A}(x, Q^2) = (Z - N) f_1 \otimes q_{1/p}, \quad (123b)$$

where f_0 and f_1 are the isoscalar and the isovector nucleon distributions in a nucleus. These distributions are given by Eq.(42) with the spectral functions \mathcal{P}_0 and \mathcal{P}_1 defined by Eq.(58). Note that the distributions f_0 and f_1 are normalized to unity.

We now discuss the pion contribution. Similar to the nucleon case, we assume the isospin relations for quark distributions in the pion: $q_{0/\pi^+} = q_{0/\pi^-} = q_{0/\pi^0}$ and $q_{1/\pi^+} = -q_{1/\pi^-}$ and $q_{1/\pi^0} = 0$. Using these relations we have for the pion correction to nuclear quark distributions with given isospin

$$q_{0/A}^\pi(x, Q^2) = f_{\pi/A} \otimes q_{0/\pi}, \quad (124a)$$

$$q_{1/A}^\pi(x, Q^2) = (f_{\pi^+/A} - f_{\pi^-/A}) \otimes q_{1/\pi}. \quad (124b)$$

Here in the first equation $f_{\pi/A}$ is the sum of the pion distributions of all charged-states. It should be emphasized that in Eqs.(124) the pion distributions refer to nuclear pion excess, since scattering off virtual pions emitted and absorbed by same nucleon (nucleon pion cloud) are accounted in the proton and neutron PDFs. For the calculation of nuclear pion distributions in our model see Sect. V C. It should be again stressed that the distributions with different isospin decouple in Eqs.(124).

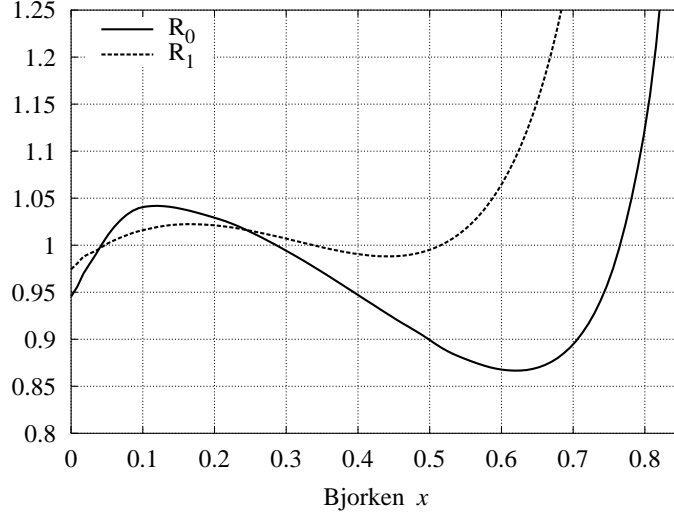


FIG. 13: Nuclear effects for the isoscalar and the isovector quark distributions in iron nucleus. The ratios R_0 and R_1 (see text) were calculated for the valence quark distributions at $Q^2 = 20 \text{ GeV}^2$. Nuclear shadowing and pion corrections are also included for the isoscalar distribution.

The isovector component should vanish in isoscalar nuclei with $Z = N$.¹⁷ However, for a generic nucleus with different number of protons and neutrons both the isoscalar and the isovector distributions are present. Heavy nuclei typically have a small excess of neutrons over the protons and the distributions f_0 and f_1 are quite different in such nuclei, as discussed in Section IV A 5. For this reason nuclear effects in PDFs depend on isospin. In order to illustrate this statement we calculate the ratios $R_0(x) = q_{0/A}(x)/(A q_{0/p}(x))$ and $R_1(x) = q_{1/A}(x)/[(Z - N)q_{1/p}(x)]$ for the iron nucleus using the proton PDFs of Ref.[39]. The results are shown in Fig. 13. We note that the full nuclear correction for $q_{0/A}$ is shown Fig. 13, *i.e.* the calculation includes effect of nuclear spectral function, off-shell correction, nuclear pion and shadowing effects. However, for the isovector quark distribution $q_{1/A}$ we did not discuss possible nuclear pion and shadowing effects.

¹⁷ It should be remarked that the condition $Z = N$ does not insure the total nuclear isospin 0. If higher-isospin states are present for a $Z = N$ nucleus, then the isovector distribution $q_{1/A}$ may be non-zero. The discussion of these issues is postponed for future studies.

2. Nuclear shadowing

In this Section we discuss coherent nuclear effects in the context of parton distributions. To this end we want to apply the approach discusses in Section IV B 2. The multiple scattering effects are generally different for different PDFs. We specify this statement by considering nuclear effects for quark distributions of different C parity, $q^{(\pm)}(x) = q(x) \pm \bar{q}(x)$. In order to simplify discussion we consider the isoscalar (anti)quark distributions, $q = u + d$ and $\bar{q} = \bar{u} + \bar{d}$. The C -odd distribution is in fact the valence quark distribution in the target $q^{(-)} = q_{\text{val}}$. The C -even distribution at small x describes the target quark sea.

In order to bridge between Section IV B and the present discussion we recall that the structure function F_1 in the LT approximation is given by C -even distribution $q^{(+)}$. The structure function F_1 is transverse helicity structure function (to be more precise, the average over left- and right-polarized transverse helicity structure function, see Eq.(19)). At small x , as discussed in Section IV B, nuclear effects are described by the propagation of hadronic component of virtual boson with the proper helicity state in nuclear environment. Equation (85) applies in the case of $q^{(+)}$.

Similarly, the structure function F_3 in the LT approximation is given by C -odd (valence) distribution $q^{(-)}$. In terms of helicity structure functions this is the asymmetry between left- and right-polarized states. Therefore, nuclear corrections to $q^{(-)}$ at small x can be described by Eq.(88). We have for coherent nuclear corrections to $q^{(+)}$ and $q^{(-)}$ quark distributions

$$\delta R^{(+)} = \frac{\delta q_A^{(+)}(x)}{q_N^{(+)}(x)} = \text{Re } f^2 \mathcal{C}_2^A / \text{Im } f, \quad (125a)$$

$$\delta R^{(-)} = \frac{\delta q_A^{(-)}(x)}{q_N^{(-)}(x)} = (2 \text{Re } f_3 f \mathcal{C}_2^A - \text{Im } f_3 f^2 \mathcal{C}_3^A) / \text{Im } f_3, \quad (125b)$$

where \mathcal{C}_2^A and \mathcal{C}_3^A are given by Eqs. (84) and (89) with effective transverse scattering amplitude $f = (i + \alpha_T) \bar{\sigma}_T / 2$. Equation (125b) determines the nuclear shadowing effect for valence quark distribution $\delta R_{\text{val}} = \delta R^{(-)}$. The amplitude f_3 describes the left-right asymmetry in the transverse amplitude. In other terms f_3 can be interpreted as the difference between $\bar{q}N$ and qN scattering amplitudes [62]. As discussed in Section IV B 2 the correction $\delta R^{(-)}$ does not depend on the specific value of the cross section asymmetry σ_3 but does depend on $\alpha_3 = \text{Re } f_3 / \text{Im } f_3$. The rate of nuclear effects for both C -even and C -odd distributions is determined by transverse amplitude f . Nuclear shadowing effect for antiquark distributions can readily be derived from Eqs. (125a) and (125b) and we have

$$\delta R_{\text{sea}} = \frac{\delta \bar{q}_A(x)}{\bar{q}_N(x)} = \delta R^{(+)} + \frac{q_{\text{val}/N}(x)}{2\bar{q}_N(x)} (\delta R^{(+)} - \delta R^{(-)}). \quad (126)$$

The results of calculation of nuclear effects for valence quark and antiquark distributions are reported in Fig. 14. The calculations account of the effects of smearing with nuclear spectral function (FMB), off-shell corrections (OS), nuclear shadowing (NS), and nuclear pion (PI) corrections. The FMB, OS, and PI corrections have been computed as discussed in Sect. VII A 1 using our model spectral function, pion distribution function¹⁸ and off-shell correction described in Sect. V. The NS correction for valence and sea distributions are

¹⁸ We note that nuclear pion effect vanishes for isoscalar valence quark distribution.

computed by Eqs. (125b) and (126) using the parameters of effective scattering amplitude derived from our fits (see Sections V G 2 and VIB).

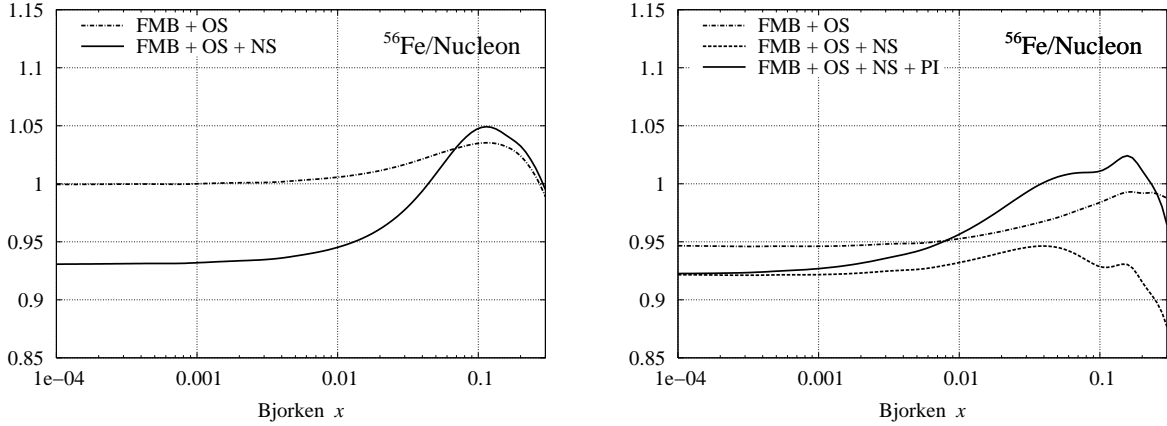


FIG. 14: Nuclear effects for isoscalar valence and sea quark distributions calculated for iron nucleus at $Q^2 = 20 \text{ GeV}^2$ (see text). The left panel displays different nuclear corrections to valence quark distribution: the dot-dashed curve if only the effect of nuclear spectral function (FMB) and off-shell (OS) corrections are taken into account, the full curve is overall nuclear correction including nuclear shadowing effect (NS). The right panel displays similar nuclear corrections for antiquark distribution. The full curve also includes the nuclear pion effect (PI), which is absent for the valence quark distribution.

A few remarks are in order. At small $x < 0.01$ the NS effect for valence quark distribution is enhanced relative to that for nuclear sea. The underlying reason for that is the enhancement of multiple scattering corrections for the cross section asymmetry as discussed in Section IV B 2. If we keep only the double scattering correction then the ratio $\delta R_{\text{val}}/\delta R_{\text{sea}}$ is given by Eq.(81). The OS correction is negative in this region. However, the combined effect of FMB and OS is somewhat different for valence and sea distributions as displayed in Fig. 14. This is attributed to different x dependence of valence and sea in the nucleon which affect the result of the averaging with nuclear spectral function. Nevertheless, in spite of these differences, the overall nuclear corrections are similar for valence and sea for $x < 0.01$.¹⁹

One observes that nuclear corrections for valence and sea distributions are different in the antishadowing region. The antishadowing effect for valence (*i.e.* positive nuclear correction) is a joint effect of two corrections both of each are positive: (1) the FMB and OS corrections and (2) the constructive interference in the multiple scattering effect which is due to a finite real part α_3 of effective scattering amplitude in the C -odd channel (for this reason shadowing becomes antishadowing, see the left panel of Fig. 14). For sea-quark distribution in the antishadowing region we observe cancellation between different effects. In this respect we remark that the contribution of the last term in Eq.(126) becomes increasingly important at $x > 0.05$, because of the ratio $q_{\text{val}/N}(x)/\bar{q}_N(x)$. This term is negative in this region and

¹⁹ Note that this discussion refers to a high $Q^2 \sim 20 \text{ GeV}^2$. At lower Q^2 the balance between different nuclear effects change.

cancels a positive nuclear pion contribution. As a result the overall nuclear correction to antiquark distribution is small for $0.02 < x < 0.2$. Note that this agrees with the results of E772 experiment, in which no enhancement of nuclear sea was observed in DY nuclear processes [14].

It should be noted that calculation of relative nuclear correction for valence quark distribution is stable with respect to the choice of the PDF set for entire region of x (see also Fig. 13 for nuclear correction to valence distributions). Nuclear effects for sea quarks also depend weakly on the particular choice of PDF for small x . However, at high x values the calculation of nuclear effects for antiquark distributions has somewhat larger uncertainties since it is sensitive to both the shape and the magnitude of the nucleon antiquark distribution (note the val/sea ratio in Eq.(126)).

B. Neutrino interactions

In this Section we calculate nuclear effects for neutrino charged-current structure functions using the model developed in the previous sections. The study of neutrino interactions is particularly interesting to this end since they are flavour sensitive and they are strongly influenced by the structure function F_3 , which is not present in the electromagnetic case. We also note that due to the low interaction probability in practice the detection of neutrinos always requires heavy nuclear targets. Therefore, the knowledge of nuclear effects is crucial for understanding of neutrino cross-sections.

In order to compute corrections to F_2^ν and F_3^ν related to the averaging with nuclear spectral function (FMB and OS effects) we apply Eqs. (40) and (41) and use the off-shell function $\delta f(x)$ extracted from the analysis of Section V G 2 for both F_2 and F_3 . Nuclear shadowing/antishadowing corrections are computed as discussed in Section IV B.

We focus here on the region of relatively high momentum transfer $Q^2 > 5 \text{ GeV}^2$ and assume that coherent nuclear interactions driven by axial current are similar to those of vector current at large Q^2 and that they can be described by the effective amplitude extracted from the analysis of Section V E to V G 3²⁰. A detailed study of nuclear effects in (anti)neutrino interactions including the low Q^2 region will be the subject of a future publication [80].

We calculate the ratios $R_2^\nu = F_2^{\nu A}/(AF_2^{\nu N})$ and $R_3^\nu = xF_3^{\nu A}/(x F_3^{\nu N})$, where N denotes the isoscalar nucleon (averaged over proton and neutron), for the most common nuclear targets used by recent neutrino experiments: ^{12}C (NOMAD [81]), ^{56}Fe (NuTeV [82], MINOS [83]), ^{40}Ar (ICARUS [84]) and ^{207}Pb (OPERA [85]). Our results for both F_2 and $x F_3$ are shown in Figures 15 and 16 for different values of Q^2 . We briefly comment on the main features that distinguish the nuclear corrections in neutrino DIS from the ones in charged-lepton DIS (F_2^μ). By comparing Fig. 7 and 15 we observe that nuclear effects for F_2^ν and F_2^μ in the coherent region are similar (note that we restrict the present discussion to relatively high Q^2). However, at large x nuclear effects for F_2^ν and F_2^μ are somewhat different. In particular, we note that $R_2^\nu > R_2^\mu$ in the dip region of $x \sim 0.6 - 0.8$. This is because the neutron excess correction is positive for F_2^ν , while it is negative for F_2^μ (see also Fig. 13). From Fig. 15 and 16 one can also observe that nuclear effects at large x are similar for neutrino F_2 and $x F_3$. However, at small x the nuclear shadowing effect for $x F_3$

²⁰ Note that the interactions of axial-vector current at low Q^2 are essentially different from those of vector current. This region requires a special analysis which goes beyond the scope of the present discussion.

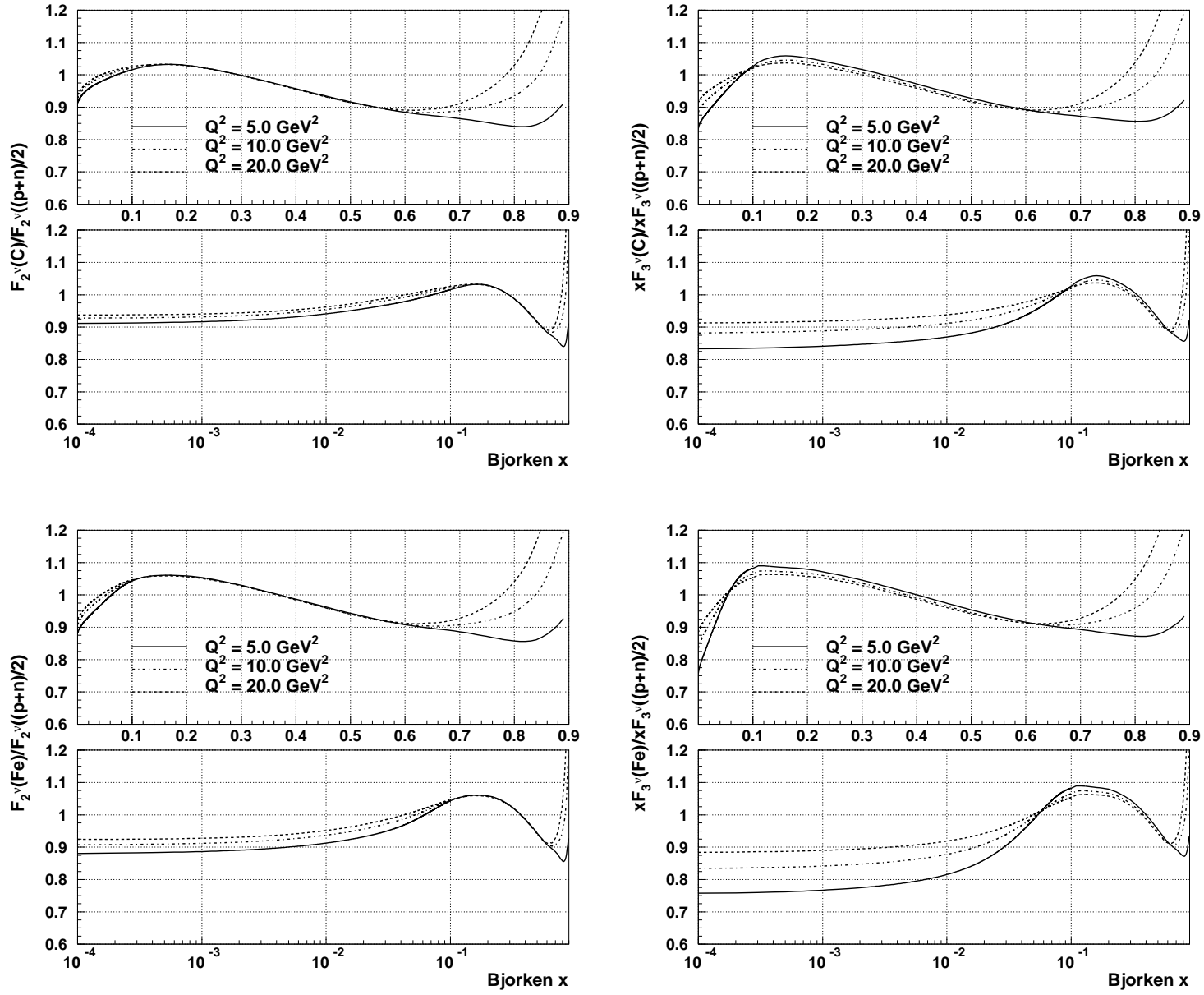


FIG. 15: Our predictions for ratios of F_2 (left plots) and xF_3 (right plots) for neutrino scattering on ^{12}C and ^{56}Fe and the corresponding values on isoscalar nucleon $(p+n)/2$. The curves are drawn for $Q^2 = 5, 10, 20 \text{ GeV}^2$ and take into account the non-isoscalarity correction.

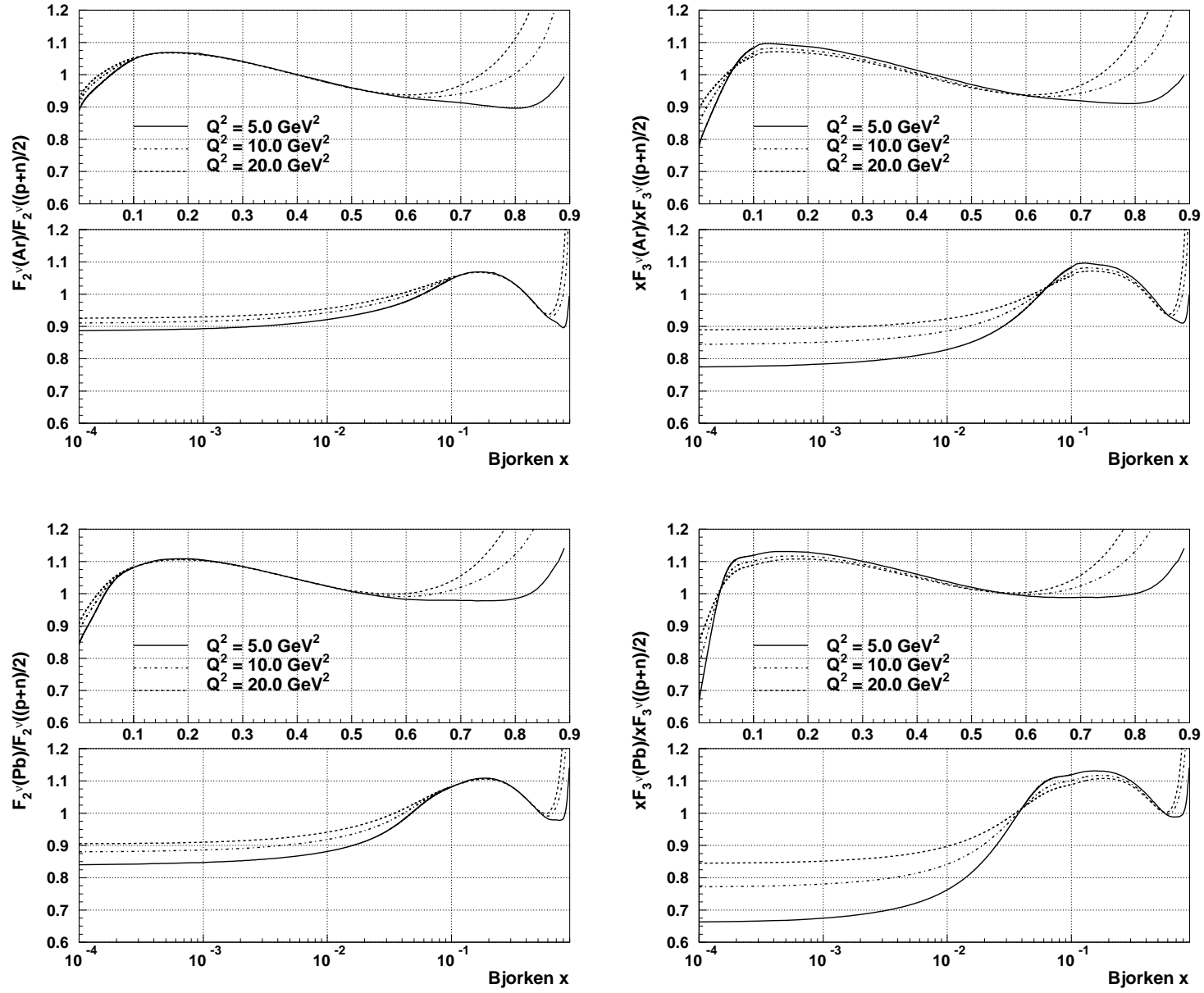


FIG. 16: Our predictions for ratios of F_2 (left plots) and xF_3 (right plots) for neutrino scattering on ^{40}Ar and ^{207}Pb and the corresponding values on isoscalar nucleon $(p+n)/2$. The curves are drawn for $Q^2 = 5, 10, 20 \text{ GeV}^2$ and take into account the non-isoscalarity correction.

is systematically larger as follows from Eq.(81).

Figure 17 illustrates different nuclear corrections to xF_3^ν for ^{207}Pb target computed at fixed Q^2 . The enhancement at intermediate x values is a joined effect of all considered nuclear correction (see also Fig. 14 and discussion in Sect. VII A 2). In the case of F_2 the “antishadowing” at $x \sim 0.1$ is due to off-shell and nuclear pion corrections.²¹ Note that the nuclear pion excess effect can be neglected in the case of xF_3 , in contrast to the case of F_2 . Indeed, in the isoscalar nucleus the pion correction depends on pion structure functions averaged over different pion states and F_3^π vanishes after such averaging. A small isovector correction which is proportional to $\pi^+ - \pi^-$ asymmetry in the nuclear pion distribution functions (see Eq.(124)) is also neglected.

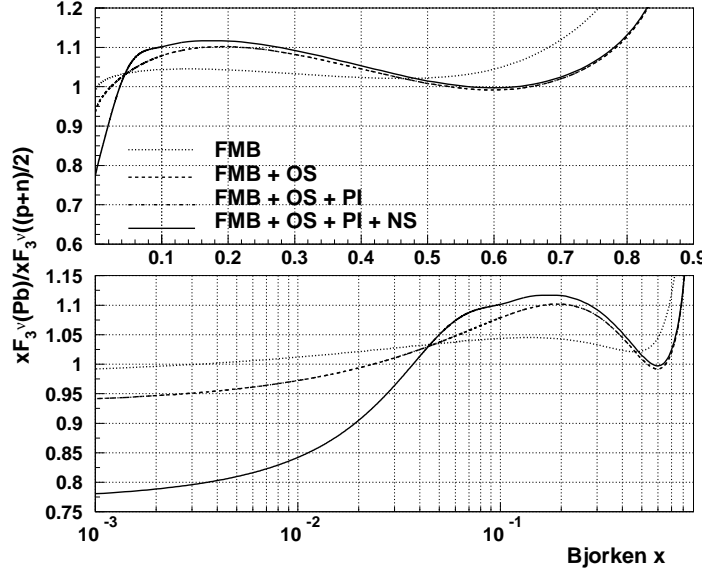


FIG. 17: Different nuclear effects calculated for neutrino xF_3 at $Q^2 = 10 \text{ GeV}^2$ for ^{207}Pb target. The labels on the curves correspond to the effects included in turn: the averaging with nuclear spectral function (FMB), off-shell correction (OS), nuclear pion excess (PI) and coherent multiple-scattering correction (NS). The calculation takes into account the target mass and the neutron excess corrections. Note that xF_3 is not corrected for pion excess effect (overlapping dashed and dashed-dotted curves).

The study of xF_3 is particularly important since it allows to check the normalization of nuclear valence quark number. As discussed in Sections VIA and VIB we require the conservation of the nuclear valence quark number in nuclei, which is an important constraint in our fits. However, the total normalization is balanced by finite contributions due to nuclear shadowing and off-shell effects. The valence quark (baryon) number of the target is related to the integral of neutrino and antineutrino averaged F_3 , the Gross–Llewellyn–Smith sum rule [90]. We remark, however, that in QCD this relation is not exact and only holds in the

²¹ See also Fig. 3 for F_2^μ . Note, however, that the neutron excess correction has a different sign for F_2^μ and F_2^ν that explains the differences between the magnitude of nuclear effects in Figs. 3 and 16.

Experiment	Targets	CC statistics ($\times 10^6$)	Data taking	Reference
NOMAD	^{12}C	1.3(0.06) $\nu(\bar{\nu})$	1995-1998	[81]
	^{27}Al	1.5(0.07) $\nu(\bar{\nu})$		
	^{56}Fe	12.5(0.6) $\nu(\bar{\nu})$		
CHORUS	^{207}Pb	14.0(0.7) $\nu(\bar{\nu})$	1994-1998	[89]
NuTeV	^{56}Fe	2.7(1.2) $\nu(\bar{\nu})$	1996-1997	[82]

TABLE V: List of recent nuclear data which can be used to study nuclear effects on neutrino structure functions.

leading twist and leading order in α_s and is renormalized by both the radiative corrections [91] and the higher-twist effects. It would be interesting to experimentally address the question of nuclear modification of this sum rule. New measurements of xF_3 from neutrino and antineutrino scattering off different nuclei would help to clarify this issue, provided they can reach a precision comparable to the size of the effects we observe in our analysis (typically 1%, see Fig. 5).

We conclude this Section by remarking that in spite of the major interest of neutrinos as a probe for nuclear effects, virtually no precise experimental information is available so far in DIS region. The only direct measurements of nuclear effects on neutrino DIS cross-sections were performed by BEBC [86] ($^{20}\text{Ne}/\text{D}$) and CDHSW [87] ($^{56}\text{Fe}/\text{p}$). However, these results are affected by large statistical and systematic uncertainties. It should be emphasized that neutrino DIS provides information complementary to that of the charged-lepton scattering and, therefore, the completion of new high-statistics measurements would have a large impact on our understanding of nuclear effects. The NOMAD experiment [81] collected large neutrino samples on ^{12}C , ^{27}Al and ^{56}Fe targets allowing a study of nuclear effects from $^{27}\text{Al}/^{12}\text{C}$ and $^{56}\text{Fe}/^{12}\text{C}$ ratios [19]. The recent NuTeV cross-section data [88] also provide information on nuclear effects in ^{56}Fe . In addition, the CHORUS experiment [89] is extracting neutrino cross-sections from the interactions collected on ^{207}Pb . Table V summarizes the various (anti)neutrino data samples.

VIII. SUMMARY

We presented a detailed phenomenological study of unpolarized nuclear structure functions for a wide kinematical region of x and Q^2 . We developed a general approach which on one side takes into account the main nuclear corrections and on the other side provides a reliable description of data on nuclear structure functions. Our complex model takes into account the QCD treatment of the nucleon structure functions and it incorporates a number of nuclear effects including nuclear shadowing, Fermi motion and nuclear binding, nuclear pions and off-shell corrections to bound nucleon structure functions for both charged-lepton and neutrino DIS.

It should be noted that the description of some nuclear corrections, such as Fermi motion and nuclear binding, is well constrained by nuclear data at low- and intermediate-energy regions. However, several nuclear effects in DIS are still not well understood. In particular, we treated the off-shell effect in the bound nucleon structure functions phenomenologically. We expressed the off-shell correction in terms of a few parameters which we extracted from data,

together with their uncertainties. We used a similar approach for the effective scattering amplitude which determines the size of the nuclear shadowing effect.

It should be emphasized that the phenomenological parameters of the model refer to the nucleon structure and for this reason they are common to all nuclei. We tested this hypothesis by performing fits to different subsets of nuclei. Overall, we obtained an excellent agreement between our calculations and data by using only 3 independent parameters.

The off-shell correction to the structure functions is related to the modification of the bound nucleon in nuclei. From this point of view, it can be considered as a new nucleon structure function which describes the deformation of the nucleon parton distributions in the nuclear environment.

We studied in detail the Q^2 and A dependencies of nuclear corrections. One important application was the calculation of nuclear effects for deuterium, which is of primary interest for the problem of the extraction of the neutron structure functions. We also applied our model to study nuclear corrections to valence and sea quark distributions, as well as the flavor (isospin) dependence of nuclear effects.

Another important application was the calculation of nuclear structure functions for neutrino scattering. In the present paper we evaluated nuclear corrections for charged-current neutrino structure functions for relatively high Q^2 , which are relevant for the analysis of existing DIS neutrino data. More detailed studies of neutrino and antineutrino interactions for both charged-current and neutral-current scattering are planned in future publications.

Acknowledgments

We would like to thank M. Arneodo for useful information on NMC data, S. Alekhin, A. Butkevich and A. Kataev for fruitful discussions on different stages of this work. The work of S.K. was partially supported by the Russian Foundation for Basic Research grant no. 03-02-17177. S.K. is grateful to CERN, where a part of this work was done, for hospitality.

APPENDIX A: PHASE SPACE IN CONVOLUTION FORMULAS

The phase space in convolution formulas is constrained by the requirement that the center-of-mass energy of bound nucleon and the virtual photon is high enough for producing physical final states. In particular, if we focus on the region of invariant masses of final states larger than a given mass M_X , the required relation is

$$W^2 \geq M_X^2, \quad (\text{A1})$$

where $W^2 = (p+q)^2$ and p the four-momentum of the bound nucleon. The inelastic channels correspond to $M_X = M + m_\pi$ and by setting $M_X = M$ we take into account the elastic channel. In this Section we discuss in detail the constraints on the integration region in the convolution formulas due to Eq.(A1). Note that Eq.(A1) is equivalent to

$$p_0 + q_0 \geq E_X, \quad (\text{A2})$$

where $E_X = (M_X^2 + (\mathbf{p} + \mathbf{q})^2)^{1/2}$ and $p_0 = M + \varepsilon$. Using this equation we can write the integral over the bound nucleon four-momentum in convolution formulas as

$$\int d^4p \theta(W^2 - M_X^2) = \int d^3\mathbf{p} \int_{E_X - q_0 - M} d\varepsilon. \quad (\text{A3})$$

This equation should be applied together with the nuclear spectral function and other functions which enter the convolution formulas. The energy integration in Eq.(A3) corresponds to the integration over the excitation energies of the residual nucleus.

We first consider a particular case when the energy dependence of the spectral function is given by

$$\mathcal{P}(\varepsilon, \mathbf{p}) = 2\pi\delta(\varepsilon - \varepsilon_{\mathbf{p}})n(\mathbf{p}), \quad (\text{A4})$$

$$\varepsilon_{\mathbf{p}} = \varepsilon_0 - \frac{\mathbf{p}^2}{2m_0}. \quad (\text{A5})$$

This case applies to the deuterium, for which $\varepsilon_0 = \varepsilon_D$ and $m_0 = M$ (see Eq.(52)), and also for the model spectral function \mathcal{P}_{MF} , for which $m_0 = M_{A-1}$ is the mass of the residual nucleus and $\varepsilon_0 = -E^{(1)}$ is the nucleon separation energy averaged over low-excitation (mean-field) configurations of the residual nucleus (see Eq.(95) and the discussion thereafter).

The energy integration in Eq.(A3) can easily be performed and inequality (A2) then becomes

$$q_0 + M + \varepsilon_{\mathbf{p}} \geq E_X. \quad (\text{A6})$$

This inequality provides the constraints on the momentum space in Eq.(A3). In order to solve it explicitly we chose the coordinate system such that the momentum transfer has only longitudinal component $q = (q_0, \mathbf{0}_{\perp}, -|\mathbf{q}|)$. Then after some algebra (A6) can be written as (we retain only the terms linear in $\varepsilon_{\mathbf{p}}$)

$$\frac{\mathbf{p}^2}{2m_*} - p_z - p_* \leq 0, \quad (\text{A7})$$

where the notations are

$$\gamma p_* = M \left[1 - x \left(1 + \frac{\Delta}{Q^2} \right) + \frac{\varepsilon_0 \gamma_2}{M} \right], \quad (\text{A8a})$$

$$m_* = \frac{m_0 |\mathbf{q}|}{m_0 + q_0 + M}. \quad (\text{A8b})$$

We also denote $\Delta = M_X^2 - M^2$, $\gamma = |\mathbf{q}|/q_0$, and $\gamma_2 = 1 + M/q_0$.

Inequality (A7) is most easily solved in terms of *longitudinal* and *transverse* coordinates, $\mathbf{p} = (\mathbf{p}_{\perp}, p_z)$. In this case, the solution to (A7) can be written as

$$\begin{cases} p_z^- \leq p_z \leq p_z^+, \\ 0 \leq \mathbf{p}_{\perp}^2 \leq T^2, \end{cases} \quad (\text{A9})$$

where $T^2 = m_*^2 + 2m_* p_*$ is maximum transverse momentum squared of the bound nucleon (for the given kinematical conditions) and p_z^{\pm} correspond to those longitudinal momenta at which the left side of (A7) crosses 0,

$$p_z^{\pm} = m_* \pm (T^2 - \mathbf{p}_{\perp}^2)^{1/2} \quad (\text{A10})$$

The momentum integral in Eq.(A3) in terms of these variables is

$$\int_{W^2 \geq M_X^2} d^3 \mathbf{p} = \pi \theta(T) \int_0^{T^2} dp_{\perp}^2 \int_{p_z^-}^{p_z^+} dp_z. \quad (\text{A11})$$

The requirement $T^2 \geq 0$ causes the constraint on possible x and Q^2 in inelastic scattering off bound nucleon.²²

We discuss now the case when the momentum is parameterized in terms of *spherical* coordinates. We introduce the azimuthal angle θ between the z -axis and the direction of the momentum, $p_z = p \cos \theta$ (here $p = |\mathbf{p}|$), and denote by $p_{\pm}(\cos \theta)$ the values of p at which the left side of (A7) is equal to 0 for the given $\cos \theta$,

$$p_{\pm}(\cos \theta) = m_* \cos \theta \pm \sqrt{(m_* \cos \theta)^2 + 2m_* p_*}. \quad (\text{A12})$$

We have two different regions, where (A7) holds:

$$\begin{cases} 0 < p_* \\ -1 \leq \cos \theta \leq 1 \\ 0 \leq p \leq p_+(\cos \theta), \end{cases} \quad (\text{A13a})$$

and

$$\begin{cases} -m_*/2 \leq p_* \leq 0 \\ c_* \leq \cos \theta \leq 1 \\ p_-(\cos \theta) \leq p \leq p_+(\cos \theta), \end{cases} \quad (\text{A13b})$$

where $c_* = (2|p_*|/m_*)^{1/2}$ and $p_{\pm}(\cos \theta)$ are given by Eq.(A12). Using these inequalities the momentum integral in convolution formula can be written in spherical coordinates as

$$\int_{W^2 \geq M_X^2} d^3 \mathbf{p} = \begin{cases} 2\pi \int_{-1}^1 d \cos \theta \int_0^{p_+(\cos \theta)} dp p^2, & \text{if } p_* > 0, \\ 2\pi \int_{c_*}^1 d \cos \theta \int_{p_-(\cos \theta)}^{p_+(\cos \theta)} dp p^2, & \text{if } -\frac{m_*}{2} \leq p_* \leq 0. \end{cases} \quad (\text{A14})$$

The first case in (A14) applies if $x < 1$ as can be readily seen from Eqs.(A8), while the last case concerns the region of x about 1 and greater than 1.

We now consider generic case of energy excitation spectrum in Eq.(A3). The upper limit of energy integration is determined by the threshold separation energy ε_{th} . We recall that in our notations for the target nucleus of A nucleons the separation energy $\varepsilon = E_0^A - E^{A-1}$, where E_0^A is the ground state energy of the target nucleus and E^{A-1} is the energy of the residual nucleus including the recoil energy. Therefore, for the given recoil momentum $\varepsilon_{\text{th}} = \varepsilon_0 - \mathbf{p}^2/(2m_0)$, where $\varepsilon_0 = E_0^A - E_0^{A-1}$ is the difference of the ground state energies

²² The equation $T^2 = 0$ determines the maximum possible x which can be achieved in DIS from bound nucleon. In application to the deuteron this gives $x = 3/2$ (neglecting Q^{-2} terms and ε_d/M corrections in Eq.(A8)). This is different from the kinematical maximum $x = M_D/M \approx 2$, which corresponds to elastic scattering from the deuteron as a whole. We comment in this respect that the estimate $x = 3/2$ was derived assuming the energies ε to be nonrelativistic. However, the events with such large x are due to high-momentum configurations $p \sim M$ in the wave function and, therefore, require fully relativistic description. The description of very large x goes beyond the scope of this paper.

of the target and the residual nucleus, $m_0 = M_{A-1}$ is the mass of the residual nucleus and $\mathbf{p}^2/(2m_0)$ its recoil energy. The constraints on the momentum space in Eq.(A3) follow from the inequality

$$E_X - q_0 - M \leq \varepsilon_{\text{th}}. \quad (\text{A15})$$

This inequality, written in terms of ε_0 and m_0 , is equivalent to (A6). Therefore, the discussion of (A6) can be taken over (A15). In particular, the solutions to (A15) in terms of the longitudinal and transverse momentum are given by Eqs.(A9) and (A10). The integration in (A3) in terms of these variables can explicitly be written as

$$\int_{W^2 \geq M_X^2} d^4p = \pi \theta(T^2) \int_0^{T^2} dp_{\perp}^2 \int_{p_z^-}^{p_z^+} dp_z \int_{E_X - q_0 - M}^{\varepsilon_{\text{th}}} d\varepsilon, \quad (\text{A16})$$

where the limits of integration are similar to those in Eq.(A11) and given by Eqs.(A8,A9,A10).

The integration in (A3) in terms of spherical coordinates can explicitly be written as

$$\int_{W^2 \geq M_X^2} d^4p = \begin{cases} 2\pi \int_{-1}^1 d\cos\theta \int_0^{p_+(\cos\theta)} dp p^2 \int_{E_X - q_0 - M}^{\varepsilon_{\text{th}}} d\varepsilon, & \text{if } p_* > 0, \\ 2\pi \int_{c_*}^1 d\cos\theta \int_{p_-(\cos\theta)}^{p_+(\cos\theta)} dp p^2 \int_{E_X - q_0 - M}^{\varepsilon_{\text{th}}} d\varepsilon, & \text{if } -\frac{m_*}{2} \leq p_* \leq 0, \end{cases} \quad (\text{A17})$$

where the notations are similar to those in Eq.(A14) and the limits of integration are given by Eqs.(A12,A13).

APPENDIX B: MULTIPLE SCATTERING COEFFICIENTS FOR UNIFORM NUCLEAR DENSITY

The magnitude of coherent nuclear effects in the C -even and C -odd structure functions F_2 and F_3 is determined by the terms \mathcal{C}_2^A and \mathcal{C}_3^A (see Eqs. (84) and (89)). These quantities can be computed analytically for uniform density distribution with a sharp edge (square well model), $\rho_A(\mathbf{r}) = \rho_0 \theta(R_A - |\mathbf{r}|)$, which is a reasonable approximation for large nuclei [67]. The nuclear radius in this model is related to the r.m.s. nuclear radius as $R_A^2 = \frac{5}{3} \langle r^2 \rangle$ and the central nuclear density is $\rho_0 = A/(\frac{4\pi}{3} R_A^3)$ with A the number of nucleons. The coefficients \mathcal{C}_2^A and \mathcal{C}_3^A are

$$\mathcal{C}_2^A = A \rho_0 R_A \varphi_2^{\text{SW}}(y), \quad (\text{B1a})$$

$$\mathcal{C}_3^A = A (\rho_0 R_A)^2 \varphi_3^{\text{SW}}(y), \quad (\text{B1b})$$

where $\varphi_{2,3}^{\text{SW}}$ are the functions of dimensionless and complex variable $y = 2i(\rho_0 f - k_L) R_A$

$$\varphi_2^{\text{SW}}(y) = [6 - 3y^2 - 2y^3 + 6(y-1)\exp(y)]/y^4, \quad (\text{B2a})$$

$$\varphi_3^{\text{SW}}(y) = 12 [-4 + y^2 + y^3/3 + (2-y)^2 \exp(y)]/y^5. \quad (\text{B2b})$$

Note that if the real part of the amplitude f and k_L can be neglected (which is a reasonable approximation for $x \ll 0.1$), then $y = R_A/l_f$ with $l_f = (\rho_0\sigma)^{-1}$ the mean free path of the particle.

-
- [1] J.J. Aubert *et al.*, Phys. Lett. B **123**, 275 (1983).
 - [2] M. Arneodo *et al.* [New Muon Collaboration], Phys. Rev. D **50**, 1 (1994).
 - [3] M. Arneodo *et al.* [New Muon Collaboration.], Nucl. Phys. B **441**, 12 (1995) [arXiv:hep-ex/9504002].
 - [4] P. Amaudruz *et al.* [New Muon Collaboration], Nucl. Phys. B **441**, 3 (1995) [arXiv:hep-ph/9503291].
 - [5] M. Arneodo *et al.* [New Muon Collaboration], Nucl. Phys. B **481**, 3 (1996).
 - [6] M. Arneodo *et al.* [New Muon Collaboration], Nucl. Phys. B **481**, 23 (1996).
 - [7] J. Ashman *et al.* [European Muon Collaboration], Z. Phys. C **57**, 211 (1993).
 - [8] G. Bari *et al.* [BCDMS Collaboration], Phys. Lett. B **163**, 282 (1985).
 - [9] S. Dasu *et al.*, Phys. Rev. Lett. **60**, 2591 (1988).
 - [10] J. Gomez *et al.*, Phys. Rev. D **49**, 4348 (1994).
 - [11] M. R. Adams *et al.* [E665 Collaboration], Phys. Rev. Lett. **75**, 1466 (1995).
 - [12] M. R. Adams *et al.* [E665 Collaboration], Z. Phys. C **67**, 403 (1995) [arXiv:hep-ex/9505006].
 - [13] J. Arrington, R. Ent, C. E. Keppel, J. Mammei and I. Niculescu, arXiv:nucl-ex/0307012.
 - [14] D. M. Alde *et al.*, Phys. Rev. Lett. **64**, 2479 (1990); M. A. Vasilev *et al.* [FNAL E866 Collaboration], Phys. Rev. Lett. **83**, 2304 (1999) [arXiv:hep-ex/9906010]; G. Moreno *et al.*, Phys. Rev. D **43**, 2815 (1991).
 - [15] K. H. Ackermann *et al.* [STAR Collaboration], Nucl. Instrum. Meth. A **499**, 624 (2003); M. Adamczyk *et al.* [BRAHMS Collaboration], Nucl. Instrum. Meth. A **499**, 437 (2003); K. Adcox *et al.* [PHENIX Collaboration], Nucl. Instrum. Meth. A **499**, 469 (2003); B. B. Back *et al.* [PHOBOS Collaboration], Nucl. Instrum. Meth. A **499**, 603 (2003).
 - [16] F. Carminati *et al.* [ALICE Collaboration], J. Phys. G **30**, 1517 (2004); ATLAS collaboration, CERN/LHCC/2004-009, LHCC I-013; P. P. Yepes [CMS Collaboration], Nucl. Phys. A **698**, 456 (2002) [arXiv:nucl-ex/0104026].
 - [17] G. A. Miller and A. W. Thomas, arXiv:hep-ex/0204007; S. Kovalenko, I. Schmidt and J. J. Yang, Phys. Lett. B **546**, 68 (2002) [arXiv:hep-ph/0207158]; S. Kumano, Phys. Rev. D **66**, 111301 (2002) [arXiv:hep-ph/0209200]; S. A. Kulagin, Phys. Rev. D **67**, 091301 (2003) [arXiv:hep-ph/0301045]; S. Kumano, arXiv:hep-ph/0307105; S. A. Kulagin, arXiv:hep-ph/0406220. S. J. Brodsky, I. Schmidt and J. J. Yang, Phys. Rev. D **70**, 116003 (2004) [arXiv:hep-ph/0409279].
 - [18] G. P. Zeller *et al.*, Phys. Rev. Lett. **88**, 091802 (2002) [arXiv:hep-ex/0110059].
 - [19] R. Petti, arXiv:hep-ex/0411032.
 - [20] J. Hylen *et al.*, Fermilab Report No. TM-2018 (1997); L. Bartoszek *et al.*, arXiv:hep-ex/0408121; D. Drakoulakos *et al.*, arXiv:hep-ex/0405002.
 - [21] Japan Proton Accelerator Research Complex, Tokai (Japan),
URL: <http://jkj.tokai.jaeri.go.jp/>.
 - [22] M. L. Mangano *et al.*, arXiv:hep-ph/0105155; A. Blondel *et al.*, CERN-2004-002; M. M. Al-sharoa *et al.* [Muon Collider/Neutrino Factory Collaboration], Phys. Rev. ST Accel. Beams **6**, 081001 (2003) [arXiv:hep-ex/0207031].

- [23] Jefferson Laboratory, Newport News (USA), URL: <http://www.jlab.org/>.
- [24] G. Piller and W. Weise, Phys. Rept. **330**, 1 (2000) [arXiv:hep-ph/9908230].
- [25] D. F. Geesaman, K. Saito, and A. W. Thomas, Annu. Rev. Nucl. Part. Sci. **45** 337 (1995).
- [26] M. Arneodo, Phys. Rept. **240**, 301 (1994).
- [27] L. L. Frankfurt and M. I. Strikman, Phys. Rept. **160** (1988) 235.
- [28] B. L. Ioffe, V. A. Khoze and L. N. Lipatov, “Hard Processes. Vol. 1: Phenomenology, Quark Parton Model”, Elsevier Science Publishers, North Holland, 1984.
- [29] C. H. Albright and C. Jarlskog, Nucl. Phys. B **84**, 467 (1975).
- [30] S. Kretzer and M. H. Reno, Phys. Rev. D **66**, 113007 (2002); [arXiv:hep-ph/0208187].
- [31] K. G. Wilson, Phys. Rev. **179**, 1499 (1969);
E. V. Shuryak and A. I. Vainshtein, Nucl. Phys. B **199**, 451 (1982).
- [32] R. Brock *et al.* [CTEQ Collaboration], Rev. Mod. Phys. **67**, 157 (1995).
- [33] L. N. Lipatov, Sov. J. Nucl. Phys. **20**, 94 (1975) [Yad. Fiz. **20**, 181 (1974)]; G. Altarelli and G. Parisi, Nucl. Phys. B **126**, 298 (1977). Yu. L. Dokshitzer, Sov. Phys. JETP **46**, 641 (1977) [Zh. Eksp. Teor. Fiz. **73**, 1216 (1977)].
- [34] W. Furmanski and R. Petronzio, Z. Phys. C **11**, 293 (1982).
- [35] W. L. van Neerven and E. B. Zijlstra, Phys. Lett. B **272**, 127 (1991); Nucl. Phys. B **383**, 525 (1992); D. I. Kazakov and A. V. Kotikov, Phys. Lett. B **291**, 171 (1992).
- [36] S. Moch, J. A. M. Vermaseren and A. Vogt, Nucl. Phys. B **688**, 101 (2004) [arXiv:hep-ph/0403192]; A. Vogt, S. Moch and J. A. M. Vermaseren, Nucl. Phys. B **691**, 129 (2004) [arXiv:hep-ph/0404111].
- [37] H. Georgi and H. D. Politzer, Phys. Rev. **D14**, 1829 (1976).
- [38] O. Nachtmann, Nucl. Phys. **B63** (1973) 237.
- [39] S. I. Alekhin, Phys. Rev. D **68**, 014002 (2003), [arXiv:hep-ph/0211096].
- [40] J. Pumplin, D. R. Stump, J. Huston, H. L. Lai, P. Nadolsky and W. K. Tung, JHEP **0207**, 012 (2002) [arXiv:hep-ph/0201195].
- [41] A. D. Martin, R. G. Roberts, W. J. Stirling and R. S. Thorne, Eur. Phys. J. C **23**, 73 (2002) [arXiv:hep-ph/0110215].
- [42] M. Gluck, E. Reya and I. Schienbein, Eur. Phys. J. C **10**, 313 (1999) [arXiv:hep-ph/9903288].
- [43] G. B. West, Ann. Phys. **74**, 464 (1972); D. Kusno and M. J. Moravcsik, Phys. Rev. D **20**, 2734 (1979); A. Bodek and J. L. Ritchie, Phys. Rev. D **23**, 1070 (1981).
- [44] S. V. Akulinichev, S. A. Kulagin and G. M. Vagradov, Phys. Lett. B **158**, 485 (1985); S. V. Akulinichev, S. Shlomo, S. A. Kulagin and G. M. Vagradov, Phys. Rev. Lett. **55**, 2239 (1985); B. L. Birbrair, A. B. Gridnev, M. B. Zhalov, E. M. Levin and V. E. Starodubsky, Phys. Lett. B **166**, 119 (1986); H. Jung and G. A. Miller, Phys. Lett. B **200**, 351 (1988); C. Ciofi degli Atti and S. Liuti, Phys. Rev. **C41**, 1100 (1990). P. J. Mulders, A. W. Schreiber and H. Meyer, Nucl. Phys. A **549**, 498 (1992). V. Barone, M. Genovese, N. N. Nikolaev, E. Predazzi and B. G. Zakharov, Z. Phys. C **58**, 541 (1993). V. V. Burov, A. V. Molochkov and G. I. Smirnov, Phys. Lett. B **466**, 1 (1999) [arXiv:nucl-th/9904050]. S. A. Gurvitz and A. S. Rinat, Phys. Rev. C **65**, 024310 (2002) [arXiv:nucl-th/0106032].
- [45] G. V. Dunne and A. W. Thomas, Phys. Rev. D **33**, 2061 (1986).
- [46] F. Gross and S. Liuti, Phys. Rev. **C45**, 1374 (1992).
- [47] S. A. Kulagin, Nucl. Phys. A **500**, 653 (1989).
- [48] S. A. Kulagin, G. Piller and W. Weise, Phys. Rev. C **50**, 1154 (1994) [arXiv:nucl-th/9402015].
- [49] S. A. Kulagin, W. Melnitchouk, G. Piller and W. Weise, Phys. Rev. C **52**, 932 (1995) [arXiv:hep-ph/9504377].

- [50] S. A. Kulagin, Nucl. Phys. A **640**, 435 (1998) [arXiv:nucl-th/9801039].
- [51] W. Melnitchouk, A. W. Schreiber and A. W. Thomas, Phys. Rev. D **49**, 1183 (1994) [arXiv:nucl-th/9311008].
- [52] S. I. Alekhin, S. A. Kulagin and S. Liuti, Phys. Rev. D **69**, 114009 (2004) [arXiv:hep-ph/0304210].
- [53] S. A. Kulagin, Nucl. Phys. Proc. Suppl. **139**, 213 (2005) [arXiv:hep-ph/0409057];
- [54] J. D. Sullivan, Phys. Rev. D **5**, 1732 (1972).
- [55] C. H. Llewellyn Smith, Phys. Lett. B **128**, 107 (1983); M. Ericson and A. W. Thomas, Phys. Lett. B **128**, 112 (1983); E. L. Berger and F. Coester, Phys. Rev. D **32**, 1071 (1985); B. L. Friman, V. R. Pandharipande and R. B. Wiringa, Phys. Rev. Lett. **51**, 763 (1983); E. E. Sapershtein and M. Z. Shmatikov, JETP Lett. **41**, 53 (1985) [Pisma Zh. Eksp. Teor. Fiz. **41**, 44 (1985)]; L. P. Kaptari, A. I. Titov, E. L. Bratkovskaya and A. Y. Umnikov, Nucl. Phys. A **512**, 684 (1990); H. Jung and G. A. Miller, Phys. Rev. C **41**, 659 (1990); D. S. Koltun, Phys. Rev. C **57**, 1210 (1998) [arXiv:nucl-th/9709033].
- [56] R. J. Glauber, Phys. Rev. **100**, 242 (1955).
- [57] V. N. Gribov, Sov. Phys. JETP **30**, 709 (1970) [Zh. Eksp. Teor. Fiz. **57**, 1306 (1969)].
- [58] R. J. Glauber and G. Matthiae, Nucl. Phys. B **21**, 135 (1970).
- [59] T. H. Bauer, R. D. Spital, D. R. Yennie and F. M. Pipkin, Rev. Mod. Phys. **50**, 261 (1978) [Erratum-ibid. **51**, 407 (1979)].
- [60] R. D. Spital and D. R. Yennie, Phys. Rev. D **9**, 128 (1974).
- [61] J. Kwiecinski and B. Badelek, Phys. Lett. B **208**, 508 (1988); N. N. Nikolaev and B. G. Zakharov, Z. Phys. C **49**, 607 (1991); S. J. Brodsky and H. J. Lu, Phys. Rev. Lett. **64**, 1342 (1990); G. Shaw, Phys. Rev. D **47**, 3676 (1993); W. Melnitchouk and A. W. Thomas, Phys. Lett. B **317**, 437 (1993) [arXiv:nucl-th/9310005]; G. Piller, W. Ratzka and W. Weise, Z. Phys. A **352**, 427 (1995) [arXiv:hep-ph/9504407]; A. Capella, A. Kaidalov, C. Merino, D. Pertermann and J. Tran Thanh Van, Eur. Phys. J. C **5**, 111 (1998) [arXiv:hep-ph/9707466]; B. Z. Kopeliovich, J. Raufeisen and A. V. Tarasov, Phys. Lett. B **440**, 151 (1998) [arXiv:hep-ph/9807211]; L. Frankfurt, V. Guzey, M. McDermott and M. Strikman, JHEP **0202**, 027 (2002) [arXiv:hep-ph/0201230]; J. W. Qiu and I. Vitev, Phys. Lett. B **587**, 52 (2004) [arXiv:hep-ph/0401062].
- [62] S. A. Kulagin, arXiv:hep-ph/9812532.
- [63] B. Badelek, J. Kwiecinski and A. Stasto, Z. Phys. C **74**, 297 (1997) [arXiv:hep-ph/9603230].
- [64] R. Machleidt, K. Holinde and C. Elster, Phys. Rept. **149**, 1 (1987).
- [65] M. Lacombe, B. Loiseau, J. M. Richard, R. Vinh Mau, J. Cote, P. Pires and R. De Tourreil, Phys. Rev. C **21**, 861 (1980).
- [66] S. Frullani and J. Mougey, Adv. Nucl. Phys. **14**, 1 (1984).
- [67] A. deShalit and H. Feshbach, "Theoretical nuclear physics. Vol. 1: Nuclear structure.", Wiley, 1974.
- [68] H. Muther and A. Polls, Prog. Part. Nucl. Phys. **45**, 243 (2000) [arXiv:nucl-th/0001007].
- [69] C. Ciofi degli Atti and S. Simula, Phys. Rev. C **53**, 1689 (1996) [arXiv:nucl-th/9507024].
- [70] J. G. Zabolitsky and W. Ey, Phys. Lett. **B76** (1978) 527.
- [71] S. A. Kulagin and A. V. Sidorov, Eur. Phys. J. A **9**, 261 (2000) [arXiv:hep-ph/0009150].
- [72] D. S. Koltun, Phys. Rev. **C9** (1974) 484.
- [73] P. D. B. Collins, "An Introduction To Regge Theory And High-Energy Physics", Cambridge Univ. Press, Cambridge, 1977.
- [74] MINUIT, Function minimization and error analysis, CERN Long Writeup D506.

- [75] K. J. Eskola, V. J. Kolhinen and P. V. Ruuskanen, Nucl. Phys. B **535**, 351 (1998) [arXiv:hep-ph/9802350]; K. J. Eskola, V. J. Kolhinen and C. A. Salgado, Eur. Phys. J. C **9**, 61 (1999) [arXiv:hep-ph/9807297].
- [76] M. Hirai, S. Kumano and M. Miyama, Phys. Rev. D **64**, 034003 (2001) [arXiv:hep-ph/0103208]; M. Hirai, S. Kumano and T. H. Nagai, Phys. Rev. C **70**, 044905 (2004) [arXiv:hep-ph/0404093].
- [77] S. y. Li and X. N. Wang, Phys. Lett. B **527**, 85 (2002) [arXiv:nucl-th/0110075].
- [78] D. de Florian and R. Sassot, Phys. Rev. D **69**, 074028 (2004) [arXiv:hep-ph/0311227].
- [79] J. H. Kim *et al.*, Phys. Rev. Lett. **81** (1998) 3595 [arXiv:hep-ex/9808015].
- [80] S. A. Kulagin and R. Petti, in preparation.
- [81] J. Altegoer *et al.* [NOMAD Collaboration], Nucl. Instrum. Meth. A **404**, 96 (1998).
- [82] D. A. Harris *et al.* [NuTeV Collaboration], Nucl. Instrum. Meth. A **447**, 377 (2000) [arXiv:hep-ex/9908056].
- [83] MINOS collaboration, Fermilab Report No. NuMI-L-337 (1998), NuMI-L-726 (2001).
- [84] S. Amerio *et al.* [ICARUS Collaboration], Nucl. Instrum. Meth. A **527**, 329 (2004).
- [85] M. Guler *et al.*, CERN/SPSC 2000-028, SPSC/P318, LNGS P25/2000.
- [86] P. P. Allport *et al.* [BEBC WA59 Collaboration], Phys. Lett. B **232**, 417 (1989).
- [87] H. Abramowicz *et al.*, Z. Phys. C **25**, 29 (1984).
- [88] V. A. Radescu [NuTeV Collaboration], arXiv:hep-ex/0408006.
- [89] E. Eskut *et al.* [CHORUS Collaboration], Nucl. Instrum. Meth. A **401**, 7 (1997).
- [90] D. J. Gross and C. H. Llewellyn Smith, Nucl. Phys. B **14**, 337 (1969).
- [91] S. G. Gorishnii and S. A. Larin, Phys. Lett. B **172**, 109 (1986); S. A. Larin and J. A. M. Vermaseren, Phys. Lett. B **259**, 345 (1991).